2016-04-11

Impacts of Disrupting Early Motor Behaviors on Spatial and Temporal Patterning of Synapses in Zebrafish Spinal Cord

Qing Yan
University of Miami, yanqing@bio.miami.edu

UNIVERSITY OF MIAMI

IMPACTS OF DISRUPTING EARLY MOTOR BEHAVIORS ON SPATIAL AND TEMPORAL PATTERNING OF SYNAPSES IN ZEBRAFISH SPINAL CORD

By

Qing Yan

A DISSERTATION

Submitted to the Faculty
of the University of Miami
in partial fulfillment of the requirements for
the degree of Doctor of Philosophy

Coral Gables, Florida

May 2016

UNIVERSITY OF MIAMI

A dissertation submitted in partial fulfillment of
the requirements for the degree of
Doctor of Philosophy

IMPACTS OF DISRUPTING EARLY MOTOR BEHAVIORS ON SPATIAL AND TEMPORAL PATTERNING OF SYNAPSES IN ZEBRAFISH SPINAL CORD

Qing Yan

Approved:

_____ Julia Dallman, Ph.D. Assistant Professor of Biology	_____ Athula Wikramanayake, Ph.D. Professor of Biology
_____ Akira Chiba, Ph.D. Professor of Biology	_____ Guillermo Prado, Ph.D. Dean of the Graduate School

_____
Stephan Züchner, M.D./Ph.D.
Professor of Human Genetics

YAN, QING (Ph.D., Biology)

Impacts of Disrupting Early Motor Behaviors on Spatial and Temporal Patterning of Synapses in Zebrafish Spinal Cord

(May 2016)

Abstract of a dissertation at the University of Miami.

Dissertation supervised by Professor Julia Dallman.
No. of pages in text. (113)

To generate rhythmic motor behaviors, both single neurons and neural circuits require a balance between excitation and inhibition (E/I balance). Disruption of E/I balance is associated with many neurodevelopmental disorders, such as seizures, autism, startle disease and glycine encephalopathy. E/I balance is maintained at both the cellular and the systems levels, and is influenced by the relative distribution of excitatory and inhibitory synapses. While the spatial and temporal patterns of excitatory and inhibitory synapses strongly associate with E/I balance, it remains unclear how perturbations of E/I balance affect the spatial and temporal patterning of synapses in *in vivo* neural circuits.

To answer this question, we investigated the spatial and temporal patterning of excitatory and inhibitory synapses in developing zebrafish spinal cord (Chapter 2). We hypothsized that excitatory and inhibitory synapses and neuronal processes follow a stable, systems-level spatial pattern on the medial-lateral axis in embryonic and larval spinal cord. Interestingly, this pattern is maintained in the zebrafish *glycine transporter 1* mutant despite the presence of perturbation of E/I balance (Chapter 3). This mutant can naturally re-establish the spinal cord E/I balance with development. We found that though the

general synapse pattern remains unchanged, subtle alterations of synapse spatial patterns take place at the beginning of the E/I balance re-establishment process.

We also investigated how a perturbation of E/I balance impacts the synaptogenesis process. To understand this, we knocked down genes encoding particular subunits of glycine receptors (GlyRs) in zebrafish embryos, and analyzed how such knockdown affects glycinergic synaptogenesis and motor behaviors (Chapter 4). We found that disruption of different GlyR subunits impacts the formation of functional glycinergic synapses in different manners: knocking down the GlyR α1 subunit leads to a reduction of GlyRs while knocking down the βb subunit disrupts the clustering of GlyRs at the post-synapses. In addition, knockdown of either subunit alters the spatial pattern of glycinergic synaptogenesis.

In conclusion, we found that E/I balance is associated with the spatial and temporal patterns of synapses at multiple levels. The systems-level pattern is stable and robust, while finer-scale patterns at cellular and dendritic levels are more flexible and likely to alter in response to perturbations of E/I balance.

Acknowledgement

First of all, I would like thank my Ph.D. advisor, Dr. Julia Dallman, for her advice, guidance, support and encouragement during all these years. She is a wonderful mentor and I have learned a lot from her. I would also like to thank my dissertation committee members, Drs. Athula Wikramanayake, Akira Chiba and Stephan Züchner for their time and commitment, and for their advice and support for my research and career. Thanks to my collaborators within and outside the Dallman lab: Dr. Lisa Ganser, Bo Zhang and Lu Zhai. I also want to thank previous and current members of the Dallman lab. Steven Sloan, Matthew Stark, Dr. Emma Back for their wonderful company and kind help in the lab. Robert Kozol, Alexander J. Abrams, and David James for all the enjoyable and insightful discussions with them and their big help with my English writing. To the undergraduate students who have helped with my project, Albert Hill, Dan Pham, and Alejandro Pinedo. And to Ricardo Cepeda for maintaining the zebrafish in great health.

I would also like to thank other colleagues in our department who helped along my way. Dr. James Baker for all his advice and help on imaging, staining and writing. Dr. Jeff Peng for helping with my Western blot. Dr. Jiang Jiang for teaching me Matlab, which means a lot for my research. Dr. Don DeAngelis for his insightful advice on the L-function analysis. Dr. Kevin Collins for his useful advice on writing and on my career.

Thanks to Dr. Martin Meyer for providing PSD-95 and SYP1 fusion protein constructs, Dr. Hiromi Hirata for his assistance in generating fast-frozen tissue sections, Dr. Rachel O. Wong and members of her lab for hosting me to learn to implement and modify their Matlab-assisted puncta-finding programs.

Special thanks to my colleague and husband, Lingyu Wang for his help, support and love. He has offered me great help with Western blot and molecular cloning. He also upgraded my laptop, and built a computer workstation at home to facilitate my data analysis. I have also gained many useful insights from discussions with him. I could not have done this without you.

TABLE OF CONTENTS

LIST OF TABLES

LIST OF FIGURES

LIST OF ABBREVIATIONS

AMPA	α-Amino-3-hydroxy-5-methyl-4-isoxazolepropionic acid
ANOVA	Analysis of variance
BDNF	Brain-derived neurotrophic factor
beo	*bandoneon*
BMP	Bone morphogenetic protein
CaMKIV	Calcium/calmodulin-dependent protein kinase type IV
CaMKK	Calcium/calmodulin-dependent protein kinase kinase
CaP motor neuron	Caudal primary motor neuron
CaV	Voltage-gated calcium channel
CDC42	Cell division control protein 42 homolog
Cdk5	Cyclin-dependent kinase 5
ChAT	Choline acetyltransferase
CNS	Central nervous system
DIC	Differential interference contrast
eEF2	Eukaryotic elongation factor 2
EGFP	Enhanced green fluorescent protein
E/I balance	Balance between excitatory and inhibitory neurotransmission
EPSC	Excitatory post-synaptic current
EPSP	Excitatory post-synaptic potential
GABA	γ-Aminobutyric acid
GEFs	Guanine nucleotide exchange factors
GFP	Green fluorescent protein
GlyR	Glycine receptor

GlyT1	Glycine transporter 1
glyt2	Glycine transporter 2
hpf	Hours post-fertilization
KA neuron	Kolmer-Agduhr neuron
IPSC	Inhibitory post-synaptic current
IPSP	Inhibitory post-synaptic potential
KS test	Kolmogorov–Smirnov test
MeCP2	Methyl CpG binding protein 2
MHCI	Major histocompatibility complex class I
MO	Morpholino
MS222	3-Aminobenzoic acid ethyl ester
M-L	Medial-lateral
NFPS	N[3-(4'-fluorophenyl)-3-(4'-phenylphenoxy) propyl]sarcosine
NMDA	N-methyl-D-aspartate
NMJ	Neuromuscular junction
Npas4	Neuronal PAS domain protein 4
PCR	Polymerase chain reaction
Plk2	Polo-like kinase 2
PSD-93	Post-synaptic density 93
PSD-95	Post-synaptic density 95
RIM	Rab3 interacting molecule
RB neuron	Rohon-Beard neuron
RRP	Readily releasable pool

RT-PCR	Reverse transcription polymerase chain reaction
SAP102	Synapse-associated protein 102
SEM	Standard error of the mean
SYP1	Synaptophysin 1
TNF-α	Tumor necrosis factor-α
TOR	Target of rapamycin
vglut2a	Vesicular glutamate transporter 2a

Chapter 1: Introduction to the E/I Balance and Synaptogenesis

Introduction

Rhythmic motor behaviors, such as breathing, walking and swimming, require coordination between excitatory and inhibitory neurotransmission[3]. During the development of the nervous system, a balance between excitatory and inhibitory neurotransmission (E/I balance) is achieved even as new neurons exit the cell cycle and integrate into the circuit[4]. Disrupting this E/I balance can result in seizures that are a common symptom in human neurodevelopmental disorders, such as autism, startle disease, and glycine encephalopathy[2, 5, 6]. To achieve E/I balance, the formation of excitatory and inhibitory synapses, i.e. the excitatory and inhibitory synaptogenesis, must be carefully regulated[7, 8]. This chapter will review the establishment and maintenance of E/I balance at both the cellular and the systems levels.

Maintenance of E/I Balance in Neural Circuits

In neural circuits, E/I balance is defined as an emergent property of excitatory and inhibitory neurotransmission to ensure functional circuit outputs that produce normal behaviors[9-11]. In a neural circuit, the ratio of excitatory and inhibitory neurotransmissions needs to be maintained around a particular set point level; E/I balance then refers to such a "set point" state.

Instead of being a passively stable set point, E/I balance in the central nervous system (CNS) is dynamically maintained by intrinsic mechanisms. This active maintenance of an E/I balance set point was first observed on individual neurons. For example, in cultured rat cortical neurons, chronic blockade of neuronal activity increases the strength of excitatory synapses, whereas blockade of inhibitory neurotransmission decreases the strength of

excitatory synapses[12]. Thus, when the system is perturbed intrinsic mechanisms adjust in a way that would restore firing patterns of the neuron. In a more recent study in cultured cortical neurons, compensatory alterations of synapse number and locations also take place to maintain E/I balance in response to perturbation[13]. Similar phenomena of synaptic changes that compensate for perturbations of E/I balance not only have been repeatedly observed in cultured neurons and brain slices[14-19], but have also been observed in neurons of intact, live animals. For example, at fruit fly (*Drosophila*) neuromuscular junctions (NMJs), E/I balance is maintained by changing pre-synaptic strength of motor neuron axon terminals[20-22]. In mouse cortical neurons in the somatosensory and visual cortices, in response to changes in activity, the number of inhibitory synapses changes compensatorily, and their locations and distributions on dendritic branches change as well[23, 24]. Dendritic dynamics of zebrafish spinal motor neurons also change compensatorily in response to decreased activity[25]. These studies support the idea that neurons possess compensatory mechanisms to maintain the E/I balance.

In addition to neuronal activity set-points, E/I balance is also maintained across neural circuits at the systems level. Several studies in rodents have shown that visual deprivation or dark rearing which decreases cortical activity, leads to increased excitatory synaptic strength across the visual cortex[26-32]. Similar changes in synaptic strength have also been observed in response to manipulation of activity across the zebrafish spinal cord[33]. Furthermore, in the embryonic clawed frog (*Xenopus*) spinal cord, enhancement of activity leads to an increased number of neurons expressing inhibitory neurotransmitters and a decreased number of neurons expressing excitatory neurotransmitters, while suppression of activity results in the opposite[34]. These observations suggest that the compensatory

mechanisms that maintain the E/I balance are not limited at the cellular level, but also function at the systems level[35, 36].

Mechanisms that Maintain E/I Balance

Mechanisms that maintain E/I balance at both the cellular and the systems levels, via synaptic strength, synapse number and positions are diverse, involving multiple cellular mechanisms as well as systems-level processes. These mechanisms lead to alterations in pre- and/or post-synaptic components, thereby maintaining the relative amount of excitatory and inhibitory neurotransmission within the set point range, i.e. E/I balance.

E/I Balance sensors

In E/I balance, many experiments have demonstrated that a set point state is dynamically maintained. Yet, how are perturbations of E/I balance detected by neurons and neural circuits? A previous modeling study has shown that the detection of changes in E/I balance requires multiple sensors[37]. At the cellular level, such detection can happen in a cell-autonomous manner via calcium-dependent signaling[15, 18, 22]. The activity of calcium/calmodulin-dependent protein kinase kinase (CaMKK) and calcium/calmodulin-dependent protein kinase type IV (CaMKIV) are required for compensatory changes of synaptic strength[18, 22]. Eukaryotic elongation factor 2 (eEF2) has also been implicated as a sensor in cultured hippocampal neurons, since it has been shown to detect disruptions in excitatory glutamatergic transmission[38, 39]. On a larger scale at the systems level, an important candidate sensor is target of rapamycin (TOR)-dependent signaling. TOR-dependent signaling is used in many systems for detecting environmental changes and regulating physiological homeostasis and growth of the organism[40]. Some recent studies

have shown that TOR-dependent signaling is also required for E/I balance maintenance in cultured mammalian CNS neurons[41] as well as at fruit fly NMJs[42]. These cellular and systems sensors detect deviation from E/I balance set point and trigger downstream compensatory regulation.

Mechanisms changing pre-synaptic neurotransmitter release

One well-studied mechanism that maintains E/I balance is the regulation of pre-synaptic neurotransmitter release. When an action potential is generated in the pre-synaptic neuron and reaches the pre-synaptic axon terminals, influx of Ca^{2+} would occur at the pre-synapses, leading to the release of vesicles filled with excitatory/inhibitory neurotransmitters into the synaptic cleft. These neurotransmitters bind to post-synaptic neurotransmitter receptors, evoking excitatory/inhibitory post-synaptic potentials (EPSPs/IPSPs) and currents (EPSCs/IPSCs) in the post-synaptic cell. Therefore, regulating the amount of pre-synaptic neurotransmitter released, by changing either the releasing frequency, or the amount of neurotransmitter filled in each vesicle, would lead to changes in synaptic strength.

This phenomena was first observed at fruit fly NMJs, where pre-synaptic voltage-gated calcium channel 2.1 (CaV2.1) modulates pre-synaptic calcium flux, which is required for pre-synaptic neurotransmitter release[43]. This modulation of pre-synaptic calcium flux alone is not sufficient to induce compensatory changes to maintain E/I balance. Molecules regulating the readily releasable pool (RRP) of pre-synaptic neurotransmitter vesicles, including Rab3, Rab3-GAP, Rab3 interacting molecule (RIM) and major histocompatibility complex class I (MHCI) are also required in compensatory regulations

of pre-synaptic neurotransmitter release[44-47]. In mammalian CNS, similar mechanisms are at work. Pre-synaptic cyclin-dependent kinase 5 (Cdk5) modulates calcium influx via CaV2.2 channels in a calcineurin-A dependent manner, which also leads to altered access to the RRP of pre-synaptic neurotransmitter vesicles.

Pre-synaptic neurotransmitter release is also regulated by extracellular signaling. At fruit fly NMJs, bone morphogenetic protein (BMP)-dependent transcription plays an important role in maintaining neural activity in the set point range[22]. In cultured mammalian cortical neurons, brain-derived neurotrophic factor (BDNF) signaling is critical for compensatory pre-synaptic changes[48]. Tumor necrosis factor-α (TNF-α) is also required for long-term changes compensatory to E/I balance perturbations, and may serve as a permissive signal to keep synapses in a state amenable to compensatory changes for E/I balance maintenance[49].

Given the nature of regulating pre-synaptic neurotransmitters, this mechanism only affects synaptic transmission, rather than synapse number or location. This regulation impacts both cellular and systems-level E/I balance.

Mechanisms regulating post-synaptic components

Regulation of post-synaptic components is the best-studied mechanism underlying the maintenance of E/I balance. The major process for the post-synaptic mechanisms is the modulation of the abundance of post-synaptic neurotransmitter receptors. Such modulation is termed "synaptic scaling"[12], which also involves multiple cellular and systems-level mechanisms.

On the cellular level, the induction of synaptic scaling can be achieved by four different processes: 1) transcriptional regulation of the expression of neurotransmitter receptors, 2) degradation of neurotransmitter receptors, and 3) surface delivery and 4) clustering of neurotransmitter receptors at post-synapses. The expression of neurotransmitter receptors can be regulated by immediate early genes, such as Homer 1a[50], polo-like kinase 2 (Plk2)[51-54], Arc[55, 56] and Narp[57]. Some other proteins, such as methyl CpG binding protein 2 (MeCP2) and neuronal PAS domain protein 4 (Npas4), also play an important role in compensatory synaptic scaling[58-61]. While most of these proteins underlie alterations in synaptic strength, Plk2 also plays a role in regulating the number of synapses[51, 54]; and Npas4 specifically regulates the number and distribution of inhibitory synapses[61].

The abundance of neurotransmitter receptors are also regulated by active protein degradation via the ubiquitin-proteasome system[62-64]. Chronic inhibition of proteasome function has been shown to block compensatory synaptic downscaling[64].

After neurotransmitter receptors are expressed and transported to the post-synapses, they also need to be clustered and anchored at the post-synapses to properly function. To cluster neurotransmitter receptors, post-synaptic proteins that hold receptors in place by interacting with other scaffolding proteins, cytoskeleton, and extracellular matrix are required. Thus, these post-synaptic proteins, including post-synaptic density 95 (PSD-95)[65-67], post-synaptic density 93 (PSD-93)[67], synapse-associated protein 102 (SAP102)[67], gephyrin[68, 69], PICK1[70] and neuroligins[65, 66, 68, 71, 72], also play significant roles in synaptic scaling. Overexpression or knocking-down of these proteins would not only change the abundance of post-synaptic neurotransmitter receptors, leading to altered synaptic strength,

but also impact the number and locations of excitatory and inhibitory synapses[61, 65, 66, 68, 69, 71, 72].

The abundance of neurotransmitter receptors at post-synapses is also regulated in a rapid manner by receptor internalization and lateral diffusing. At excitatory glutamatergic post-synapses, both α-amino-3-hydroxy-5-methyl-4-isoxazolepropionic acid (AMPA) receptors and N-methyl-D-aspartate (NMDA) receptors can be actively internalized during compensatory synaptic downscaling[18, 73-76]. Receptor internalization has not been reported at inhibitory post-synapses. Yet, a previous study has demonstrated that in response to manipulated neural activity, glycine receptors can diffuse laterally from the post-synaptic membrane to the non-synaptic regions of the cellular membrane, or *visa versa*, to compensatorily regulate the synaptic strength of inhibitory glycinergic synapses[19].

Systems-level signaling pathways also play a crucial role in synaptic scaling. For example, BMP, BDNF and TNF-α signaling have all been shown to contribute to the post-synaptic synaptic scaling[22, 49, 77-81]. Multiple studies have also revealed roles of other signals in synaptic scaling, including Beta3-integrins[82] and retinoic acid[83, 84]. Therefore, at post-synapses, cellular and system-level mechanisms work together to maintain E/I balance by regulating synaptic strength and synapse number and locations.

E/I Balance Maintenance and Synaptogenesis

Many mechanisms involved in the maintenance of E/I balance also contribute to synaptogenesis; therefore, these molecules and signaling pathways do not only modulate synaptic strength, but also regulate both how many and where excitatory and/or inhibitory synapses form. Similar mechanisms act at different stages of synaptogenesis, from the initial specification to stabilization, and to later activity-dependent synaptic development.

Some proteins that maintain E/I balance play a critical role in the specification of synapses. MeCP2 and Npas4 are two best-studied examples. MeCP2 knockout neurons exhibit a 40% reduction in excitatory synapse numbers[85]. Knocking down Npas4 leads to 50% reduction in inhibitory synapse number, whereas overexpression of Npas4 doubles inhibitory synapse number[86]. The cell adhesion molecules, neuroligins, are also vital for synapse specification. They bind to pre-synaptic molecule nerexin; this interaction is critical for synaptogenesis. In fruit flies, mutations in neuroligin 1 decreases synaptic growth[87]. In mammalian CNS neurons, overexpression of neuroligin 1, 2 or 3 would increase synapse numbers[65, 71, 88], while neuroligin 2 overexpression specifically increases inhibitory synapse numbers[88]. Knocking down neuroligin 1, 2 or 3 would lead to reduction of excitatory synapse numbers[71]. *In vivo* knockout of neuroligin 1-3 in mice does not alter synapse numbers, but neurotransmission of both excitatory and inhibitory synapses fail, leading to a reduction of numbers of functional synapses[89]. Therefore, mechanisms found at the level of isolated neurons may not hold in the live animals. The *in vivo* determination of synapse numbers is still being discovered.

Post-synaptic scaffolding proteins like PSD-95 and gephyrin, stabilize newly formed synapses[90]. PSD-95 is the major scaffolding protein at excitatory post-synapses; in cultured mammalian CNS neurons, its overexpression reduces the number of inhibitory synapses, while its knockdown leads to reduction of excitatory synapse numbers and increase of inhibitory synapse numbers[65]. On the other hand, gephyrin is the major scaffolding protein at inhibitory post-synapses; its overexpression increases inhibitory synapse number, and its knockdown decreases inhibitory synapse number[69]. Actually, the maintenance of newly formed synapses by these post-synaptic scaffolding proteins also stabilizes axonal or

dendritic filopodia; these filopodia then extend from the synapse formation site to form stable axonal or dendritic branches. The branches without synapse formation are found to be transient, which cannot be stabilized and mature, and will be retracted shortly[90-92]. Therefore, post-synaptic scaffolding proteins are critical for the stabilization of synapses as well as the formation of axonal and dendritic branches.

Once a synapse is formed, secreted signaling molecules that mediate E/I balance maintenance, such as BMP, BDNF and TNF-α, are also important in the development and maturation of synapses. BMP signaling activates downstream regulations of actin cytoskeleton, which is important for the growth of post-synaptic terminals[22, 93]. BDNF signaling has been associated to the maturation of inhibitory synapses in mammalian CNS[94]. TNF-α level plays a role in regulating synapse loss[95, 96]. These secreted signals usually form a local gradient, so as to globally regulate synapse formation[97].

Both cellular and global E/I balance maintenance mechanisms play essential roles in synaptogenesis, and thereby largely influence the number and locations of excitatory and inhibitory synapses. A recent study found that the relative distribution of excitatory and inhibitory synapses impacts E/I balance[98]. This indicates that the pattern of synaptogenesis and E/I balance can largely influence each other. Yet, how perturbations of E/I balance affect the pattern of synaptogenesis is not well understood.

Hypothesis

I hypothesize that well-maintained E/I balance is associated with a stable pattern of excitatory and inhibitory synaptogenesis. In Chapter 2, I tested the hypothesis that a stable pattern of relative distribution of excitatory and inhibitory synapses exist at the systems level as E/I balance is maintained during circuit development. I also hypothesized that the

pattern of synaptogenesis changes in association with re-establishment of E/I balance after genetic perturbation in Chapter 3. Finally, I tested the hypothesis that perturbation of E/I balance would disrupt the process of synaptogenesis, which is described in Chapter 4.

Chapter 2: Systems-Level Pattern of Excitatory and Inhibitory Synapses in Developing Zebrafish Spinal Cord Circuit

The data presented in this chapter has been submitted to *Journal of Comparative Neurobiology* in January, 2016. I designed and conducted all the experiments, and performed all the Matlab image processing and data analysis. The Ripley's L-function analysis was a collaboration with another graduate student, Bo Zhang, with advice from Dr. Don DeAngelis. Statistical tests in this chapter was a collaboration with another graduate student, Lu Zhai. Zebrafish care and husbandry was provided by Ricardo Cepeda.

Background

E/I balance is critical for rhythmic motor behaviors, like breathing, walking and swimming, which are generated by the spinal cord circuit[3]. During the development of the spinal circuit, though new neurons are exiting the cell cycle and integrating into the circuit, and new synaptic connections are forming, E/I balance is still maintained throughout this development[4]. Yet, how E/I balance is maintained during such dynamic circuit development is still unclear.

It has been suggested that E/I balance can be impacted by the relative distribution of excitatory and inhibitory synapses[98], which often form distinct territories on post-synaptic dendrites[99, 100]. However, previous studies have focused on dendritic branches of single neurons, while E/I balance is a phenomenon that is observed and maintained not only at the level of individual neurons but also globally at the level of neural circuits[33-36]. Therefore, to further understand E/I balance in the spinal locomotory circuit, we investigate the distributions of excitatory and inhibitory synapses at the systems level.

In the spinal cord, neuronal somas in the medial spinal cord are flanked by lateral neuropils that are enriched in both excitatory and inhibitory synapses[101]. While neuron types in the spinal circuit are well characterized, the organization of the spinal neuropil remains largely uncharted. Although the zebrafish spinal neuropil lacks the obvious layering reported in the optic tectum neuropil[102], previous studies have shown a function-related medial-lateral (M-L) organization of interneuron processes[103-105]. Here, we set out to map synapses in the zebrafish spinal neuropil to provide insights into how the arrangement of excitatory and inhibitory synapses associates with the functionally relevant M-L axis of the neuropil.

The zebrafish (*Danio rerio*) spinal circuit has some unique characteristics that lend themselves to the study of how excitatory and inhibitory synapses are spatially distributed. This circuit consists of a similar variety of neuron types as that of mammals but has fewer cells per type[3], simplifying analysis. Furthermore, zebrafish embryos and larvae perform stereotyped rhythmic motor behaviors, which can be used as direct readouts for E/I balance[4]. To test whether excitatory and inhibitory synapses form different territories at the systems level, we quantified synapse distributions in the zebrafish spinal neuropil at two qualitatively different developmental stages: 48 hours post-fertilization (hpf), a late embryonic stage characterized by rapid neurogenesis, synaptogenesis and simple behaviors, and 120 hpf, a larval stage when most neurons are integrated into motor circuits supporting a larger repertoire of rhythmic motor behaviors[106, 107]. To visualize excitatory and inhibitory synapses, we used two antibodies against specific post-synaptic scaffolding proteins commonly used as proxies for stabilized synapses: anti-PSD-95 for excitatory synapses and anti-gephyrin for inhibitory synapses[90, 91, 108]. We adopted a statistical

program from plant ecology to quantify spatial distributions of excitatory and inhibitory synapses across the neuropil[109, 110]. In addition to analyzing the distributions of excitatory and inhibitory synapses, we also analyzed glutamatergic and glycinergic neuronal processes along the M-L axis of the spinal cord. To understand how this M-L pattern is associated with the growth of lateral extending post-synaptic neuronal dendrites in the neuropil, we tracked dendritic morphology of caudal primary motor neurons during development. Such an analytic strategy allowed us to elucidate the distributions of excitatory and inhibitory synapses/processes, and to understand how motor neuron dendrites grow into this systems-level structure as they achieve an expanded behavioral repertoire.

Materials and Methods

Fish care and embryo rearing

Experiments were conducted on offspring from *Danio rerio* wild-type (WT) strains AB, Tubingen, and BWT (a fish store strain from Long Island) as well as transgenic lines *Tg(vglut2a:dsred)* and *Tg(glyt2:gfp)*[107, 111, 112]. Zebrafish were maintained on a 14-hour light and 10-hour dark cycle at 28.5 °C and fed twice daily. Fertilized eggs were obtained by natural crossing after removing a divider at first light. Embryos were raised in glass petri dishes with system water (water that houses the adult fish) at 28.5 °C in an incubator with the same light/dark cycle, and staged according to Kimmel, 1995[113]. Zebrafish embryos and larvae were collected between 24 and 120 hpf. All animal protocols were approved by the Institutional Animal Care and Use Committee of University of Miami.

Antibody characterization

A PSD-95 antibody (clone 6G6-1C9, mouse IgG 2a, EMD Millipore Corporation, Billerica, MA) was used to label excitatory post-synapses[114]. This antibody does not work in Western blot with zebrafish protein samples (our unpublished data). Therefore, to test the utility of this antibody for immunohistochemistry, we overexpressed zebrafish PSD-95-EGFP fusion protein[90], and showed that the PSD-95 antibody can recognize overexpressed PSD-95-EGFP (Figure 2.1A). To confirm specificity of staining with the

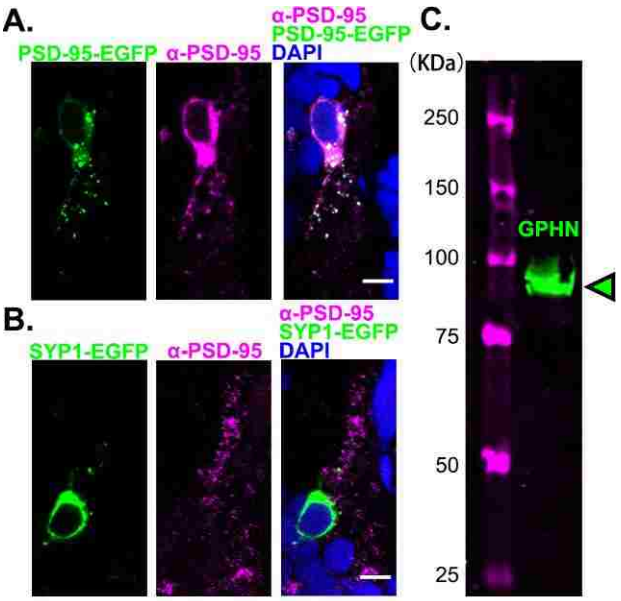

PSD-95 antibody, a zebrafish pre-synaptic protein synaptophysin 1 (SYP1) fused with EGFP[91] was overexpressed and was shown not to colocalize with PSD-95 antibody staining (Figure 2.1B), indicating that the PSD-95 antibody can specifically label zebrafish PSD-95 at post-synapses.

A gephyrin antibody (clone mAb4a, mouse IgG1, Synaptic Systems, Göttingen, Germany) was used to label inhibitory post-synapses. The specificity of this gephyrin antibody in zebrafish was verified with Western blot, yielding a single band of the expected size of ~93 kilodalton (Figure 2.1C). This antibody has been used in a previous study for labeling inhibitory synapses in zebrafish and revealed a punctate pattern representing individual inhibitory post-synapses that were shown to colocalize with the glycine receptor[115].

Immunohistochemistry of post-synaptic scaffolding proteins

Cryosectioning and antibody staining of WT zebrafish embryos at 48 hpf and larvae at 120 hpf were performed as previously described[116]. Briefly, anesthetized zebrafish embryos or larvae were embedded in O.C.T. compound (Tissue-Tek, Sakura, Torrance, CA) and gradually frozen in liquid nitrogen. 30 μm-thick transverse sections from the middle of fish trunk (within 5 segments of the anus) were then collected on a cryostat (CM-1850, Leica, Wetzlar, Germany) at -25 ℃ and mounted on poly L-lysine coated slides (Newcomer Supply, Middleton, WI) prior to a 10-minute fixation in 4% formaldehyde (diluted from 16%, Pierce, Thermo Fisher Scientific, Rockford, IL). Sections were immunostained with anti-PSD-95 (mouse IgG2a, 1: 500) and anti-gephyrin (mouse IgG1, 1: 500). Staining was carried out using the Sequenza slide staining system (Thermo Fisher

Scientific). Alexa 568-conjugated goat anti-mouse IgG2a (1:2000, Molecular Probes, Thermo Fisher Scientific) and Alexa 488-conjugated goat anti-mouse IgG1 (1:2000, Molecular Probes) were used as secondary antibodies. Stained sections were mounted in Vectashield/DAPI (Vector Laboratories, Burlingame, CA). Images were captured on a confocal microscope (TCS SP5, Leica) using a 1.4 NA 63× oil objective (Leica). Images were acquired at 0.08 × 0.08 × 0.4 μm voxel size.

Identification and counting of synapses

Confocal images were processed using Image J (NIH). To avoid the impact of variation along the anterior-posterior axis, we analyzed PSD-95 and gephyrin puncta in three images (one each near the top, the middle, and the bottom of the stack) from a representative z-stack in each fish. Measurements from these three images were averaged and these averaged values were then used to calculate the mean and the standard error of the mean (SEM) for a given sample and to conduct statistical tests between samples. Image brightness and contrast were adjusted to maximize visibility of synaptic puncta and reduce background noise before using a customized Matlab (Math Works, Natick, MA) program to identify, localize and count PSD-95 and gephyrin puncta as described in previous studies [115, 117, 118]. Briefly, the Matlab program first thresholded the image iteratively by sampling every other gray value between 0 and 255, identifying local peaks in intensity. Each peak represented the center of a punctum. Only puncta with diameters ranging from 0.15 to 2 μm were counted. Adjacent puncta were separated according to the positions of their peaks. Then, all possible puncta were filtered according to their peak intensity, average intensity, size and internal contrast (the difference between the highest and lowest intensities within

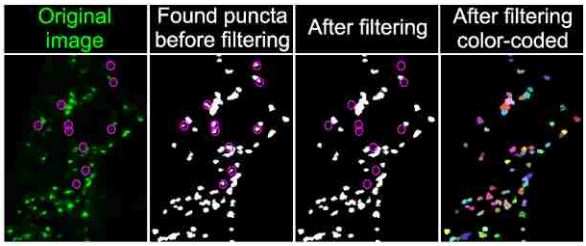

[redacted]

a given punctum, which becomes more stringent as its filtering value increases). The filtering criteria were adjusted for each image by comparing the filtered puncta to the original image to optimally separate the actual puncta and false-positive selections (Figure 2.2). The final outputs of this Matlab program provided the total numbers of PSD-95 and gephyrin puncta in each image as well as the spatial coordinates of each punctum in the image.

The total puncta number was defined as the number of all the given type of puncta in one transverse-section view of the spinal cord. To calculate puncta density, we measured the area of puncta type-specific background staining in Image J. The puncta density was defined as the total puncta number divided by this area in a transverse-section.

Analysis of synapse distribution patterns in the spinal neuropil

To determine the distribution of excitatory and inhibitory synapses in the neuropil, we conducted the Ripley's L-function statistics in Programita software[109, 110]. This spatial statistic quantifies the distribution of points in space, and classifies the given distribution as either clumped/clustered, random or regular/dispersed. The Ripley's L-function results

were represented in L-function curves. Figure 2.3 provides examples for L-function curves generated from Matlab-generated different dot distributions.

In our L-function analysis, the location of each synapse was provided by the output of our puncta-finding Matlab program; a single image from the middle of each z-stack was used for the L-function analysis. To define the boundary of the spinal neuropil, we wrote a Matlab script to draw boundaries around the irregularly shaped neuropil regions. Since Programita could only analyze a single study area with specified boundary each time, in each image, only one side (left or right) of the spinal neuropil was randomly picked for the analysis. Data of all the fish at the same stage were treated as repeated trials to generate separate PSD-95 and gephyrin L-function curves.

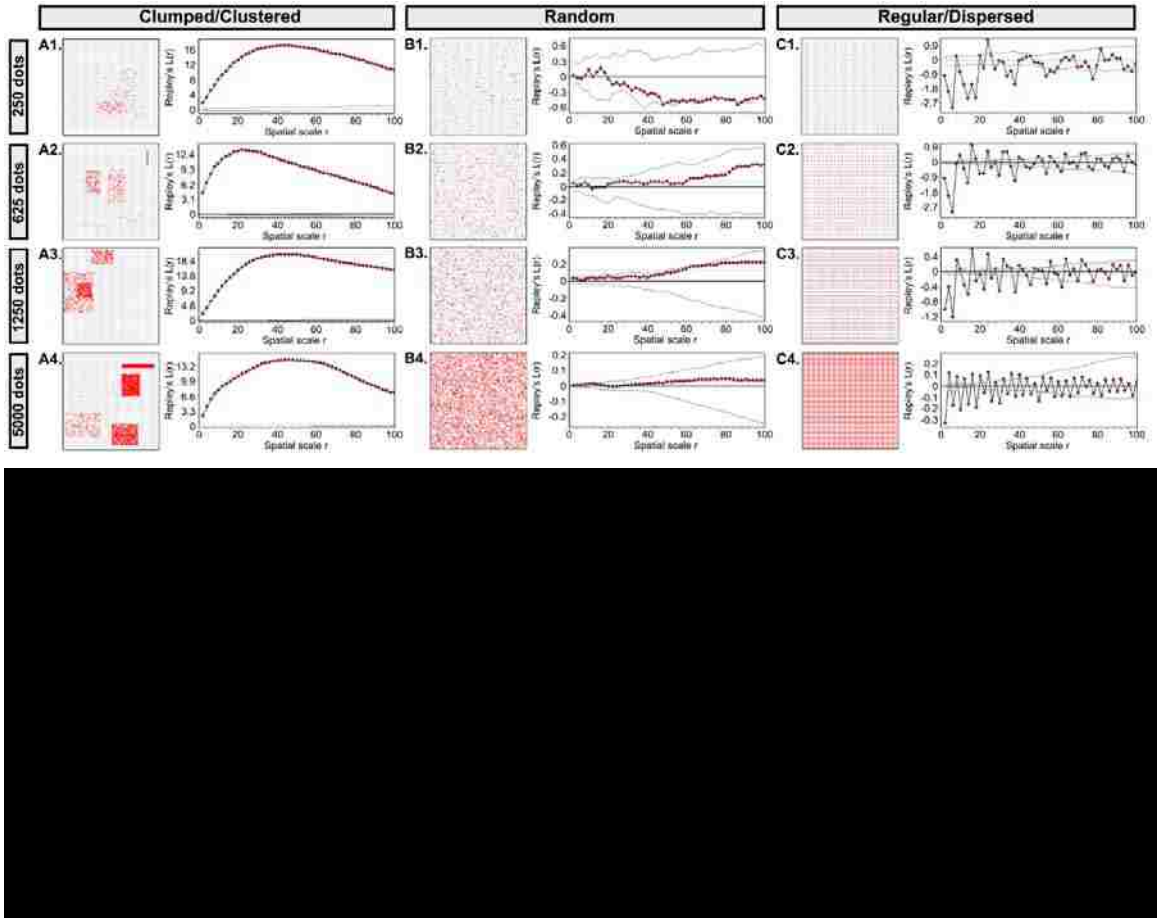

During the L-function analysis, the univariate spatial pattern (clumped/random/regular) of puncta was analyzed using Ripley's K(r) function. The K(r) function was defined as the expected number of puncta within distance r from a randomly chosen point. Under complete spatial randomness, $K(r) = \pi r^2$, which is the area of a circle with radius r. L(r) was defined as $\sqrt{(K(r)/\pi) - r}$; the expected value of L(r) was zero under the null hypothesis of complete spatial randomness for the given distribution of puncta. To account for random variations, 95% confidence envelopes were generated for expected L(r) values under the null hypothesis. These confidence envelopes were obtained from 500 simulations using a random arrangement of puncta and random translation, i.e. changing positions of puncta randomly in simulations. When the observed L(r) values were larger or smaller than the confidence envelopes of the expected L(r), the spatial patterns (clumped/clustered or regular/dispersed, respectively) of the puncta were statistically significant at distance r. Since distance r represented the radius of sampling circles in the analysis, we set our maximum scale as 40 μm, about half the height of spinal cord transverse sections.

To determine the distribution of excitatory and inhibitory synapses relative to one another, we also conducted bivariate L-function analysis with the coordinates of both PSD-95 and gephyrin puncta. This bivariate pattern analysis quantified how one type of punctum was distributed relative to each focal punctum of the other type to examine whether the two puncta types occur on average more or less frequently as near neighbors than expected if they were randomly distributed. The bivariate K function $K_{EI}(r)$ is defined as the expected number of one type of punctum (gephyrin, referred as Pattern I) within a given distance r of an arbitrary punctum of the other type (PSD-95, referred as Pattern E), divided by λ_I, the density of Pattern I puncta: $\lambda_I K_{EI}(r) = E[\#(\text{points of Pattern I} \leq$

r from an arbitrary punctum of Pattern E)] ; E[] is the expectation operator and # represents "the number of". Under independence of the two puncta patterns, $K_{EI}(r) = \pi r^2$, regardless of the individual univariate patterns. The L-function for bivariate analysis was defined as $L_{EI}(r) = \sqrt{(K_{EI}(r)/\pi) - r}$. A 95% confidence envelopes of the $L_{EI}(r)$ functions were calculated from 500 simulations of the null model of complete spatial randomness, which assumed independence between puncta Patterns E and I. $L_{EI}(r)$ values larger than the confidence envelope indicated that there were on average significantly more Pattern I gephyrin puncta within distance r of Pattern E PSD-95 puncta than expected under independence (positive correlation). Similarly, $L_{EI}(r)$ values smaller than the confidence envelope indicated on average significantly less Pattern I gephyrin puncta than expected within distance r of Pattern E PSD-95 puncta (negative correlation).

Analysis of synapse distributions along the M-L axis

To quantify the M-L distribution of excitatory and inhibitory synapses, we wrote a Matlab program to identify the midpoints between the most lateral and the most medial puncta along the dorsal-ventral axis in each neuropil region. By connecting these midpoints together, we generated a midline to bisect each neuropil region. In this way, we could calculate the numbers of PSD-95 and gephyrin puncta located in each half to calculate the proportions of excitatory and inhibitory synapses in the lateral half of the neuropil.

To capture M-L distribution patterns independent of an outlined neuropil, we wrote a Matlab script to divide the spinal cord into 100 bins along the horizontal axis, allowing us to calculate the M-L frequencies of PSD-95 and gephyrin puncta. For each image, the data from the left and right halves (50 bins/hemi-spinal cord) were pooled together for analyses

of the frequency distribution of PSD-95 and gephyrin puncta from the most medial (0%) to the most lateral (50%) spinal cord.

Retrograde labeling of caudal primary motor neurons

To label caudal primary (CaP) motor neurons, 24-96 hpf WT embryos and larvae were anesthetized in 0.001% 3-aminobenzoic acid ethyl ester (MS222, Sigma-Aldrich, St. Louis, MO), transferred to a room-temperature slanted agarose plate (1.2% agarose (Promega, Madison, WI) in system water), and injected in ventral musculature in anal segments with a 25% solution of 10,000 molecular weight Texas Red dextran (Molecular Probes, Life Technologies, Grand Island, NY) in 10% Hanks' buffer (GIBCO, Thermo Fisher Scientific) as previously described[119]. Injected zebrafish were then transferred to system water to recover and to allow retrograde transport of the dextran dye to fill the entire motor neuron for about 24 hours before fixation, sectioning and imaging.

Tracing CaP motor neuron dendritic arbors

Images of Texas Red dextran-labeled CaP motor neurons were processed using Image J. The brightness and contrast were adjusted to maximize visibility of dendritic branches and reduce background noise. Tracing and reconstruction of dendritic arbors were done in Neuromantic (version 1.7.5; http://www.rdg.ac.uk/neuromantic/). Since labeled motor neuron dendrites are continuous three-dimensional structures, they could be easily distinguished from speckled background staining in z-stack images. The lateral distance of CaP motor neuron dendrites was defined as the horizontal distance between the lateral boundary of the soma and the most lateral tip of the dendritic arbor in the traverse section.

We also measured the average width of one neuropil region (there are two neuropil regions in each spinal cord transverse section) at each stage; to increase the sample size, we measured the width of the neuropil in sections with successfully labeled motor neurons as well as in sections without labeled neurons.

Cryosectioning and imaging of fish with labeled interneurons or motor neurons

Embryos and larvae from *Tg(vglut2a:dsred)/Tg(glyt2:gfp)* transgenic lines were collected at 48 and 120 hpf, respectively. Dextran-injected WT embryos and larvae were collected 24 hours after the injection. Collected zebrafish embryos and larvae were anesthetized in 0.001% MS222 prior to fixation with 4% formaldehyde for 24 hours at 4 ℃, and followed by overnight incubation in 30% sucrose solution at 4 ℃. Embryos and larvae were then embedded in tissue freezing medium (TFS, Durham, NC) and frozen at -20 ℃ in the cryostat. 30 μm-thick transverse sections from the middle of fish trunk (within 5 segments of the anus) were collected at -20 ℃ and mounted on poly L-lysine coated slides. Sections were then washed with 1× phosphate buffered saline (1× PBS, diluted from 10× PBS, Cellgro, Corning, Manassas, VA) with 0.4% Trition-X (Avantor, Center Valley, PA) in the Sequenza slide staining system before mounting in Vectashield/DAPI. Images were acquired at 0.08 × 0.08 × 0.4 μm voxel size on the confocal microscope using the 1.4 NA 63× oil objective.

Analysis for the M-L territories of neuronal processes in the neuropil

Images of *Tg(vglut2a:dsred;glyt2:gfp)* transverse spinal cord sections were processed in Image J. The brightness and contrast were adjusted to maximize visibility of neuronal

processes and reduce background noise. For analysis, the section with the best signal-to-noise ratio for DsRed and GFP in the spinal neuropil was chosen from each z-stack for the analysis. For each of these images, one side of the two spinal neuropil regions (left and right) was chosen randomly for the analysis. To avoid the interference of the fluorescence of neuronal somas, a rectangle that encompassed the widest region of each neuropil was analyzed. The height of the rectangle was 40-60% of the neuropil height, and was adjusted to make sure that neuropil, whose shape was irregular, would occupy no less than 80% (48 hpf) or 90% (120 hpf) of the area in the rectangle. The mean intensities of DsRed and GFP pixels at each M-L position were analyzed in Image J using the "Plot Profile" function. This output was then normalized to a 0-100 relative intensity scale, in which 0 corresponds to the background intensity and 100 corresponds to the maximal intensity. To compare the overall M-L distribution trends of glutamatergic (DsRed) and glycinergic (GFP) processes, we used Matlab to fit curves to the respective fluorescent intensity values of all fish at each stage. At 48 hpf, the DsRed curve adjusted $R^2 = 0.4139$ (the sum of squares due to error (SSE) = 1.322×10^{-5}), and the GFP curve adjusted $R^2 = 0.6021$ (SSE = 9.35×10^{-4}); at 120 hpf, the DsRed curve adjusted $R^2 = 0.7411$ (SSE = 5.14×10^{-4}), and the GFP curve adjusted $R^2 = 0.7555$ (SSE = 8.47×10^{-4}).

Statistics

Statistical tests were conducted in JMP 11 Pro (SAS Institute Inc., Cary, NC). When data satisfied the requirements for independence, normality and homogeneity of variance, they were analyzed by ANOVA. Within the same developmental stage, PSD-95 and gephyrin data were extracted from the same fish. Therefore, to account for variability among

different individuals, the unit "fish" was set as a random blocking variable. The p values for the first-order interaction in two-way ANOVA and the second-order interaction in three-way ANOVA are reported in results unless noted otherwise. When the p values for these interactions were not significant, the significant main effects in two-way ANOVA and the significant first-order effects in three-way ANOVA are also reported in results. Bonferroni correction was applied for *post hoc* student's t-tests. For data that didn't pass tests of normality, the Mann-Whitney U test was used to determine statistical significance. Kolmogorov–Smirnov (KS) tests were conducted to compare cumulative probability distributions.

Results

Excitatory and inhibitory synaptogenesis exhibits distinct developmental dynamics

Using antibodies against excitatory post-synaptic protein PSD-95 and inhibitory post-synaptic protein gephyrin, we mapped the location of individual excitatory and inhibitory synapses in spinal cord transverse sections in 48 hpf embryos and 120 hpf larvae (Figure 2.4A-B). At both stages, excitatory and inhibitory synapses are enriched in the spinal neuropil, lateral to neuronal somas. As development progresses and more synapses are formed, the neuropil region becomes significantly wider (48 hpf 14.31 ± 0.64 % of the spinal cord width, n = 15 fish; 120 hpf 24.07 ± 0.70 % of the spinal cord width, n = 9 fish; Mann-Whitney U test, p = 0.0002; Figure 2.4C).

Using a custom Matlab program to identify each synaptic punctum [115, 117, 118], we determined how the numbers of excitatory and inhibitory synapses change from the embryonic to the larval stage. Our analysis shows distinct developmental dynamics for

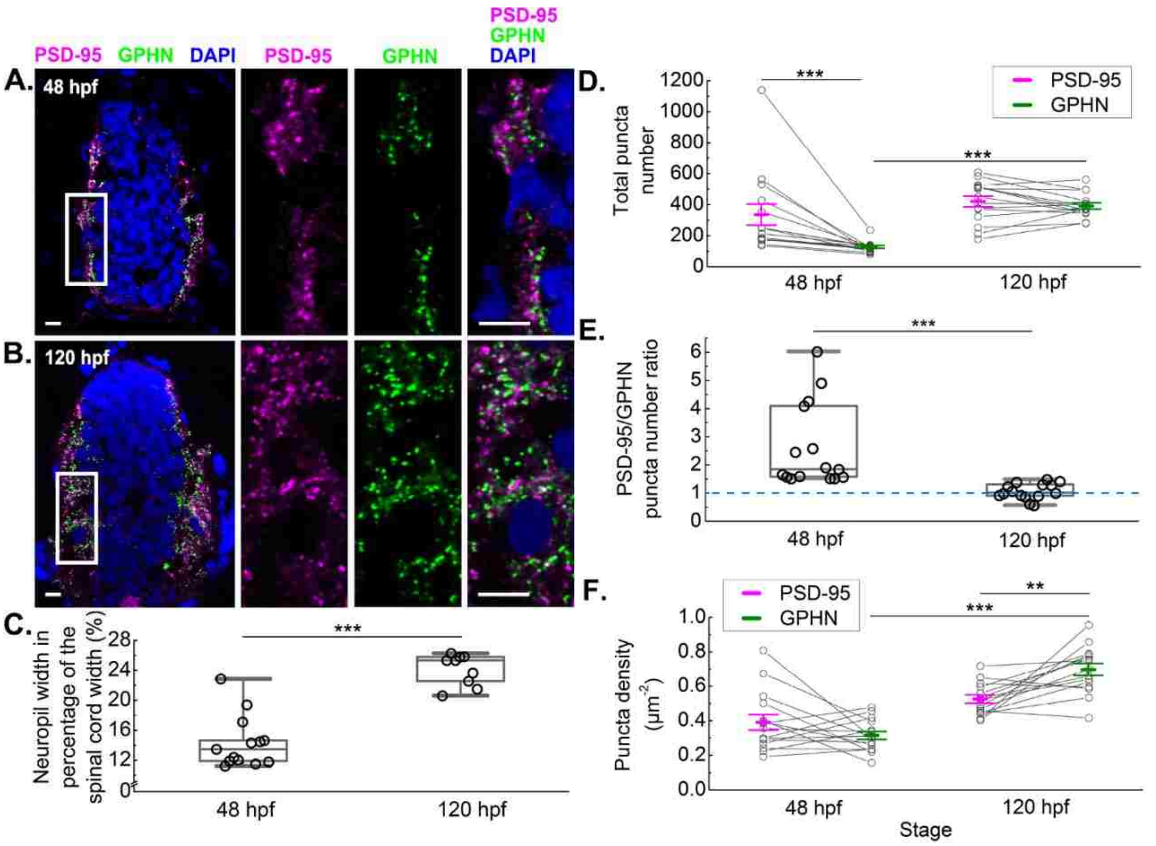
PSD-95 GPHN DAPI
PSD-95
GPHN
PSD-95 GPHN DAPI
A.
48 hpf
B.
120 hpf
C.
Neuropil width in percentage of the spinal cord width (%)
48 hpf
120 hpf
D.
Total puncta number
PSD-95
GPHN
E.
PSD-95/GPHN puncta number ratio
F.
Puncta density (μm-2)
Stage

[redacted]

excitatory and inhibitory synapses (two-way ANOVA, puncta type × stage $F(1, 28) = 7.27$, $p = 0.0117$). While the number of PSD-95 puncta varies between individual fish, the average number does not change significantly with development (48 hpf 336.00 ± 67.26, n = 15 fish; 120 hpf 420.98 ± 34.35, n = 15 fish). By contrast, the number of gephyrin puncta varies less between individual fish and does increase significantly during development (48 hpf 128.47 ± 9.37, n = 15 fish; 120 hpf 391.73 ± 20.05, n = 15 fish; $p < 0.001$). With respect to the excitatory/inhibitory synapse ratio, at 48 hpf, there are significantly more PSD-95 puncta than gephyrin puncta ($p < 0.001$), which is evident in every individual fish examined (Figure 2.4D). Therefore, at 48 hpf, the ratio of PSD-95 to gephyrin puncta number (E/I puncta ratio) is heavily skewed towards excitation, however, by 120 hpf, the E/I puncta ratio declines to nearly 1 (48 hpf 2.61 ± 0.38, n = 15 fish; 120 hpf 1.07 ± 0.07, n = 15 fish; Mann-Whitney U test, $p < 0.0001$; Figure 2.4E). In summary, excitatory synaptogenesis initially outpaces inhibitory synaptogenesis; by 120 hpf, however, inhibitory synapses catch up, resulting in a more equal E/I puncta ratio.

As with numbers of puncta, we also found that the densities of PSD-95 and gephyrin puncta are developmentally dynamic (two-way ANOVA, puncta type × stage $F(1, 56) = 14.15$, $p = 0.0004$). Though there are more PSD-95 puncta than gephyrin puncta at 48 hpf (Figure 2.4D), their densities are similar (PSD-95 0.39 ± 0.04 μm^{-2}, n = 15 fish; gephyrin 0.32 ± 0.02 μm^{-2}, n = 15 fish). While the density of PSD-95 puncta stays constant during development, the density of gephyrin puncta significantly increases from 48 to 120 hpf ($p < 0.001$). At 120 hpf, with similar total numbers (Figure 2.4D), gephyrin puncta exhibit a higher density than PSD-95 puncta (PSD-95 0.53 ± 0.02 μm^{-2}, n = 15 fish; gephyrin 0.70 ± 0.04 μm^{-2}, n = 15 fish; $p < 0.01$; Figure 2.4F). These observations indicate distinct

developmental dynamics for PSD-95 and gephyrin puncta, and that gephyrin puncta are more clumped overall than PSD-95 puncta.

Excitatory and inhibitory synapses exhibit distinct spatial patterns during spinal circuit development

To determine the developmental changes of synapse distributions in the landscape of the neuropil, we analyzed post-synaptic puncta with an analytic method known as Ripley's L-function. This spatial statistic has been widely used in ecology to analyze the distribution of objects in a landscape, and provides powerful point-pattern analysis[109, 110]. Ripley's L-function compares the observed distribution of puncta to a null model of random distribution, and can detect distribution patterns at all scales (r, Figure 2.5A), from the immediate neighborhood to the entire study area[109, 110]. As a result, at any spatial scale, Ripley's L-function can assign puncta distributions to one of three patterns: clumped, random or dispersed (see Materials and Methods; Figure 2.5A and Figure 2.3). With this approach, we found that PSD-95 and gephyrin puncta exhibit distinct spatial patterns. At 48 hpf, PSD-95 puncta are randomly distributed in the spinal neuropil (Figure 2.5B) while gephyrin puncta are clumped (Figure 2.5C). With development, both PSD-95 and gephyrin puncta become more dispersed (Figure 2.5E-F). Interestingly, at both stages, the L-function curves for both puncta types show highly dispersed distributions within a 10 μm scale compared to more random or clumped distributions at larger scales. Such a drop in L-function curves at small scales is typical of point patterns that exhibit regular spacing (Figure 2.3C1-C4). These L-function results at small spatial scales indicate that both

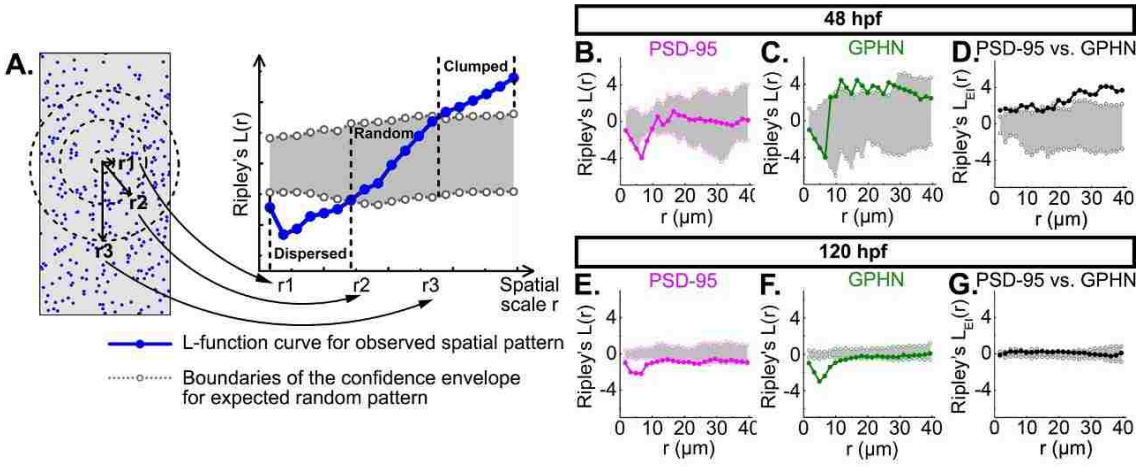

excitatory and inhibitory synapses tend to maintain a certain distance from other synapses of the same type.

We also examined how excitatory and inhibitory synaptic puncta distribute with respect to puncta of the other type (Figure 2.5D and G). In striking contrast to the highly dispersed small-scale pattern seen within puncta type, we no longer see such a dispersed pattern

between puncta types. This relative analysis shows that PSD-95 and gephyrin puncta clump at 48 hpf (Figure 2.5D) and randomly distribute at 120 hpf with respect to each other (Figure 2.5G).

In summary, excitatory and inhibitory synapses exhibit distinct spatial patterns during development. Irrespective of developmental stages, inhibitory synapses tend to be more clumped than excitatory synapses. With development, synapses in general become more dispersed. Furthermore, both excitatory and inhibitory synapses exhibit regular spacing at small spatial scales, within but not between synapse types.

Excitatory and inhibitory synapses are enriched in distinct medial-lateral (M-L) regions in the spinal neuropil

Using a custom Matlab program to divide neuropil regions into medial and lateral halves (see Materials and Methods; Figure 2.6A), we quantified the enrichment of excitatory and inhibitory puncta along the M-L axis. We found a greater portion of PSD-95 puncta than gephyrin puncta in the lateral half of the neuropil at 48 hpf (PSD-95 53.42 ± 1.21 %, n = 15 fish; gephyrin 41.54 ± 2.75 %, n = 15 fish; $p < 0.001$; Figure 2.6B). This pattern of enrichment holds at 120 hpf (PSD-95 58.10 ± 1.08 %, n = 15 fish; gephyrin 46.23 ± 0.88 %, n = 15 fish; $p < 0.001$; two-way ANOVA, puncta type × stage $F(1, 28) = 0.00$, $p = 0.9993$; puncta type $F(1, 28) = 68.89$, $p < 0.0001$; Figure 2.6B). These data indicate that the distinct M-L enrichment of excitatory and inhibitory synapses is established by 48 hpf and sharpened by 120 hpf.

Given the observed M-L enrichment of excitatory and inhibitory synapses, we examined the frequency distributions of PSD-95 and gephyrin puncta along the M-L axis

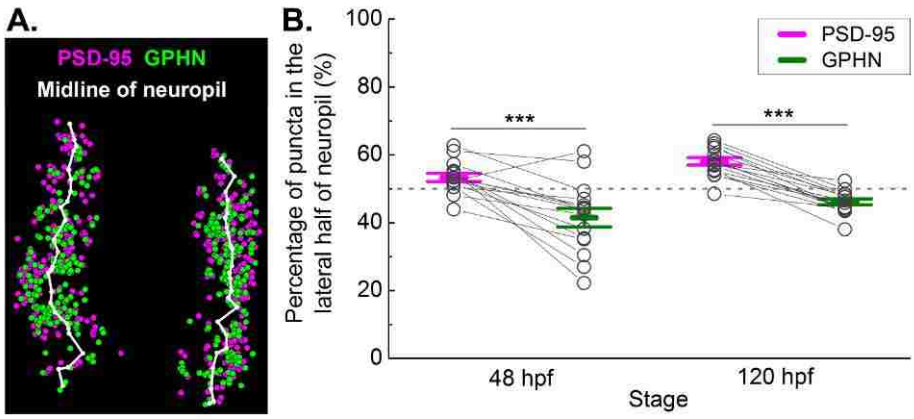

(Figure 2.7A). At 48 hpf, PSD-95 puncta decorate the cell body region in the most medial spinal cord and are enriched in the lateral neuropil, while gephyrin puncta are most abundant in the medial neuropil region adjacent to neuronal somas (Figure 2.7B). The cumulative probability curves show a statistically significant difference between the M-L distributions of PSD-95 and gephyrin puncta at this stage (KS test, $p = 0.0397$; Figure 2.7B). At 120 hpf, both PSD-95 and gephyrin curves are largely excluded from the medial cell body region and enriched in the neuropil (Figure 2.7C).

This developmental difference in M-L distribution is more evident when each hemi-cord is divided into five M-L zones (Zone 1-5) with Zone 1 starting at the midline and Zone 5 ending at the lateral edge of the spinal cord (three-way ANOVA, zone × puncta type × stage $F(4,114) = 10.29$, $p < 0.0001$; Figure 2.7A). At 48 hpf, ~10% of PSD-95 puncta are

Figure 2.7 PSD-95 and gephyrin puncta show distinct medial-lateral distributions and developmental dynamics
(A) M-L distribution analysis. A representative spinal cord section (upper panel) stained for PSD-95 (magenta), gephyrin (GPHN, green), and DAPI-labeled nuclei (blue). The spinal cord midline is defined as 0%, with spinal cord lateral edges defined as 50%. A stylized section (lower panel) shows the division of five medial-lateral (M-L) zones (Zone 1: 0-10%, Zone 2: 11-20%, Zone 3: 21-30%, Zone 4: 31-40%, Zone 5: 41-50%) used in (D)-(I). In (B)-(I), the cyan/blue regions in the background indicate Zones occupied by neuronal somas at 48 (cyan) and 120 hpf (blue). (B-C) M-L distributions of PSD-95 and gephyrin puncta at 48 (B) and 120 hpf (C). Average percentages of PSD-95/total PSD-95 and gephyrin/total gephyrin distributed at 1% intervals along the M-L axis at each stage (48 hpf, n = 10; 120 hpf, n = 15) are graphed. Inserts show the cumulative probability curves. (D-E) Bar graphs compare the percentages of PSD-95 and gephyrin puncta in each zone at 48 (D) and 120 hpf (E). (F-G) Bar graphs compare the numbers of PSD-95 or gephyrin puncta in each zone at 48 (F) and 120 hpf (G). (H-I) Bar graphs compare puncta numbers at 48 and 120 hpf in the five M-L zones for PSD-95 (H) and gephyrin puncta (I). Statistical tests in the inserts in (B)-(C) are KS test. Statistical tests in (D)-(E) and (F)-(I) are three-way ANOVA, followed by *post hoc* Bonferroni corrections. Asterisks indicate statistical significance (* $p \leq 0.05$, ** $p \leq 0.01$, *** $p \leq 0.001$).

found near the midline where gephyrin is largely absent (Zone 1, $p < 0.001$; Table 2.1). Both PSD-95 and gephyrin puncta are most abundant laterally, with gephyrin puncta significantly more enriched in Zone 4 adjacent to neuronal somas ($p < 0.001$; Table 2.1; Figure 2.7D). As the spinal cord develops, the neuropil region makes up a greater proportion of the spinal cord (Figure 2.4C; cyan/blue shading in Figure 2.7B-I), occupying the lateral half of Zone 4 and all of Zone 5 at 48 hpf, and expanding to the most lateral quarter of Zone 3 and all of Zones 4 and 5 at 120 hpf (Figure 2.4C; Figure 2.7D-E). At both 48 and 120 hpf then, gephyrin puncta are more enriched than PSD-95 in zones adjacent to cell bodies (Figure 2.7D-E). PSD-95 puncta, on the other hand, are more enriched in Zone 5 at 120 hpf, which corresponds to the most lateral part of the neuropil ($p< 0.001$; Table 2.1; Figure 2.7E).This developmental change in M-L distributions is also clearly reflected in the absolute numbers of synaptic puncta (three-way ANOVA, stage × enriched in Zone 5 at 120 hpf, which corresponds to the most lateral part of the neuropil

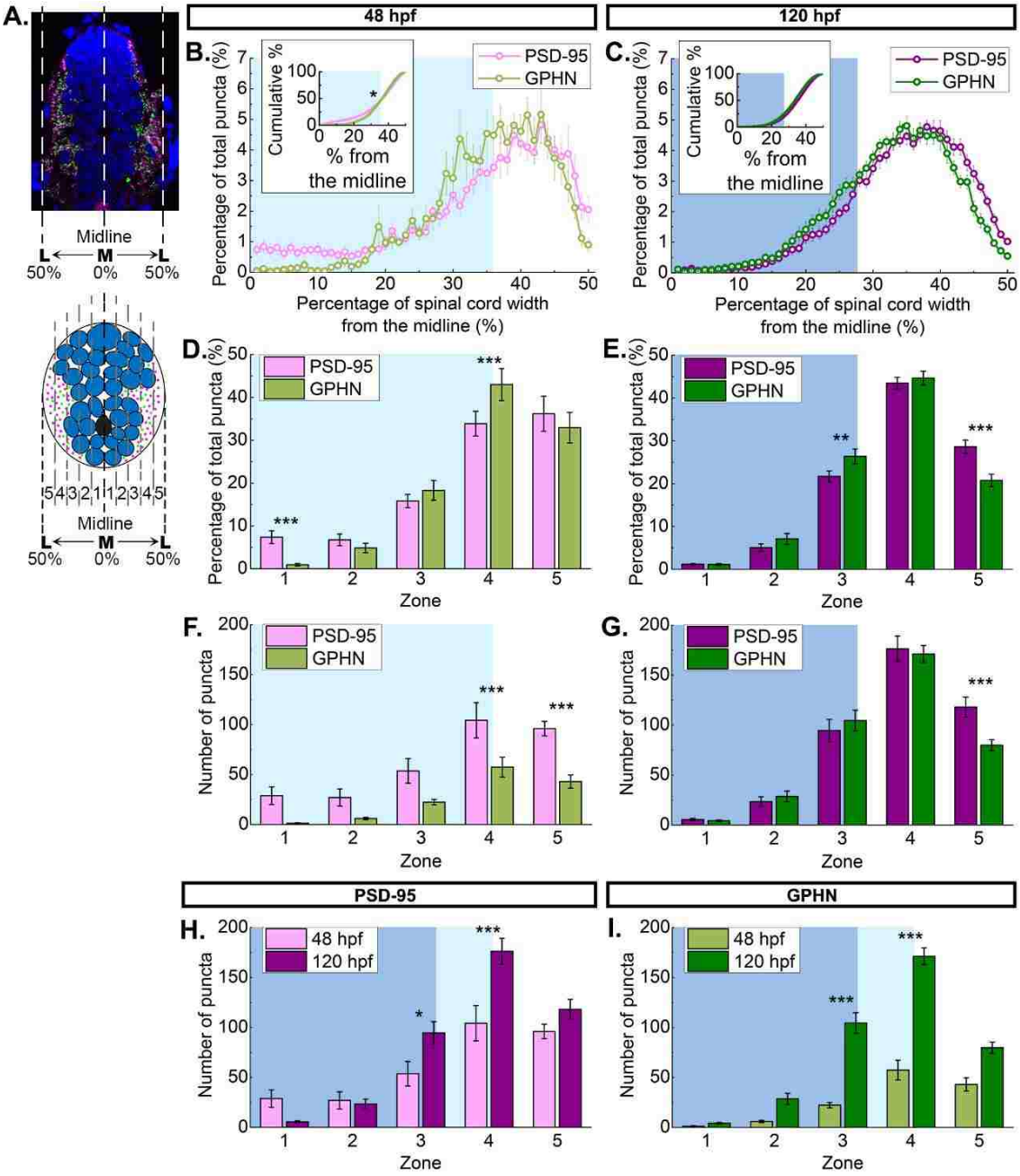

(p< 0.001; Table 2.1; Figure 2.7E).This developmental change in M-L distributions is also clearly reflected in the absolute numbers of synaptic puncta (three-way ANOVA, stage × zone × puncta type $F(4,109) = 1.02$, $p = 0.4028$; stage × zone $F(4, 87) = 24.65$, $p < 0.0001$; zone × puncta type $F(4, 109) = 4.94$, $p = 0.0011$; stage × puncta type $F(1, 109) = 30.29$, $p < 0.0001$; Figure 2.7F-I). At 48 hpf, there are significantly more PSD-95 than gephyrin puncta (Figure 2.4C). This trend is reflected in all zones, though the differences between

Table 2.1 PSD-95 and gephyrin puncta distributions in medial-lateral zones
Numbers show the PSD-95 and gephyrin puncta distributions in the medial-lateral (M-L) zones in Figure 2.7. Zone 1 is the most medial and Zone 5 is the most lateral. Puncta numbers correspond to the data in Figure 2.7F-I. Frequencies correspond to the data in Figure 2.7D-E. Numbers are means +/- SEM. 48 hpf n = 10 fish, 120 hpf n = 15 fish.

Data type	Stage	Puncta type	M-L zones				
			Zone 1	Zone 2	Zone 3	Zone 4	Zone 5
Puncta number	48 hpf	PSD-95	28.83 ± 8.79	27.01 ± 8.55	53.65 ± 12.28	104.22 ± 17.64	95.97 ± 7.21
		Gephyrin	1.21 ± 0.46	5.95 ± 1.13	22.32 ± 2.69	57.40 ± 9.93	42.97 ± 6.64
	120 hpf	PSD-95	5.51 ± 1.05	22.39 ± 4.83	94.51 ± 11.25	176.23 ± 12.90	118.02 ± 10.07
		Gephyrin	4.29 ± 0.71	28.59 ± 5.44	104.59 ± 10.26	171.24 ± 8.42	79.84 ± 5.54
Frequency	48 hpf	PSD-95	7.36 ± 1.49 %	6.75 ± 1.37 %	15.82 ± 1.55 %	33.88 ± 2.88 %	36.19 ± 4.10 %
		Gephyrin	0.93 ± 0.32 %	4.83 ± 1.10 %	18.30 ± 2.30 %	42.99 ± 3.73 %	32.95 ± 3.56 %
	120 hpf	PSD-95	1.18 ± 0.18 %	5.07 ± 0.88 %	21.68 ± 1.29 %	43.46 ± 1.37 %	28.61 ± 1.57 %
		Gephyrin	1.13 ± 0.19 %	7.11 ± 1.26 %	26.37 ± 1.74 %	44.64 ± 1.61 %	20.76 ± 1.45 %

PSD-95 and gephyrin puncta numbers are only statistically significant in the neuropil region ($p < 0.001$ for both Zones 4 and 5; Table 2.2; Figure 2.7F). At 120 hpf, when the numbers of PSD-95 and gephyrin puncta become more evenly matched (Figure 2.4C), there are still significantly more PSD-95 puncta than gephyrin puncta in Zone 5 ($p < 0.001$; Table 2.1; Figure 2.7G). Therefore, though the overall E/I puncta ratio is about 1 at this stage, the E/I puncta ratio in Zone 5 is skewed towards excitation.

To assess developmental dynamics of PSD-95 and gephyrin puncta along the M-L axis, we compared each puncta type across 48 and 120 hpf. Zones 3 and 4 exhibit significant developmental increases in puncta numbers for both PSD-95 and gephyrin (Zone 3 PSD-95 $p < 0.05$; Zone 4 PSD-95 $p < 0.001$; Zone 3 gephyrin $p < 0.001$; Zone 4 gephyrin $p < 0.001$; Table 2.1). None-the-less, while PSD-95 puncta numbers decrease medially in Zone 1 and increase laterally in Zones 3 and 4 (Table 2.1; Figure 2.7H), gephyrin puncta numbers increase across all zones (Table 2.1; Figure 2.7I).

These results show that excitatory and inhibitory synapses are enriched in distinct M-L zones by the late embryonic stage. Such M-L enrichment is sharpened at the larval stage with distinct developmental dynamics for excitatory and inhibitory synapses, and a stable enrichment of excitatory synapses in the most lateral neuropil.

Enrichment of excitatory and inhibitory neuronal processes matches the M-L enrichment of post-synaptic puncta

To test whether excitatory and inhibitory neuronal processes also show differential enrichment along the M-L axis, we quantified M-L neuropil territories occupied by glutamatergic and glycinergic neuronal processes. To do this, we used a zebrafish *vglut2a:dsred;glyt2:gfp* double transgenic line, in which all glutamatergic neurons express DsRed and all glycinergic neurons express GFP[107, 111, 112]. In the spinal cord, glutamate and glycine are the major excitatory and inhibitory neurotransmitters, respectively; thus, most excitatory and inhibitory neuronal processes are labeled, enabling the analysis for their respective neuropil territories.

We find that at both 48 and 120 hpf, glutamatergic and glycinergic neuronal processes exhibit similar M-L enrichment as excitatory and inhibitory post-synaptic puncta: the glycinergic processes are enriched in the medial neuropil and the glutamatergic processes are enriched in the lateral neuropil (Figure 2.8). To quantify this spatial pattern, we analyzed the mean intensity of vglut2a:DsRed and glyt2:GFP in the neuropil. At both 48 and 120 hpf, the peaks of GFP and DsRed intensities are located in the medial and lateral neuropil, respectively. At 48 hpf, since the neuropil is still narrow and the spinal cord circuit is rapidly developing, both DsRed and GFP intensity distributions exhibit large

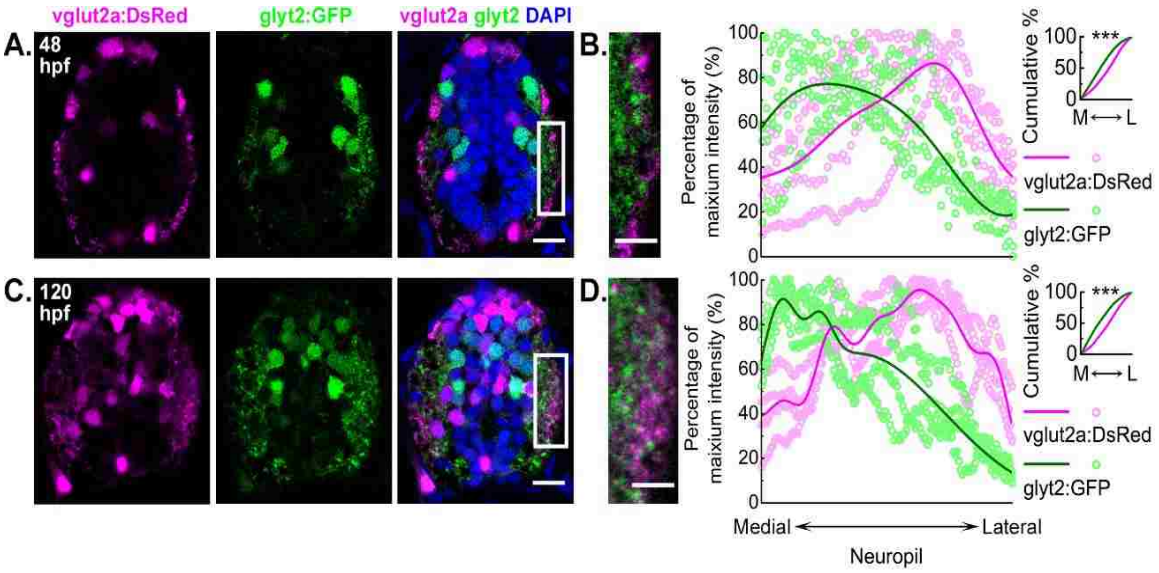

variations; still, their cumulative probability distributions are significantly different (KS test, $p = 6.53 \times 10^{-5}$; Figure 2.8B). At 120 hpf, there is much less variation for both DsRed and GFP, making the M-L patterns more obvious, with a corresponding highly significant difference in their cumulative probability distributions (KS test, $p = 7.21 \times 10^{-9}$; Figure 2.8D). In summary, the excitatory and inhibitory neuronal processes and post-synaptic puncta exhibit similar patterns of M-L enrichment in the neuropil.

Primary motor neuron dendrites grow into the highly structured spinal neuropil

To understand how post-synaptic motor neuron dendrites fit into this excitatory-inhibitory neuropil structure, we tracked the growth of caudal primary (CaP) motor neuron dendrites from 48 to 120 hpf. In spinal locomotory circuits, mature motor neurons integrate hundreds to tens of thousands of synaptic inputs from excitatory and inhibitory interneurons. To make these contacts during development, motor neurons extend their dendrites laterally into the spinal neuropil[101]. CaP motor neurons are one of the earliest-born motor neurons in zebrafish spinal cord[120]. Axons of CaP motor neurons project to synapse on the ventral muscles by 21 hpf[120], therefore, to retrogradely label their dendrites, we injected Texas-Red dextran into ventral musculature[119]. At 48 hpf, dendrites of these neurons are still quite short and variable in number (Figure 2.9). Dendrites become less variable in number (Figure 2.9C), extend laterally from 72 to 96 hpf, and eventually form a complex, multi-branching dendritic arbor by 120 hpf (Figure 2.9A and C). This dendritic growth is strongly correlated with the widening of the spinal neuropil over the same time period (adjusted $R^2 = 0.9587$, $p = 0.0139$; Table 2.3).

Figure 2.9 Primary motor neurons extend dendrites into the growing lateral neuropil from 48 to 120 hpf
(A) The diagram above the micrographs shows the organization of tightly packed cell bodies (grey) in a spinal cord transverse section. Black cells represent the primary motor neurons whose axons exit the spinal cord to innervate muscle. Below the diagram, representative images show full spinal cord transverse sections with retrogradely labeled motor neurons (yellow) at four developmental stages, 48, 72, 96 and 120 hpf. DAPI labels nuclei (blue). To capture dendritic morphology, the motor neuron channel is a z-projection of confocal images from a 30-µm transverse section. In 48 and 120 hpf images, some ventral-projecting secondary motor neurons are also labeled. Caudal primary (CaP) motor neurons are indicated by white arrowheads. Since other tissues also take up the dextran, which happens more often at earlier stages, speckled background staining and boundary of the spinal cord are also visible. Scale bar, 10 µm. Lower panels show zoomed-in images of the labeled CaP motor neurons as well as tracings of the dendritic arbor at each stage. Scale bar, 5 µm. (B) There is a strong correlation between neuropil widening (neuropil width/spinal cord width) and growth of CaP motor neuron (MN) dendrites (dendrite lateral distance/spinal cord width) during development. Data represent the means at four developmental stages, 48, 72, 96 and 120 hpf. Error bars represent SEM (neuropil width: 48 hpf, n = 15 fish; 72 hpf, n = 19 fish; 96 hpf, n = 15 fish; 120 hpf, n = 9 fish; motor neuron dendrites: 48 hpf, n = 7 neurons; 72 hpf, n = 8 neurons; 96 hpf, n = 9 neurons; 120 hpf, n = 4 neurons). Adjusted $R^2 = 0.9759$ ($p \leq 0.01$). (C) Numbers of primary dendrites per CaP motor neuron during development. Each circle represents one individual CaP motor neuron. Error bars represent SEM. No significant difference is found between different stages (one-way ANOVA, $F(3, 16) = 0.14$, $p = 0.9335$).

Although both the neuropil width and the lateral extent of CaP dendrites increase about 50% from 48 to 120 hpf, the total number of primary dendrites per CaP motor neuron stays relatively constant during this period (48 hpf 8.25 ± 0.67, n = 8 neurons; 72 hpf 8.60 ± 0.40, n = 5 neurons; 96 hpf 8.33 ± 0.33, n = 3 neurons; 120 hpf 8.00 ± 0.41, n = 4 neurons; one-way ANOVA, $F(3, 16) = 0.14$, $p = 0.9335$; Figure 2.9C). This indicates that most of the primary dendrites are formed around 48 hpf when the number of dendrites is highly variable and are thereafter stabilized to average 8-9 primary dendrites per cell. Therefore, motor neuron dendrites grow and branch laterally into a widening neuropil that is already structured with respect to excitatory and inhibitory enrichment along the M-L axis.

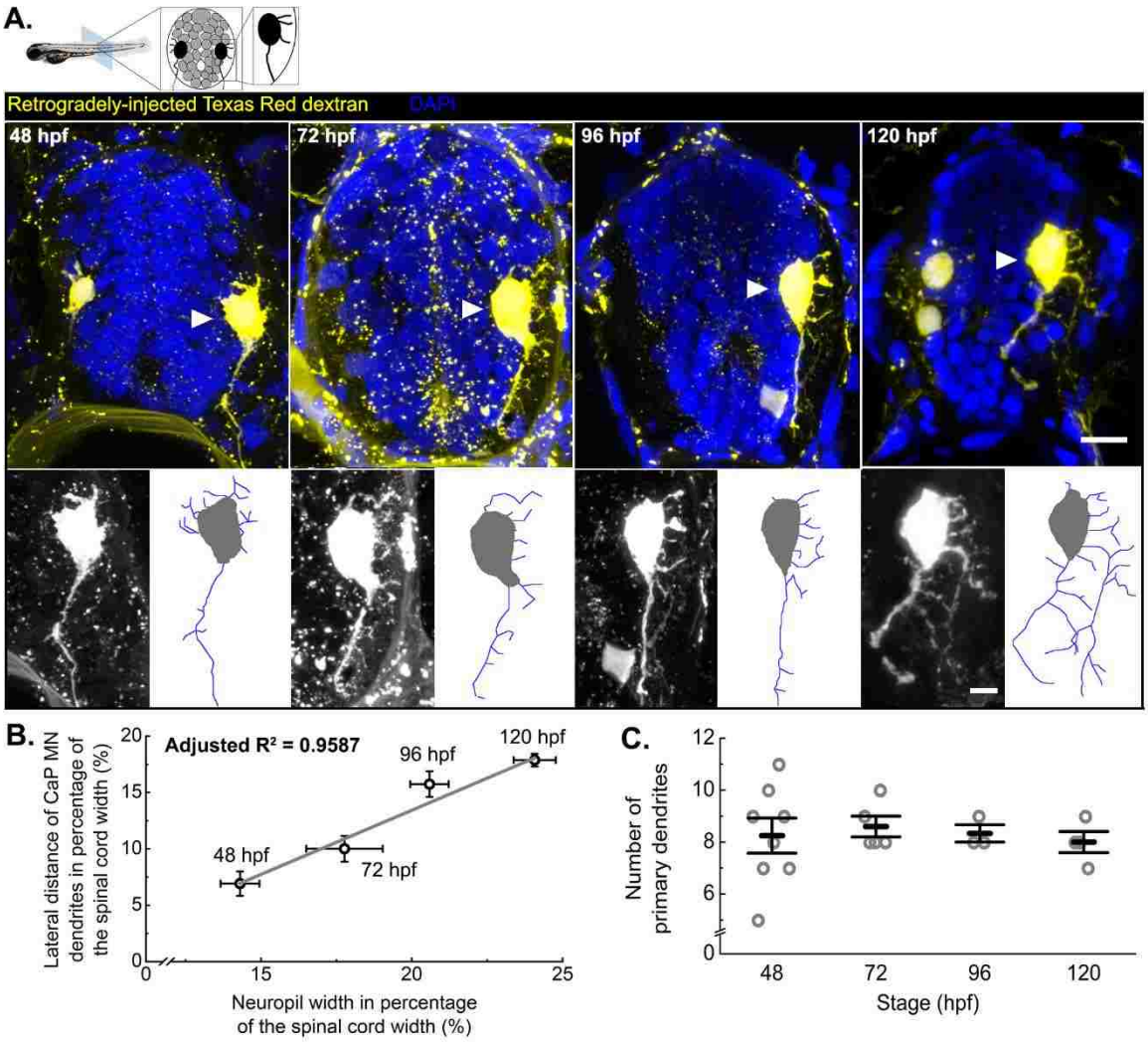

Discussion

In this study, we labeled both excitatory and inhibitory post-synapses in the zebrafish spinal neuropil to directly compare their relative spatial positions and developmental dynamics. While most other studies of synapse distribution patterns focus on individual neurons[100, 118, 121-130], our study finds robust structure at the systems level that provides a framework for spinal circuit connectivity.

Table 2.2 Widening of the spinal neuropil and the lateral extension of caudal primary motor neuron dendrites from 48 to 120 hpf
Both original measurements in µm and the percentages of spinal cord width are listed. Numbers are means +/- SEM. CaP MN, caudal primary motor neuron. Relative neuropil width: 48 hpf, n = 15 fish; 72 hpf, n = 19 fish; 96 hpf, n = 15 fish; 120 hpf, n = 9 fish; relative lateral distance of motor neuron dendrites: 48 hpf, n = 7 neurons; 72 hpf, n = 8 neurons; 96 hpf, n = 9 neurons; 120 hpf, n = 4 neurons.

	48 hpf	**72 hpf**	**96 hpf**	**120 hpf**
Neuropil width (µm)	3.44 ± 0.55	8.83 ± 0.60	10.33 ± 0.42	11.17 ± 0.40
Neuropil width in % of spinal cord width	14.31 ± 0.64 %	17.77 ± 1.27 %	20.59 ± 0.64 %	24.07 ± 0.70 %
Lateral distance of CaP MN dendrites (µm)	3.00 ± 0.37	5.35 ± 0.66	8.11 ± 0.54	8.86 ± 0.13
Lateral distance of CaP MN dendrites in % of spinal cord width	6.92 ± 1.08 %	10.01 ± 1.14 %	15.74 ± 1.13 %	17.88 ± 0.56 %

Systems-level regulation of excitatory and inhibitory synaptogenesis

By quantifying synapses at embryonic and larval stages, we identified different developmental trajectories for excitatory and inhibitory synapses. Unlike mammalian embryos, embryonic zebrafish can already generate coordinated rhythmic motor behaviors, e.g., escape behavior, which enables newly hatched larvae to evade predators even before they can see or hear well[131-135]. Indeed, at the embryonic stage, excitatory and inhibitory synapses already exhibit spatial patterning that is maintained and sharpened at later stages. Thus, the spatial enrichment of excitatory and inhibitory synaptic connections is germane to the spinal neuropil, and is likely to be fundamental to the establishment of spinal circuit connectivity and function.

None-the-less, one pattern that is unique to the embryonic stage is the presence of excitatory PSD-95 in the middle of the spinal cord, a region mostly populated by

undifferentiated precursors[136]. By the larval stage, both these precursors and the medial PSD-95 puncta disappear as neurons exit the cell cycle and differentiate[137]. These medial PSD-95 puncta could mediate excitatory drive for spontaneous activity known to be required for aspects of neuronal differentiation[138]. Medial PSD-95 puncta could also be pre-patterned post-synapses that cluster neurotransmitter receptors prior to pre-synaptic innervation. Such a phenomenon has been reported at mammalian and zebrafish neuromuscular junctions[139, 140]. These possibilities suggest that excitatory post-synaptic scaffolding proteins serve unique roles in embryonic neuronal precursors.

Excitatory and inhibitory synapses also exhibit qualitatively distinct developmental dynamics. From embryonic to larval stages, the number of inhibitory synapses significantly increases whereas the number of excitatory synapses remains fairly constant. Such differences in synaptic dynamics occur despite the fact that both excitatory and inhibitory neurons are added during this time[104, 107]. One possibility is that excitatory and inhibitory synapses undergo different pruning processes[141-143], with inhibitory synapses gradually added during development while excitatory synapses are simultaneously pruned and formed to maintain constant numbers. Future studies are needed to elucidate distinct rules of engagement for excitatory and inhibitory synapse formation and maintenance.

How could the M-L excitatory and inhibitory patterns arise?

Our study shows excitatory and inhibitory synapses form domains of enrichment along the M-L axis in the spinal neuropil. One possible explanation for this pattern would be an M-L segregation of excitatory and inhibitory interneuron somas. However, in the zebrafish spinal cord, excitatory and inhibitory neuronal somas occupy similar M-L domains[107]

(Figure 2.8A and C). Rather, our findings suggest that this M-L structure of excitatory and inhibitory synapses can be partly explained by the M-L segregation of excitatory and inhibitory neuronal processes (Figure 2.8), pointing to early developmental guidance cues as a mechanism to set up the M-L neuropil patterning. Indeed, there is ample precedent for such patterning and underlying cues. For example, in the rat striatum, cholinergic fibers are enriched laterally in the neuropil[144] due to an M-L gradient of nerve growth factor[145]. In the mouse spinal cord, Sonic hedgehog secreted from the floor plate forms an M-L gradient that restricts serotonergic axon growth to the lateral neuropil[146]. In the fly nerve cord, Slit and Netrin are secreted from the midline, signaling through Robo and Frazzled, respectively, to direct growth of motor neuron dendrites[147-149] as well as the positioning of longitudinal axons along the M-L axis[150]. In vertebrates, the Robo/Slit signal is not only crucial for the lateral positioning of longitudinal tracts from the brain to the spinal cord[146, 151], but also controls the M-L positioning of commissural axons after crossing the midline[152]. Though the role of Robo/Slit signaling in the lateral positioning of neuronal processes has not been extensively studied in zebrafish, Robo 1-4 are expressed in zebrafish spinal cord during development[153-159], suggesting that they could contribute to the M-L segregation of excitatory and inhibitory neuronal processes. Since the positions of neuronal processes can be regulated by guidance cues in a population-specific manner[160], and some transcription factors are able to activate distinct gene sets in excitatory and inhibitory neurons[161], excitatory and inhibitory processes may follow different guidance cues during circuit formation, thereby resulting in the M-L pattern of excitatory and inhibitory neuronal processes and synapses.

Ripley's L-function provides a method for analyzing synapse patterns at the systems level

Here, we adopted Ripley's L-function[109, 110] to determine whether synapse distributions change as the circuit develops. Like other spatial statistics, such as the nearest neighbor analysis[162], Ripley's L-function compares the observed distribution of puncta to a null model of random distribution. Unlike the nearest neighbor analysis, which detects distribution structures only in the immediate neighborhood and can be largely impacted by the area chosen, Ripley's L-function is a second-order statistic that detects homogeneity at all scales in the entire study area[109, 110]. Thus, it is suitable for analyzing puncta distributions in a complex and relatively large (compared to synaptic puncta) study area like the spinal neuropil, and is therefore of great utility for systems-level analyses.

By using Ripley's L-function, our study reveals some interesting spatial phenomena at the systems level. First, for the distributions of all puncta types, including the relative distributions between excitatory and inhibitory puncta, the Ripley's L-function shows that their patterns become more dispersed with development. This trend towards dispersed distributions may result from more diverse neuron groups forming synapses in less occupied neuropil regions. Since synapses from the same neuron group tend to cluster in a similar domain on post-synaptic neurons[124], the developmental increase in the diversity of pre-synaptic neuron groups may lead to more dispersed distribution patterns of synapses.

In analyses of either excitatory or inhibitory puncta, the Ripley's L-function shows a hyper-dispersed pattern[110] at spatial scales under 10 μm. Such regular spacing between synapses of like type has been observed in individual mouse retinal ganglion neurons[122] and hippocampal pyramidal neurons[124]. Our results indicate that such regular spacing of adjacent synapses of the same type exists even at the neuropil level, between synapses in

different neurons, suggesting that there may be intrinsic, system-level mechanisms underlying this spacing between synapses of the same type.

The Ripley's L-function analysis also shows a more clumped distribution for the inhibitory puncta than the excitatory puncta overall. This is consistent with the higher densities of the inhibitory puncta (Figure 2.4F). Clumping of inhibitory synapses has been observed on proximal dendrites at the cellular level[100, 123]. Our study indicates that inhibitory synapses also clump proximally to neuronal somas at the systems level.

Linking patterns at the cellular level to patterns at the systems level

Many phenomena revealed by our systems-level analyses have been previously found at the level of single dendritic branches and/or neurons. These include spatial patterning such as a regular spacing between adjacent synapses of the same type[124] and clumping of inhibitory synapses[100, 123]. These phenomena also include temporal patterns like the developmental decrease of the E/I puncta ratio, which has also been observed to a lesser extent at the cellular-level in bi-stratified, direction-selective retina ganglion cells[122]. These findings indicate that patterns at the cellular level may reflect processes at work on the systems level.

The systems-level patterns also suggest possible mechanisms that produce patterns at the cellular level. In this study, we examined the dendritic morphologies of caudal primary motor neurons, whose somas locate medial to the spinal neuropil and dendrites extend and branch laterally throughout the M-L excitatory and inhibitory structures in the neuropil. If a similar M-L pattern of excitatory and inhibitory synapses also exist on motor neuron dendrites, it would form a proximal-distal dendritic pattern: excitatory synapses enriched

on lateral, distal dendrites and inhibitory synapses enriched on medial, proximal dendrites. This proximal-distal pattern has been observed in mammalian cortical and hippocampal pyramidal neurons[99, 100, 123, 163], in which inputs from distal excitatory synapses are amplified with a higher gain[164] and proximal inhibitory synapses delay, block, and shape the dendritic spikes initiated from the distal dendrites[165-170]. If similar patterns of excitatory and inhibitory synapses exist on motor neuron dendritic arbors, then similar integrative rules may also apply to zebrafish spinal motor neurons. Interestingly, even at 120 hpf when the overall E/I puncta ratio is close to 1, the E/I puncta ratio in the most lateral neuropil occupied by distal dendrites still skews towards excitation. On the other hand, the proximal "gating" by medial inhibitory synapses may facilitate quick inhibition of motor neurons, which is required to generate alternating left-right bending in swimming behaviors[115, 171, 172]. Taken together, the high E/I puncta ratio in the most lateral neuropil could play an important role in boosting excitatory inputs, while the inhibitory synapses enriched in the medial neuropil are probably vital for inhibiting motor neurons during alternating left-right bending.

While our study reveals a distribution pattern between excitatory and inhibitory synapses at the systems level for the first time, it remains unclear how this pattern is related to synapse distribution patterns at the cellular level. There are two possibilities: 1) that synapse distribution patterns are unique on individual neurons; and patterns from different neurons converge to form the pattern observed at the neuropil level, and 2) that synapse spatial patterns are globally regulated at the systems level, which thereby determines neuronal dendritic morphologies and the cellular-level patterns. Distinguishing these possibilities would provide important insights into the way neural circuits are organized:

bottom-up or top-down. To bridge this gap, techniques are needed to label excitatory and inhibitory synapses on visualized single neurons in the circuit. Synapse-staining strategies are often incompatible with labeling of neuronal morphology, due to their distinct requirements for fixation[116, 173]. Thus, novel techniques that allow simultaneous labeling of excitatory and inhibitory synapses and individual neurons would facilitate observations of excitatory and inhibitory synapse patterns on diverse spinal neurons, without the side effect of overexpressing post-synaptic scaffolding proteins[65, 69]. Such novel techniques include mGRASP[123], intrabodies for PSD-95 and gephyrin[174] and ENABLED labeling strategy[175], all of which have previously been successfully established in mammals[123, 124, 174, 175]. Future work applying these techniques in zebrafish will allow us to understand how synapse patterns at different levels impact each other, thus providing valuable insights into how neural circuits are organized and how their organization enables their function.

Conclusions

By comparing the distributions of PSD-95 and gephyrin puncta, we found that excitatory and inhibitory synapses exhibit distinct temporal and spatial patterns in the zebrafish spinal circuit. Excitatory synapses outpace inhibitory synapses during early synaptogenesis while inhibitory synapses are more clumped in distribution at both early and late stages. Furthermore, excitatory and inhibitory synapses exhibit distinct enrichment along the M-L axis, which is probably caused at least in part by distinct M-L neuropil territories occupied by excitatory and inhibitory neuronal processes. Such M-L patterns for excitatory and inhibitory synapses and neuronal processes are established early in development, and are later refined as the circuit matures. Our observations suggest that synapse distribution is structured even at the systems level, and that excitatory and

inhibitory synaptogenesis are differentially regulated during zebrafish spinal circuit development.

Chapter 3: Synapse Pattern Alteration during Re-Establishment of E/I balance in Zebrafish Spinal Cord

For data presented in this chapter, I designed and conducted the experiments, and performed analyses for neuron numbers, and synaptic puncta localization. The Ripley's L-function analysis was a collaboration with another graduate student, Bo Zhang, with advice from Dr. Don DeAngelis. Another graduate student, Lu Zhai, offered advice on the design of the statistical tests used in this chapter. Some experiments and analyses were done with the assistance of undergraduate students Albert Hill and Dan Pham. Retrogradely labeling of CaP motor neurons and quantification the numbers and length of CaP dendritic branches were conducted by Albert Hill. The number of glycinergic neurons per segment in fish larvae was analyzed by Dan Pham.

Background

Neurological diseases, including seizures, autism, startle disease and glycine encephalopathy, are associated with disruption of E/I balance[2, 5, 6, 8, 176], however, due to the remarkable resilience of the nervous system, E/I balance in many instances can re-establish behavioral outputs of neural circuits. One example is the zebrafish *glycine transporter 1* (*glyt1*) mutant[177, 178]. GlyT1 is the major glycine transporter that both sets basal glycine levels in the cerebrospinal fluid and remove glycine from synaptic clefts after synaptic transmissions. Mutating the *glyt1* gene leads to excessive nervous system glycine. Because glycine is the major inhibitory neurotransmitter in the hindbrain and spinal cord, normal function of the spinal cord circuit is disrupted in *glyt1* mutants, with tonic inhibitory signaling causing embryonic paralysis. Despite persistent high glycine, *glyt1* mutants

naturally recover motor behaviors at the larval stage[1, 177, 178] (Figure 3.1), indicating that the spinal cord E/I balance could be re-established by intrinsic mechanisms.

The mechanisms underlying the gradual recovery of behavior and re-establishment of E/I balance in *glyt1* mutants are not well understood yet. A previous study showed that *glyt1* mutants downregulate their glycine receptors late in their recovery process (Figure 3.2; the third and fourth rows). Recovery of motor function, however, starts much earlier by 50 hpf. This gradual recovery is reflected in synaptic recording. At the embryonic paralysis stage, the amplitude of inhibitory post-synaptic potentials (IPSPs) in the mutant spinal motor neurons is twice as the WT level; from this time point, the IPSP amplitudes in *glyt1* mutants gradually decrease during the recovery process (Figure 3.2; the second

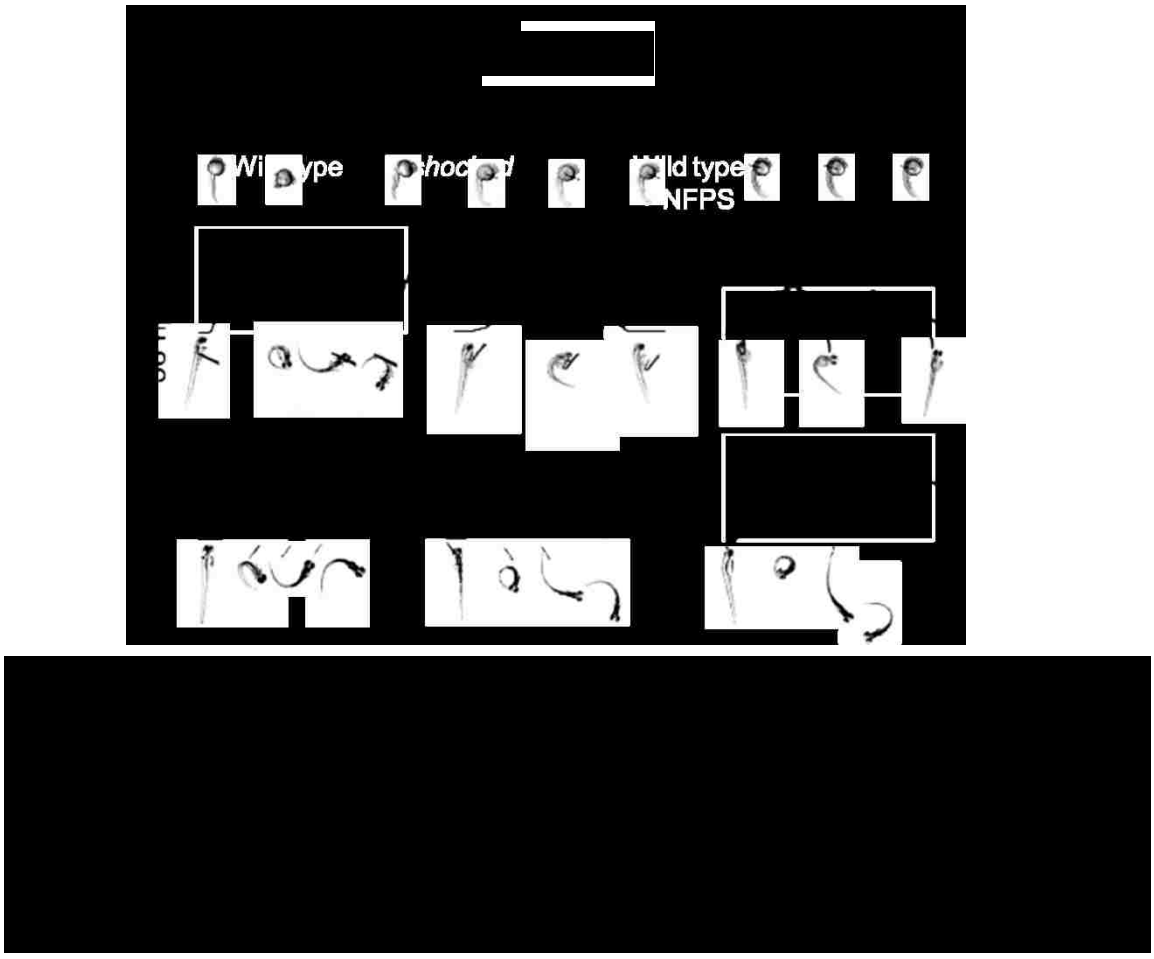

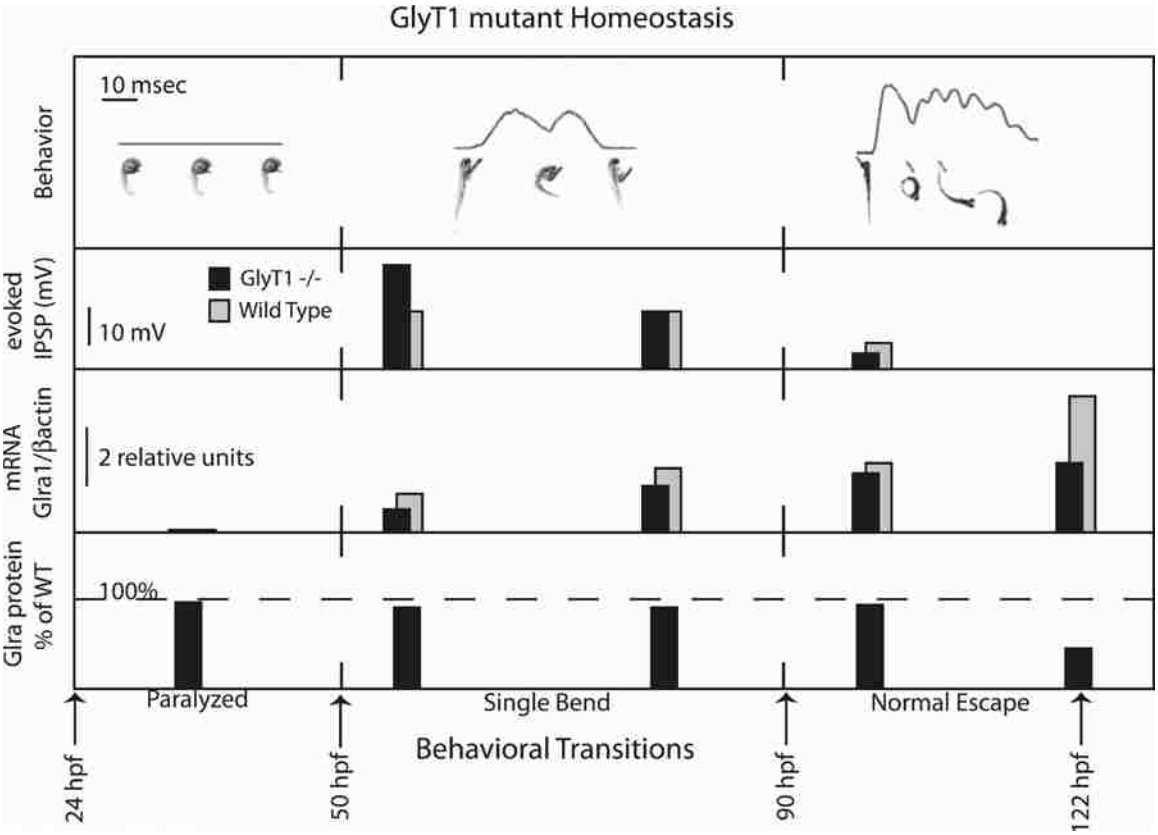

row), and match the level of excitatory post-synaptic potentials at the complete recovery. Yet, during the recovery process of *glyt1* mutants, the expression levels of ion channels and neurotransmitter receptors are largely maintained at the WT level. Therefore, the early physiological changes reflect post-translational mechanisms that compensate for the genetic perturbation of E/I balance; yet these mechanisms largely remain unknown.

Such post-translational compensation could be achieved by 1) changing the numbers of neurons expressing excitatory and inhibitory neurotransmitters, and/or 2) changing the wiring pattern in the spinal cord via regulation of the number and spatial patterning of excitatory and inhibitory synaptogenesis. Compensatory changes in numbers of neurons expressing excitatory and inhibitory neurotransmitters has been reported in frog spinal cord[34]. The pattern of synaptogenesis, as mentioned in previous chapters, is closely associated with and impacts E/I balance[7, 8, 88]. Previous *in vivo* observations have shown synapse number and locations alter to maintain E/I balance[23, 24, 179]. Therefore, to understand the recovery of motor behaviors in *glyt1* mutants, we tested the hypotheses that the re-establishment of E/I balance in *glyt1* mutants is associated with changed numbers of excitatory and inhibitory neurons, and/or altered patterns of excitatory and inhibitory synaptogenesis.

To test this hypothesis, we studied 72 hpf *glyt1* mutant larvae that have just initiated motor recovery. We first labeled neurons that express the four major types of neurotransmitters in the spinal cord, glutamate, glycine, acetylcholine, and γ-aminobutyric acid (GABA), with florescent protein labeling or immunostaining, to quantify the numbers of neurons using each type of neurotransmitter. We also immunostained post-synaptic scaffolding proteins, PSD-95 at excitatory post-synapses and gephyrin at inhibitory post-synapses to visualize the locations of excitatory and inhibitory synapses simultaneously. To understand the spatial patterns of synaptogenesis, we conducted the medial-lateral (M-L) analysis with custom Matlab programs to study whether the systems-level M-L enrichment pattern of excitatory and inhibitory post-synapses and pre-synaptic neuronal processes is altered during the re-establishment of E/I balance in the *glyt1* mutant. To

investigate whether synapse distributions at different spatial scales alter during this re-establishment, we adopted the spatial statistic, Ripley's L-function to quantify distribution patterns of excitatory and inhibitory synapses at different spatial scales. In addition, we tracked the changes in dendritic branching of caudal primary motor neurons to further understand the dendritic-level changes of synaptogenesis patterns. This strategy allowed us to investigate the association between alterations of synapse spatial patterns and the re-establishment of E/I balance. Such an understanding of E/I balance re-establishment will also shed light on potential treatments for many neurological disorders.

Materials and Methods

Fish care and embryo rearing

Experiments were conducted on offspring from *Danio rerio* WT strains AB, Tubingen, and BWT (a fish store strain from Long Island), transgenic lines *Tg(vglut2a:dsred)* and *Tg(glyt2:gfp)*[107, 111, 112], and the *glyt1* mutant. Heterozygous zebrafish with the *shocked* te301 allele (hereafter referred to as the *glyt1* mutant) were obtained from the Max Planck Institute, Tübingen, Germany[1, 178]. Zebrafish were maintained on a 14-hour light and 10-hour dark cycle at 28.5 °C and fed twice daily. Fertilized eggs were obtained by natural crossing after removing a divider at first light. Embryos were raised in glass petri dishes with system water (water that houses the adult fish) at 28.5 °C in an incubator with the same light/dark cycle, and staged according to Kimmel, 1995[113]. Zebrafish embryos and larvae were collected between 24 and 96 hpf. Homozygous *glyt1* mutant embryos were identified at 30 hpf based on the absence of normal coiling behavior. All animal protocols were approved by the Institutional Animal Care and Use Committee of University of Miami.

Labeling of spinal neurons using different types of neurotransmitters

To test whether the recovery of *glyt1* mutants involves a change in the number of neurons expressing excitatory or inhibitory neurotransmitters, we labeled and counted the numbers of glutamatergic, glycinergic, cholinergic, and GABAergic spinal neurons per segment. Glutamatergic and glycinergic interneurons were labeled using transgenic lines *Tg(vglut2a:dsred)* and *Tg(glyt2:gfp)*[107, 111, 112], respectively, and labeled live WT and *glyt1* mutant larvae were imaged at 72 hpf. Prior to imaging, fish larvae were anesthetized in MS222 and mounted in 1.2% agarose. Images were taken on the confocal microscope with a 1.2 NA 63× water objective (Leica). Cholinergic and GABAergic neurons were labeled by whole-mount immunostaining. Briefly, 72 hpf WT and *glyt1* mutant larvae were fixed in 4% formaldehyde at 4 °C for 24 hrs and washed in 1 × PBS as well as 1 × PBS with 1% Triton-X. To increase the penetration of antibodies into the spinal cord, we cut the heads, yolks and ventral muscles of fixed larvae, and treated cut samples in 20% acetone for 7 mins at -20 °C. To label cholinergic neurons, anti-choline acetyltransferase (polyclonal goat IgGs, 1:50, Millipore) was used as the primary antibody[180], and Alexa 633-conjugated donkey anti-goat IgGs (1:2000, Molecular Probes) was used as the secondary antibody. To label GABAergic neurons, anti-GABA (polyclonal rabbit IgGs, 1:500, Sigma-Aldrich) was used as the primary antibody[107, 181], and Alexa 568-conjugated goat anti-rabbit IgGs (1:2000, Molecular Probes) was used as the secondary antibody. Tissue samples were incubated overnight at 4 °C in the antibodies used. Samples were mounted on slides in Vectashield/DAPI, and imaged on the confocal microscope using the 1.4 NA 63× oil objective. Differential interference contrast (DIC) images were also captured for

identification of segment boundaries. All images were acquired at 0.08 × 0.08 × 1.0 μm voxel size.

Immunohistochemistry of post-synaptic scaffolding proteins and counting of synaptic puncta

Cryosectioning and antibody staining of WT and *glyt1* mutant zebrafish larvae at 72 hpf were performed as described in Chapter 2. Sections were immunostained with anti-PSD-95 (clone 6G6-1C9, mouse IgG2a, 1: 500, EMD Millipore Corporation) and anti-gephyrin (clone mAb4a, mouse IgG1, 1: 500, Synaptic Systems). Staining was carried out using the Sequenza slide staining system (Thermo Fisher Scientific). Alexa 568-conjugated anti-mouse IgG2a (1:2000, Molecular Probes) and Alexa 488-conjugated anti-mouse IgG1 (1:2000, Molecular Probes) were used as secondary antibodies. Stained sections were mounted in Vectashield/DAPI. Images were captured on the confocal microscope using the 1.4 NA 63× oil objective, acquired at 0.08 × 0.08 × 0.4 μm voxel size. Puncta finding was performed with a custom Matlab program as described in Chapter 2. The resulted puncta number information was used to calculate total puncta numbers and puncta densities with Image J.

Analyses of synapse distribution patterns in the spinal cord

To compare synapse distribution patterns in WT and *glyt1* mutants, we conducted the analysis of synapse distributions along the medial-lateral axis and Ripley's L-function spatial statistic. The procedures of these analyses were the same as described in Chapter 2.

Labeling neuronal processes and analysis for the medial-lateral territories of neuronal processes in the neuropil

Larvae from *Tg(vglut2a:dsred)/Tg(glyt2:gfp)* transgenic lines with WT or homozygous *glyt1* mutant genetic background were collected at 72 hpf. These larvae were cryosectioned and processed for imaging as described in Chapter 2. Images were acquired at 0.08 × 0.08 × 0.4 µm voxel size on the confocal microscope using the 1.4 NA 63× oil objective. The analysis of medial-lateral (M-L) neuropil territories of neuronal processes was performed in Image J as described in Chapter 2. In WT, the vglut2a:DsRed curve adjusted $R^2 = 0.7764$ (the sum of squares due to error (SSE) = 3.24×10^{-4}), and the glyt2:GFP curve adjusted $R^2 = 0.8006$ (SSE = 4.68×10^{-4}). In *glyt1* mutants, the vglut2a:DsRed curve adjusted $R^2 = 0.7122$ (SSE = 4.12×10^{-4}), and the glyt2:GFP curve adjusted $R^2 = 0.8122$ (SSE = 3.69×10^{-4}).

Retrograde labeling of caudal primary motor neurons

To label caudal primary (CaP) motor neurons, 72 hpf WT and *glyt1* mutant embryos were anesthetized in MS222 and injected in ventral musculature in anal segments with a 25% solution of 10,000 molecular weight Texas Red dextran in 10% Hanks' buffer, as described in Chapter 2. Injected zebrafish were then transferred to system water to recover and to allow retrograde transport of the dextran dye to fill the entire motor neuron for about 24 hours before fixation and imaging. Embryos with labeled CaP motor neurons were collected at 96 hpf, fixed in 4% formaldehyde at 4 °C for 24 hrs, washed in 1 × PBS, and mounted in Vectashield/DAPI. Images were captured on the confocal microscope using the 1.4 NA 63× oil objective, acquired at 0.08 × 0.08 × 0.4 µm voxel size. Images were

processed using Image J to maximize visibility of dendritic branches and reduce background noise.

Statistics

Data were tested for independence, normality and homogeneity of variance before they were analyzed by student's t-test or ANOVA. Bonferroni correction was applied for *post hoc* student's t-tests following ANOVA. P values for ANOVA and the *post hoc* Bonferroni correction were provided in the results unless otherwise noted. For two-group-comparison data that passed tests for normality but didn't pass tests for homogeneity of variance, the student's t-test for heteroscedastic (unequal variance) samples was used to determine statistical significance. For multiple-group-comparison data didn't pass tests for homogeneity of variance, Dunnett's tests was used to determine statistical significance. KS tests were conducted to compare cumulative probability distributions.

Results

glyt1 mutant and WT larvae have similar numbers of excitatory and inhibitory spinal neurons

In 72 hpf WT and *glyt1* mutants, we labeled spinal neurons using the four major neurotransmitters in the spinal cord: glutamate, glycine, acetylcholine and γ-aminobutyric acid (GABA). Glutamate and glycine are the major excitatory and inhibitory neurotransmitters in the spinal cord, respectively; acetylcholine is used by motor neurons and a very small portion of excitatory interneurons, while GABA is used by a small portion of inhibitory interneurons[107, 182].

To label cholinergic and GABAergic neurons, we conducted immunostaining with antibodies against choline acetyltransferase (ChAT) and GABA, respectively. The main cholinergic neurons are motor neurons, which occupy the ventral to the dorsal-middle spinal cord. There is no clear separation of the dorsal-middle neurons and the ventral neurons (Figure 3.3A). Therefore, we compared the total numbers of cholinergic neurons in WT and *glyt1* mutants, and found the numbers are very similar ($F(1,7) = 2.39$, $p = 0.1732$; Figure 3.3B).

GABAergic neurons could be separated into two distinct groups based on locations: a dorsal group and a ventral group (Figure 3.4A). A part of the ventral group is a specific neuron type called Kolmer-Agduhr (KA) neurons, which have characteristic dorsal cilia that contact the central canal[183]. Therefore, we counted the dorsal, and the ventral KA and non-KA GABAergic neurons in WT and *glyt1* mutant spinal cord. Though *glyt1* mutants have fewer dorsal GABAergic neurons than WT, this difference is not statistically

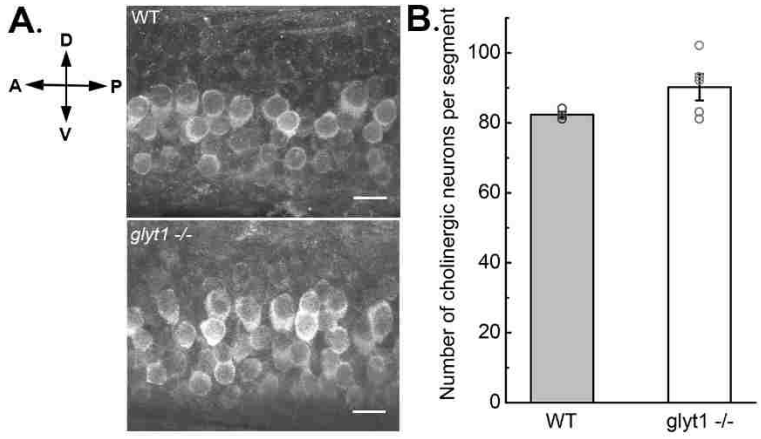

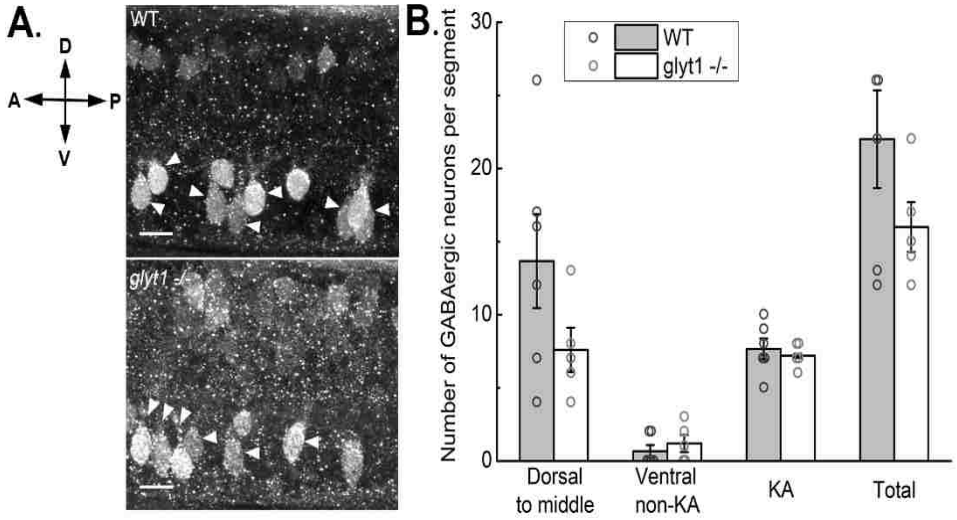

significant. The numbers of ventral GABAergic neurons, both KA and non-KA neurons, are similar in WT and *glyt1* mutants (Dunnett's test p = 1.0000 for all the four comparisons between WT and *glyt1* mutants; Figure 3.4B).

We labeled glutamatergic and glycinergic neurons using transgenic lines *Tg(vglut2a:dsred)* and *Tg(glyt2:gfp)* in which glutamatergic neurons are labeled with DsRed and glycinergic neurons are labeled with GFP, respectively[107, 111, 112]. For both glutamatergic and glycinergic neurons, the labeled neurons could be divided into two major groups by their dorsal-ventral locations: neurons in the dorsal to middle region above the

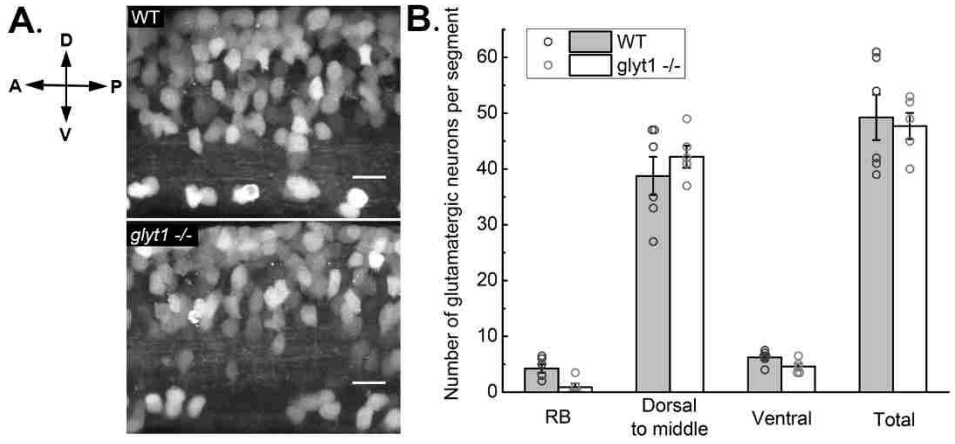

spinal central canal, and the ventral neurons located below the central canal (Figure 3.5A and 3.6A). In glutamatergic neurons, there is also an additional neuron group located in the most dorsal spinal cord with much larger cell bodies compared to other glutamatergic neurons; those are a type of sensory neuron specific to fish and amphibian embryos and early larvae, known as the Rohon-Beard (RB) neurons[184]. We did not observe any significant difference in either glutamatergic or glycinergic neurons between WT and *glyt1* mutant; they have similar number of neurons in each group for both glutamatergic (Dunnett's test p = 1.0000 for all the four comparisons between WT and *glyt1* mutants; Figure 3.5B) and glycinergic neurons (Dunnett's test p = 1.0000 for all the three comparisons between WT and *glyt1* mutants; Figure 3.6B).

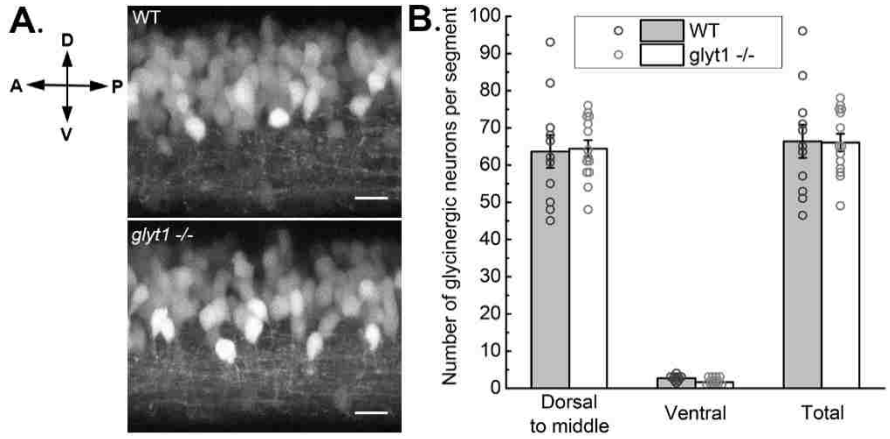

In summary, the numbers of spinal neurons using the four major types of neurotransmitters do not differ in *glyt1* mutants and WT. Therefore, the re-establishment of E/I balance in the mutants cannot be explained by alterations of neurotransmitter phenotypes.

Neuropil territories of excitatory and inhibitory neuronal processes exhibit the same pattern in WT and glyt1 mutants

Since glutamatergic and glycinergic neuronal processes exhibit a medial-lateral (M-L) neuropil pattern during spinal cord development (see Chapter 2), we investigated whether the M-L neuropil territories of excitatory and inhibitory neuronal processes are altered in

glyt1 mutant. To do this, we utilized the zebrafish *vglut2a:dsred;glyt2:gfp* double transgenic line to label glutamatergic neurons with DsRed (Figure 3.5A) and glycinergic neurons with GFP[107, 111, 112] (Figure 3.6A). Since glutamate and glycine are the major excitatory and inhibitory neurotransmitters used in vertebrate spinal cord, respectively, this double transgenic line allowed us to label most excitatory and inhibitory interneurons in the spinal cord. We found that *glyt1* mutant neuronal processes form similar M-L neuropil patterns as WT: vglut2a:DsRed^{+} processes enriched in the lateral neuropil and glyt2:GFP^{+} processes enriched in the medial neuropil (Figure 3.7). In both WT and *glyt1* mutants, the peaks of GFP and DsRed intensities are located in the medial and lateral neuropil,

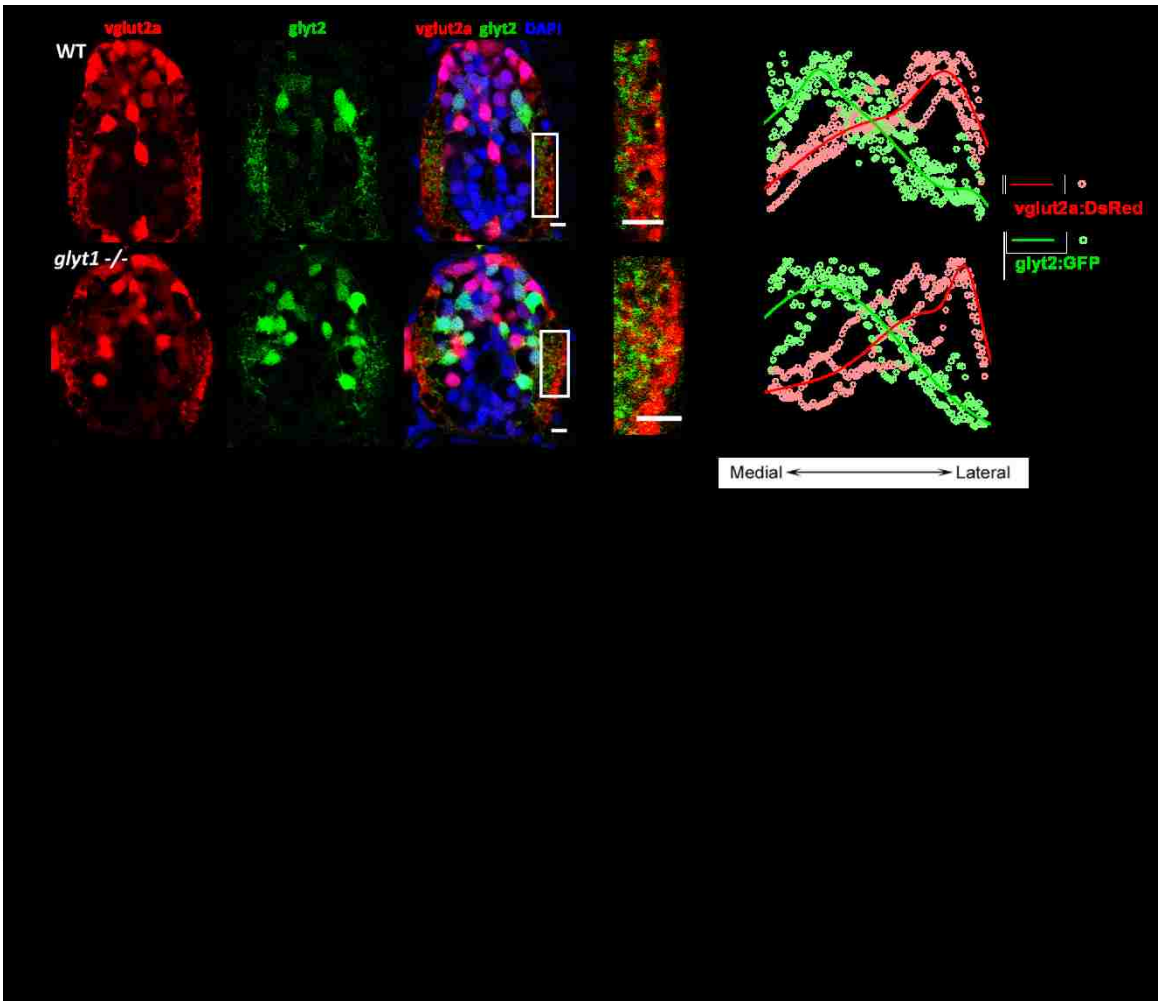

respectively (Figure 3.7B and D). Therefore, the systems-level M-L pattern of excitatory and inhibitory pre-synaptic neuronal processes is maintained in the *glyt1* mutants.

Both excitatory and inhibitory synapses exhibit higher densities in the glyt1 mutant

To test whether there is any alteration in the pattern of synaptogenesis during the re-establishment of spinal E/I balance in the *glyt1* mutants, we charted excitatory and inhibitory synapses by immunostaining the post-synaptic proteins, PSD-95 at excitatory post-synapses and gephyrin at inhibitory post-synapses in 72 hpf WT and *glyt1* mutant. At 72 hpf, both WT and *glyt1* mutant spinal cords exhibit a similar structure as observed in 48 and 120 hpf WT (see Chapter 2), with both excitatory and inhibitory synapses locating lateral to neuronal somas and enriched in the neuropil (Figure 3.8A and B).

Using a custom puncta-finding Matlab program, we compared the numbers of excitatory and inhibitory synapses in WT and *glyt1* mutant. Interestingly, the number of either excitatory or inhibitory synapses does not differ between WT and *glyt1* mutants (PSD-95 $F(1,17) = 2.09$, $p = 0.1706$; gephyrin $F(1,17) = 2.02$, $p = 0.2911$; Figure 3.8C and D). As a result, the ratio of PSD-95/gephyrin puncta numbers (E/I puncta ratios) in the *glyt1* mutants is also similar to WT, at a ratio nearly 1 ($F(1,17) = 0.0053$, $p = 0.9428$; Figure 3.8E).

We also compared puncta densities in WT and *glyt1* mutant. Increased puncta densities in *glyt1* mutants were observed for both PSD-95 and gephyrin (student's t-tests, PSD-95 $p = 3.4362 \times 10^{-5}$, gephyrin $p = 0.0004$; Figure 3.8F and G). Since the numbers of PSD-95 and gephyrin puncta in WT and *glyt1* mutants cannot explain the difference in puncta

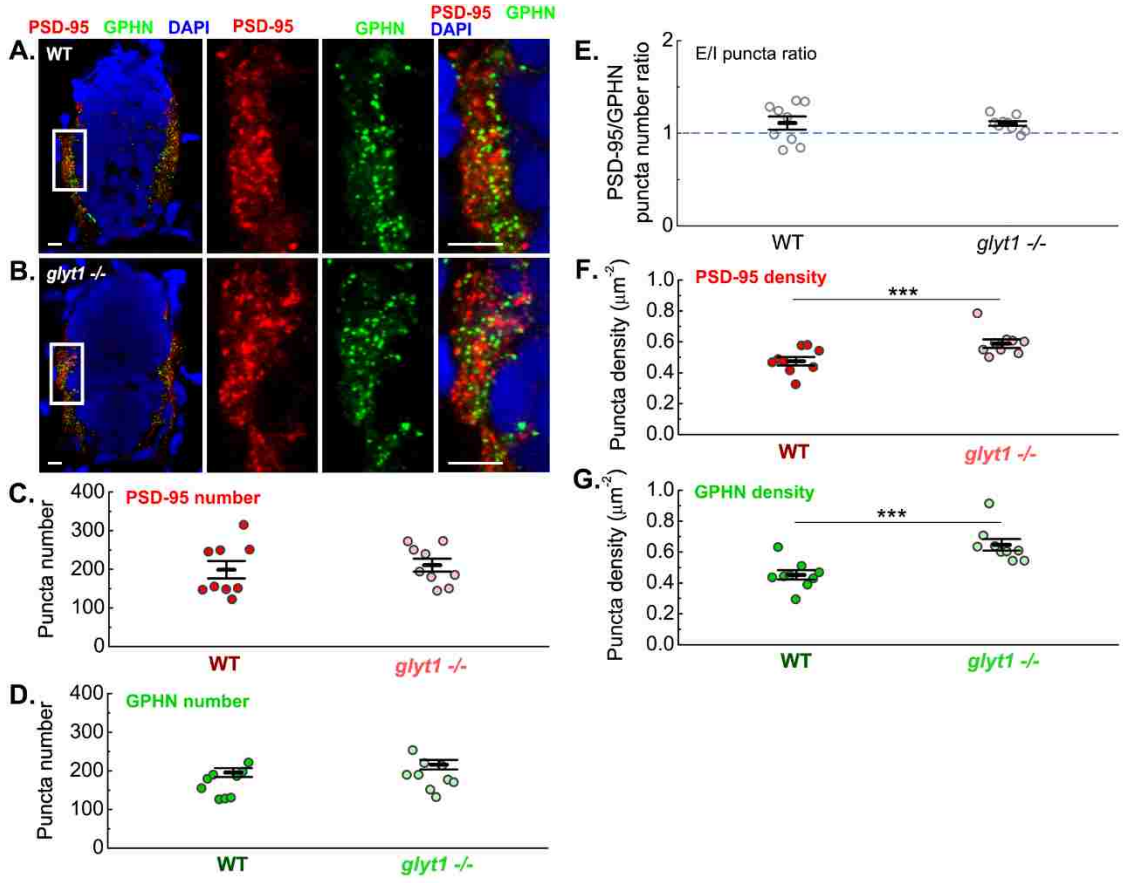

densities, the higher excitatory and inhibitory puncta densities in *glyt1* mutants indicate a change in the spatial patterns of synapses.

In summary, compared to WT, the *glyt1* mutants exhibit higher synapse densities at 72 hpf. This increase of puncta density exists at both excitatory and inhibitory synapses, and is not caused by a formation of more synapses, thus indicating that synapses are more clumped in the *glyt1* mutant.

Regular spacing between adjacent excitatory synapses increases while inhibitory synapses are more clumped in glyt1 mutant spinal cord

To determine the changes in spatial patterns of synapses in the *glyt1* mutants, we performed the Ripley's L-functions. This spatial statistical analysis allowed us to determine the distribution patterns of PSD-95 and gephyrin puncta in WT and *glyt1* mutant spinal neuropil, quantitatively testing whether the puncta distributions are clumped/clustered, random, or regular/dispersed[109, 110] (Figure 2.5A). At small spatial scales, PSD-95 puncta in both WT and *glyt1* mutants exhibit highly dispersed pattern; however, the mutant PSD-95 puncta remain dispersed until a much larger scale compared to WT (Figure 3.9A and D). Since such dispersed patterns at small scales are signs of regular spacing between adjacent puncta (Figure 2.3C1-C4), the patterns of PSD-95 indicate that adjacent excitatory synapses maintain regular spacing at larger special scales in the *glyt1* mutants. At lager spatial scales, PSD-95 puncta exhibit random distributions in both WT and *glyt1* mutants. Gephyrin puncta also exhibit such regular spacing at small scales in both WT and *glyt1* mutants. In contrast to PSD-95 puncta, the scales for such spacing in both genotypes are similar. However, at large scales, while gephyrin puncta distribute randomly in WT, they are more clumped in the *glyt1* mutants (Figure 3.9B and E).

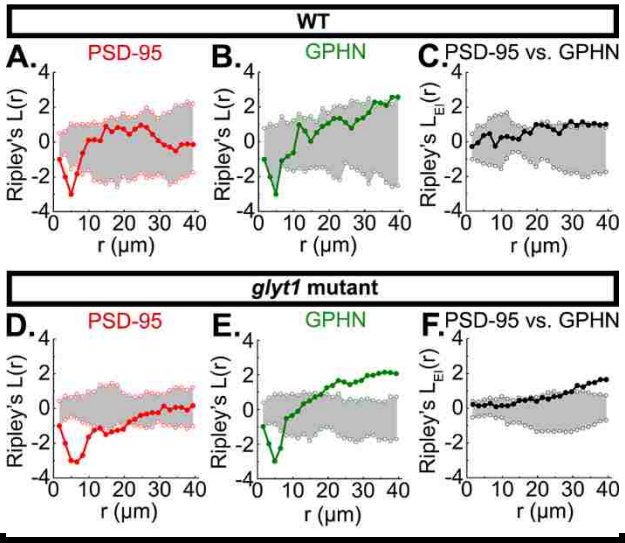

We also quantified the relative distribution patterns between excitatory and inhibitory synaptic puncta. While the distributions of PSD-95 and gephyrin puncta are generally independent from each other (Figure 3.9C and F; within the gray confidence envelope), the pattern in *glyt1* mutants is more clumped at large scales compared to that in WT. This suggests that excitatory and inhibitory synapses tend to locate closer each other in the mutant spinal neuropil, which is consistent with the higher puncta densities in the mutants (Figure 3.8F and G).

Therefore, in 72 hpf *glyt1* mutants, the distribution patterns of excitatory and inhibitory synapses are distinct in the following ways: excitatory synapses exhibit regular spacing between each other at larger spatial scales while inhibitory synapses are more clumped. In addition, the localization of excitatory and inhibitory synapses are more closely associated with each other.

The M-L pattern of excitatory and inhibitory synapses is maintained in glyt1 mutants

Given that excitatory and inhibitory synapses form a stable systems-level medial-lateral (M-L) pattern in spinal neuropil during normal development (see Chapter 2), we then tested whether this M-L pattern is altered in *glyt1* mutant. By dividing the spinal neuropil regions into the medial and lateral halves in Matlab (Figure 3.10A), we quantified the proportion of PSD-95 and gephyrin puncta locating in the lateral half of the neuropil. WT and *glyt1* mutants exhibit the same pattern: around 60% of PSD-95 puncta are enriched in the lateral half of the neuropil, while significantly less gephyrin puncta locate there (genotype × puncta type $F(1,35) = 0.08$, $p = 0.7870$; puncta type $F(1, 35) = 79.95$, $p = 1.0 \times 10^{-7}$, *post hoc* Bonferroni $p < 0.0001$; Figure 3.10B).

We further analyzed the M-L synapse patterns in the five M-L zones in WT and *glyt1* mutants (Figure 3.11A). In both WT and *glyt1* mutants, gephyrin is more enriched than PSD-95 in Zone 3 and 4, the most medial neuropil region (WT: Zone 3 $p < 1.0 \times 10^{-7}$, Zone 4 $p < 0.05$; *glyt1 -/-*: Zone 3 $p < 0.01$, Zone 4 $p < 0.05$), while PSD-95 is more enriched in Zone 5, the most lateral neuropil (Zone 5: WT $p < 1.0 \times 10^{-14}$, *glyt1 -/-* $p < 1.0 \times 10^{-7}$; genotype × puncta type × Zone $F(4,79) = 2.37$, $p = 0.0595$; puncta type × Zone $F(4,79) = 53.95$, $p < 0.0001$; Zone $F(4,79) = 321.86$, $p < 0.0001$). Though in both WT and *glyt1*

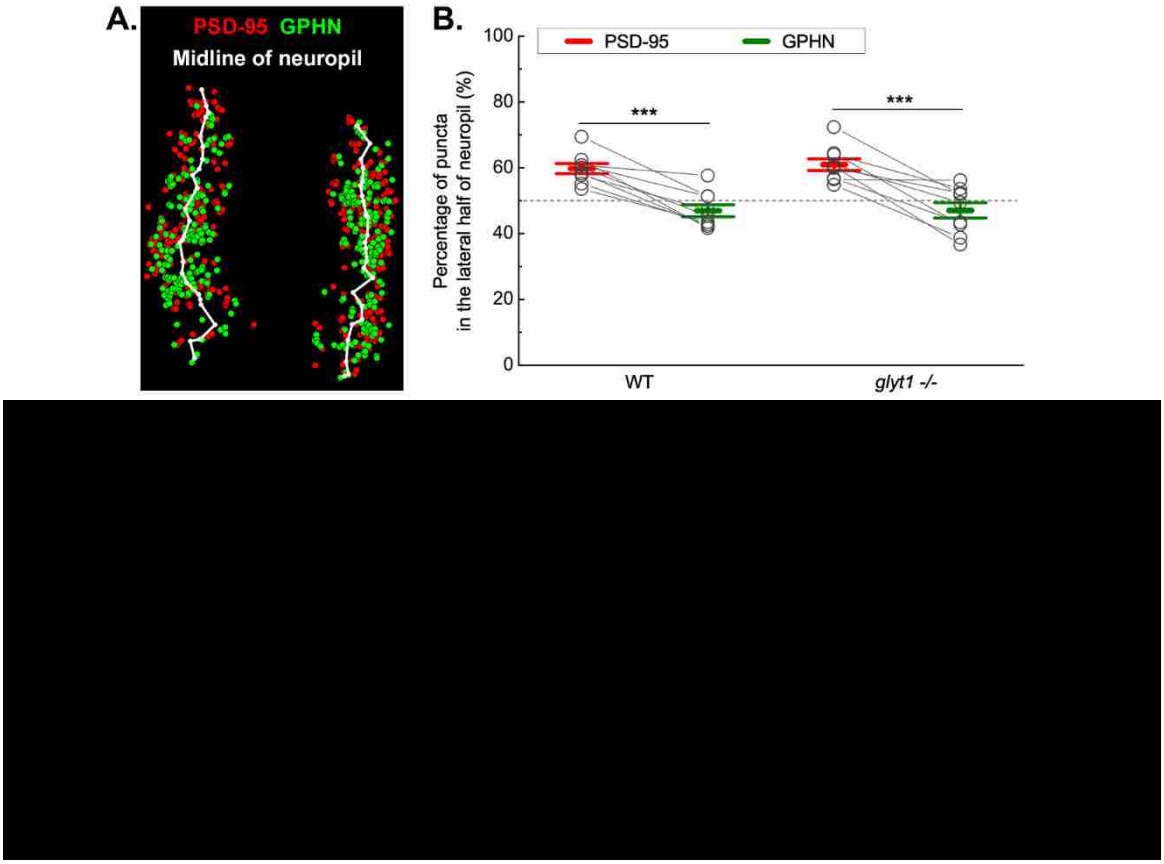

mutants, there are similar numbers of excitatory and inhibitory synapses at this stage (Figure 3.8E), significant differences between PSD-95 and gephyrin puncta numbers still exist in Zone 5, the most lateral zone, in both WT and *glyt1* mutants (in both WT and *glyt1* -/- $p < 1.0 \times 10^{-6}$; genotype × puncta type × Zone $F(4,79) = 0.27$, $p = 0.8938$; puncta type × Zone $F(4,79) = 28.88$, $p < 0.0001$; Zone $F(4,79) = 111.16$, $p < 0.0001$). There is no significant difference in puncta frequencies or number distributions in any zone between WT and *glyt1* mutants (frequency: genotype $F(1,79) = 0.48$, $p = 0.4894$; puncta number: genotype $F(1,79) = 2.18$, $p = 0.1613$; Figure 3.11D-G). Interestingly, when we overlaid the mutant puncta frequency distribution curves onto the WT ones, we found subtle differences: in *glyt1* mutants, the frequency distributions of both PSD-95 and gephyrin exhibit narrower peaks compared to WT, and the peak frequency values are higher in the mutants as well; the curves shift slightly towards the lateral neuropil, making both types of

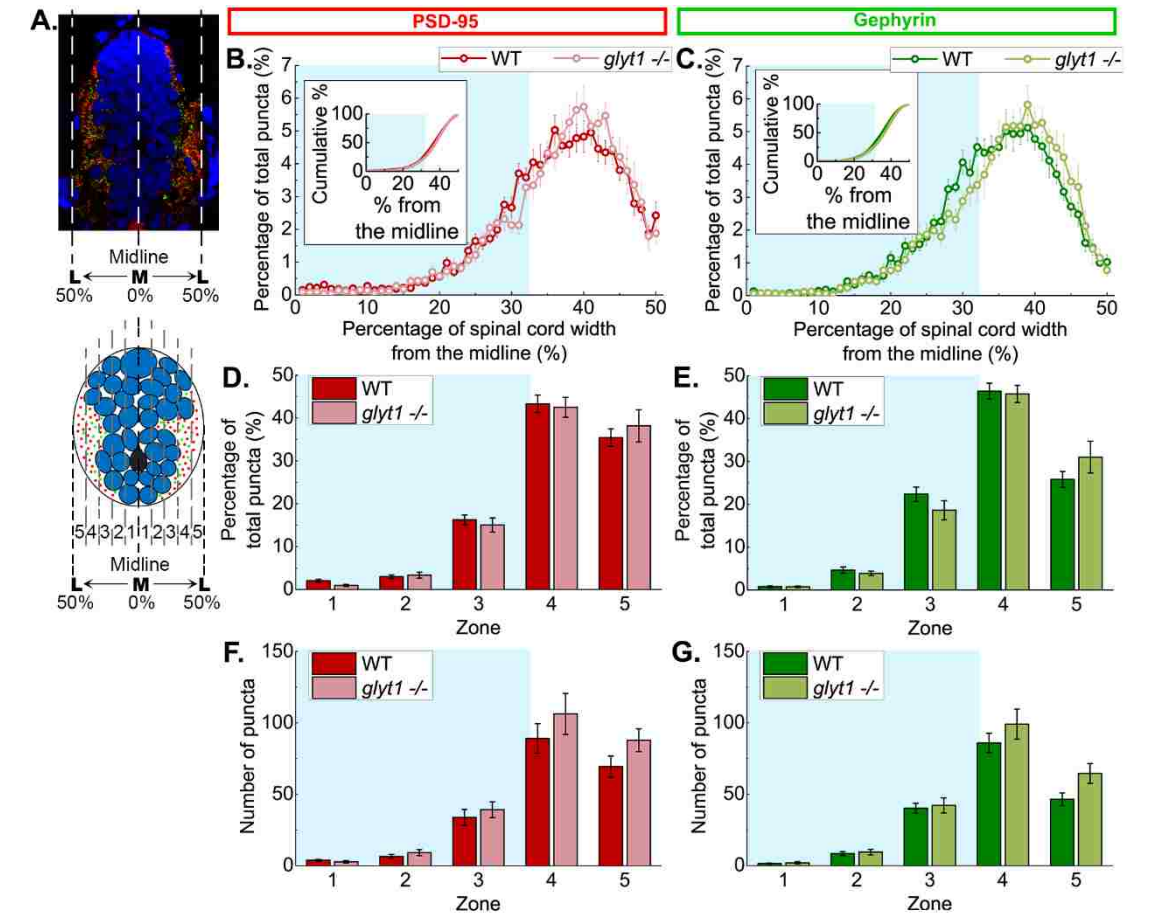

puncta more enriched in the middle neuropil compared to those of WT (Figure 3.11B and C). Such enrichment is consistent with the higher puncta densities observed in the *glyt1*

mutants (Figure 2.6F and G), though this difference in spatial patterns is so subtle that the KS tests for cumulative probability did not detect any statistical significance ($p = 0.9802$ for both PSD-95 and gephyrin; Figure 3.11B and C; inserts).

Therefore, similar to the system-level M-L pattern of pre-synaptic neuronal processes (Figure 3.7), despite of E/I balance perturbation in the *glyt1* mutants, the systems-level M-L synapse pattern is still maintained in the spinal cord.

Caudal primary motor neurons form more small dendritic branches in the glyt1 mutant

To understand how the post-synaptic motor neuron dendrites change in the *glyt1* mutants, we analyzed the branching of caudal primary (CaP) motor neuron dendritic arbors. A previous study has shown that the dendritic dynamics of zebrafish spinal motor neurons can alter in response to perturbations of E/I balance[25]. Since CaP motor neuron dendrites do not become highly branched until 96 hpf or later (Figure 2.9A), we injected Texas-Red dextran into ventral musculature of 72 hpf zebrafish larvae to retrogradely label CaP motor neurons[119], and imaged and analyzed CaP motor neuron dendritic branching patterns at 96 hpf (Figure 3.12A). We found that compared to WT, the *glyt1* mutants have a higher proportion of CaP motor neurons with secondary or tertiary dendrites (Figure 3.12B). This difference accompanies difference in the length of dendritic branches, which was defined as the distance from the starting point the measured dendritic branch to its first branching point to smaller dendrites. Compared to WT, the mutant neurons have shorter primary dendritic branches and longer secondary and tertiary branches (Figure 3.12C). Though the differences are not statistically significant ($p > 0.05$ for all branch orders,

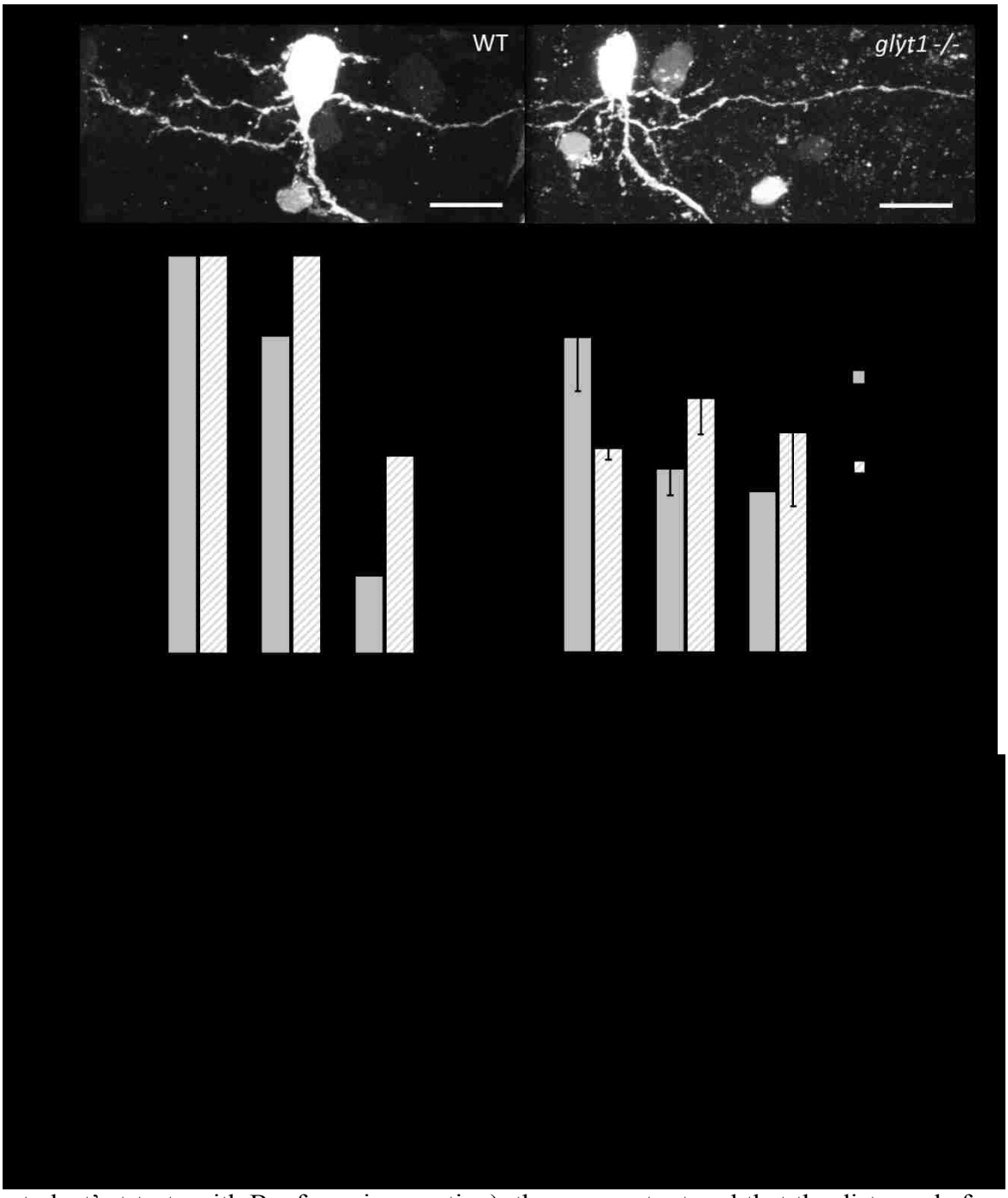

student's t-tests with Bonferroni correction), they suggest a trend that the distance before branching is shortened in the mutant dendrites.

Taken together, the mutant CaP motor neuron dendrites start to branch out earlier during their extension, and they also form more small branches, which are probably associated with the subtle changes of synapse spatial patterns in the mutant.

Discussion

In this study, we compared the spatial patterns of synapses in WT and *glyt1* mutants at the beginning of the mutant's recovery process. Interestingly, we found that the systems-level patterns observed in WT are maintained in the *glyt1* mutant. Rather, the mutants alter synapse spatial patterns at much finer scales. These results indicate that the re-establishment is likely associated with fine-scale regulation of synapse distributions, rather than alteration of the general, system-level pattern.

Spatial patterns of synapses in the glyt1 mutant spinal cord

We found that the system-level pattern of excitatory and inhibitory synapses and neuronal process is maintained in the *glty1* mutant spinal cord; instead, changes of synapse spatial patterns occur at much finer scales. Given that this systems-level pattern is established early in development and also maintained through the spinal cord development, this pattern exhibits incredible stability in developmental changes and in the *glyt1* mutant genetic perturbation. Therefore, this systems-level pattern likely provides a stable framework for spinal connectivity which is fundamental for generating functional motor behaviors. This pattern may even be fundamental to allow the re-establishment of E/I balance in the *glyt1* mutants. Future studies are needed to understand specific roles that this systems-level pattern plays in maintaining E/I balance.

Subtle changes in synapse distribution patterns take place in the *glyt1* mutant spinal cord, with increased clumping of both excitatory and inhibitory synapses (Figure 3.7F and G) towards the middle of the neuropil (Figure 3.10B and C). This means that both excitatory and inhibitory synapses exhibit a trend of leaving their original enriched zones; and this is likely associated with the change of motor neuron dendritic branching in the

glyt1 mutant. These subtle changes occur in the 72 hpf mutants, corresponding to the initiation of the recovery process. Therefore, our results support the hypothesis that E/I balance in the *glyt1* mutants is re-established by subtle changes in synapse distributions, rather than alteration of the general pattern.

Synapse distribution alters without changing the numbers of synapses

While previous findings of alterations of synapse distribution in response to perturbations of E/I balance usually accompany changes in synapse numbers[23, 24, 61, 161], our study shows that the synapse distributions alter in the *glyt1* mutants without changing the numbers of synapses, suggesting that the regulations of synapse distributions and synapse numbers can be uncoupled. While there are only limited studies that have recorded changes in both synapse numbers and distributions, a previous study has provided similar implications. In mouse brain whisker-to-barrel pathway, 24 hr whisker stimulation leads to increased numbers of both excitatory and inhibitory synapses as well as a rearrangement of inhibitory synapse locations; however, 4 days after the stimulation, when the E/I balance in the neural pathway is recovered and synapse numbers decline to the normal levels, the distribution pattern of inhibitory synapses never come back to the baseline[23]. It is possible that neural circuits allow multiple wiring topologies in generating functional behaviors; and this may also explain the remarkable resilience of the nervous system to perturbations of E/I balance[11, 185].

Dendritic branching patterns of motor neurons in the glyt1 mutant

In our study, we found that CaP motor neuron dendrites exhibit enhanced branching in the *glyt1* mutant. Previous studies have also revealed dendritic changes of motor neurons in response to perturbations of E/I balance[25, 186]. In zebrafish spinal cord, when E/I balance is disrupted by decreasing neuronal excitability, the dendritic filopodia of primary motor neurons become less dynamic[25], suggesting that a similar phenomenon may also take place in CaP motor neurons of the *glyt1* mutant. A previous study in zebrafish retina shows that stabilization of dendritic branches by formation of synapses is required for further branching of the dendrites[90]. Therefore, one explanation of the increased CaP motor neuron dendritic branching in the *glyt1* mutants is that decreased dendritic dynamics lead to quicker stabilization of dendritic branches, thereby resulting in increased branching.

Another previous study of mouse embryonic motor neurons with defects in glycine transmission has also shown increased branching of motor neurons[186]. This is curious since the zebrafish *glyt1* mutants in our study have excessive glycine transmission, which would be expected to show the opposite phenomenon to the glycine transmission-defect mice. Given that the glycine transmission-defect mice exhibit disrupted E/I balance with abnormally high excitatory neurotransmission[186], the enhanced dendritic branching in motor neurons is likely associated with increased excitation. Since in our study, the *glyt1* mutants are at the beginning of their motor recovery, the increased motor neuron dendritic branching is probably an initiating sign of E/I balance re-establishment. Further studies are needed to test this hypothesis.

Motor neuron dendritic integration in glyt1 mutants

In 72 hpf *glyt1* mutant larvae, we observed changes in both synapse spatial patterns and motor neuron dendritic branching, which are likely linked with each other. Mutant synapses are compressed in the middle neuropil, and compared to WT, slightly shifted towards the lateral, while the branching point of motor neuron primary dendrites shifts medially in *glyt1* mutants. Therefore, in mutant motor neurons, there are likely increased surface area of secondary dendrites, with more synapses locating there.

This change of dendritic property and synapse locations would probably change the input integrations in *glyt1* mutant motor neurons. Previous studies on brain pyramidal neurons have revealed the existence of dendritic domains with distinct synaptic inputs, excitability and modulation with in the same dendritic arbor[163, 164]. Another previous study in a mouse model of Alzheimer's disease showed that decreased dendritic length and branching in mouse cortical pyramidal neurons are associated with neuronal hyperexcitability; their computational modeling has demonstrated that this dendritic morphological change itself is sufficient to explain the neuronal hyperexcitability[187]. Therefore, it is possible that the *glyt1* mutant motor neurons are re-arranging dendritic domains with altered dendritic physiological properties to establish new integration patterns that more favorable for mutant motor functions.

Unlike in mammalian brain neurons[163, 187-191], the dendritic properties in zebrafish motor neurons remain largely uncharted. Future studies that determine the morphological and physiological properties of dendritic arbors in zebrafish motor neurons would provide valuable insights into understanding the maintenance of E/I balance in the spinal locomotory circuits.

Conclusions

By comparing the spatial patterns of PSD-95 and gephyrin puncta in 72 hpf WT and *glyt1* mutant spinal cords, we found that the systems-level medial-lateral (M-L) patterns of synapses and neuronal processes are maintained, while subtle changes of synapse distributions occur in the *glyt1* mutant. In the mutants, excitatory synapses exhibit regular spacing at larger spatial scales, and inhibitory synapses are more clumped across the spinal neuropil. Excitatory and inhibitory synapses are also more clumped with each other, with their M-L enrichment territories compressed towards the middle of the neuropil. Consistent with changes of synapse distribution, mutant CaP motor neurons also exhibit enhanced dendritic branching. These alterations of synapse distributions occur independent of changes in synapse numbers. Our observations suggest that subtle changes of synapse distribution, rather than alterations of the general pattern, are associated with the initiation of motor recovery in the *glyt1* mutants, and that regulations of synapse numbers and distributions can be uncoupled.

Chapter 4: Blocking Inhibition Disrupts Glycinergic Synaptogenesis in Zebrafish Spinal Cord

This study was a collaboration with Dr. Lisa Ganser. I established the immunostaining method to simultaneously label glycinergic receptors and inhibitory post-synaptic scaffolding protein gephyrin, and conducted the image analysis to reveal glycinergic synaptogenesis patterns. The data presented in this chapter was published in *Neurobiology of Disease* in 2013[115] with me as a co-first author.

Background

While E/I balance and synaptogenesis are strongly associated with each other[7, 8], how perturbations of E/I balance disrupt synaptogenesis is still not completely understood. Imbalanced excitatory and inhibitory synaptogenesis is associated with multiple human diseases[8], one of which is human startle disease, also known as hyperekplexia[6]. Startle disease is an inherited disease with disrupted spinal cord E/I balance. Patients exhibit exaggerated startle reflexes and abnormally tense muscles, which may also be accompanied by suspension of breathing[192], and thus can cause brain damage and/or sudden infant death[193]. These symptoms are caused by reduced glycinergic neurotransmission. Because glycine is the major inhibitory neurotransmitter in vertebrate hindbrain and spinal cord, reduced inhibitory signaling is thought to explain the hyperexcitable phenotype. In startle disease patients, mutations have been found in genes encoding glycine receptor (GlyR) α1 and β subunits, five of which come together to form the pentameric GlyRs[2, 6, 193] (Figure 4.1). Given that glycinergic transmission has been reported to play an important role in neuronal differentiation and circuit development[186, 194], the reduction of glycinergic transmission may also impact synaptogenesis process.

However, how synaptogenesis is altered by mutations in GlyR subunit genes is not well understood.

Human startle disease can be caused by mutations in genes encoding either the GlyR α1 subunit (*GLYRA1*)[192, 195] or the β subunit (*GLRB*)[196]. Mutations in *GLRB* are often associated with more severe clinical phenotypes however, including gaze disorders, breathing difficulties, learning difficulties and developmental delay[197-199]. We set out to model the α1 and β subunit forms of startle diseases in zebrafish to better understand mechanisms underlying such phenotypic difference between losing GlyR α1 and β subunit

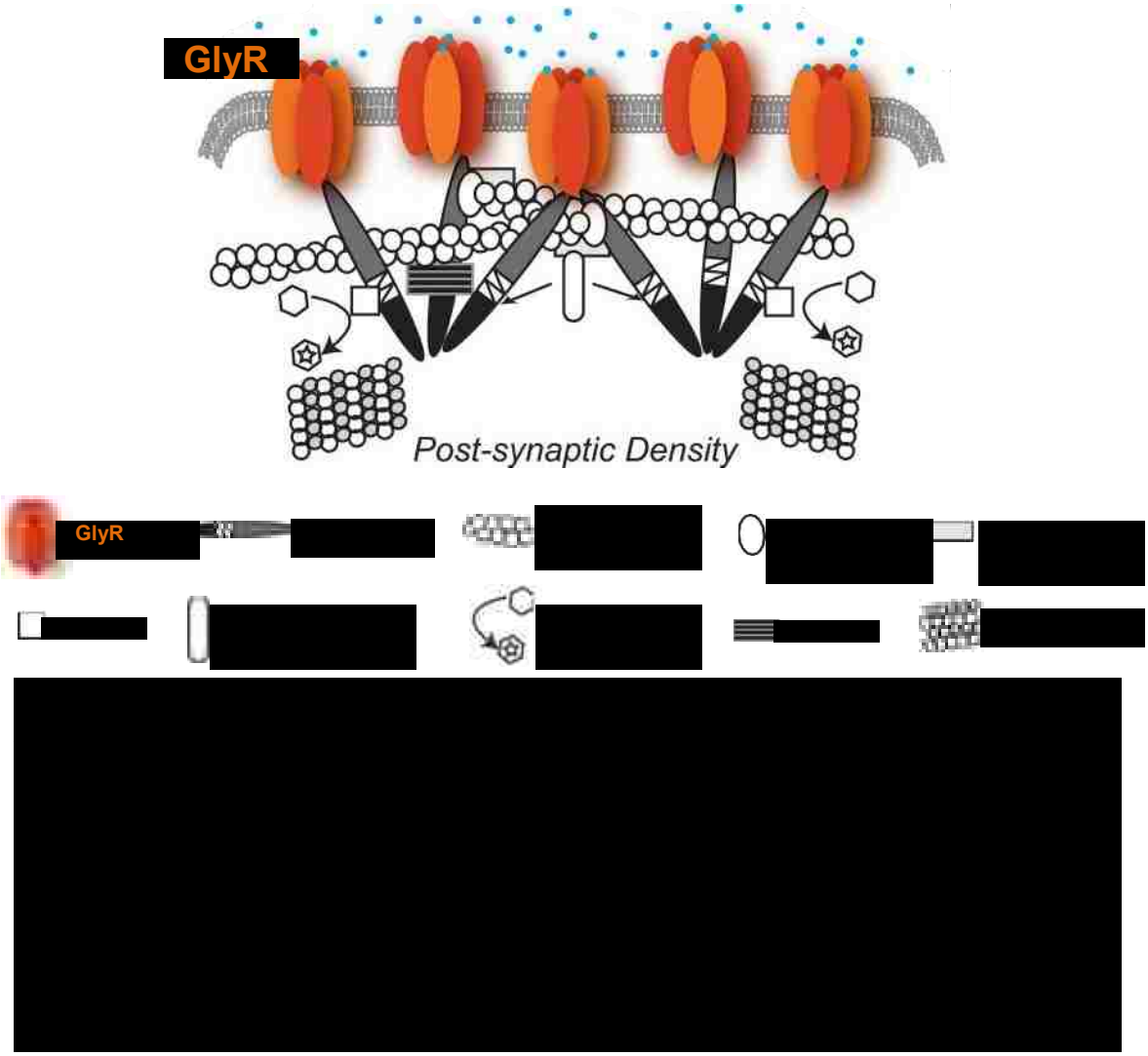

mutations[197-199]. At post-synapses, each functional GlyR consists of five subunits, including two α subunits and three β subunits. There are at least four independent genes (*GLRA1-4*) encoding α subunits and one gene (*GLRB*) encoding the β subunits in humans. α subunits bind glycine, and β subunits interact with post-synaptic scaffolding protein gephyrin to link GlyR to the cytoskeleton[2] (Figure 4.1). Despite such well-known functions, it remains unclear what roles these different subunits play during glycinergic synaptogenesis, and how that is associated with the phenotypic difference in startle disease.

In this study, we hypothesized that GlyR α and β subunits play distinct roles in glycinergic synaptogenesis, which is associated to different behavioral phenotypes after disruption. We tested this hypothesis in zebrafish since both GlyR α and β subunit genes can be readily knocked down by antisense morpholino injection[200]; also, given the well-characterized stereotyped motor behaviors in zebrafish, the resulting behavioral phenotypes can be easily qualified[4, 201]. While humans have five known GlyR subunit genes (*GLRA1-4* and *GLRB*), zebrafish genome contains seven GlyR subunit genes (*glra1*, *glra2*, *glra3*, *glra4a*, *glra4b*, *glrba* and *glrbb*)[171] due to whole genome duplication early in the evolution of teleosts[202]. Despite this duplication, previous studies have shown that mutations in *glrbb* gene lead to bilateral contractions of the axial muscles, which cannot be compensated by *glrba* function; and this zebrafish mutant *bandoneon* (*beo*) has been viewed as a model for human startle disease[171, 203]. Since mutations in *GLRA1* and *GLRB* genes have been identified in human startle disease patients[2, 6, 192, 193, 195, 196], we targeted to *glra1* and *glrbb* genes in zebrafish.

To compare the synaptogenesis patterns and behavioral phenotypes associated with disruption of GlyR α1 and βb subunits, we used splice-site morpholinos[204] to knock down

glra1 and *glrbb* genes. We immunostained with antibodies against GlyR and post-synaptic scaffolding protein gephyrin to analyze glycinergic synaptogenesis patterns in *glra1* and *glrbb* morphants. We also analyzed embryonic motor behaviors in these morphants to identify the phenotypic range after knocking down each gene. With this strategy, we were able to reveal different roles of α1 and βb subunits in glycinergic synaptogenesis and the link between glycinergic synaptic transmission and functional rhythmic motor behaviors.

Materials and Methods

Fish care and embryo rearing

Experiments were conducted on offspring from *Danio rerio* WT strains AB, Tubingen, and BWT (a fish store strain from Long Island). Zebrafish were maintained on a 14-hour light and 10-hour dark cycle at 28.5 °C and fed twice daily. Fertilized eggs were obtained by natural crossing after removing a divider at first light. Embryos were raised in glass petri dishes with system water at 28.5 °C in an incubator with the same light/dark cycle, and staged according to time in hpf and Kimmel, 1995[113]. All animal protocols were approved by the Institutional Animal Care and Use Committee of University of Miami.

Splice-site targeted morpholino knockdown

We designed splice site-targeted morpholinos (MOs) against *glra1* and *glrbb* based upon the appropriateness of the sequence for effective MO knockdown, with 50% GC content and multiple mismatches to related genes. To control for possible off-target effects, two independent MOs were designed against intron/exon boundaries shared among all *glra1* transcripts: *glra1*MOex4 5'-GAATTGTCCTCTCACCTTATACTGT-3' and *glra1*MOex7 5'-CTTCCCTGAAACACAGAGAGTATGT-3'. The *glra1*MOex4 targeted

the 3' acceptor site of *glra1* exon 4 that encodes amino acids involved in glycine binding[205], and the *glra1*MOex7 targeted the 5' donor site of *glra1* exon 7 that encodes the first two membrane-spanning domains (M1 and M2) (Figure 4.2 A). Since the phenotype of target zebrafish *glrbb* mutant *beo* has been described previously[203], off-target effects were not a concern for the *glrbb* MO. Therefore, we designed one splice site-targeted MO against 3' acceptor site of *glrbb* exon 5, one of the largest exons upstream of the transmembrane domains (Figure 4.2C): *glrbb*MOex5 5'-GAGAGCATTAAAGTTCACCTCATGC-3'. Standard control MO (Gene Tools, LLC, Philomath, OR) was used for control MO injection. Lyophilized MOs were resuspended in water as 1 mM stocks, stored at room temperature, and heated for 5 min to 65 °C prior to use. For injection, stock solutions were diluted in a filtered solution of 1% (w/v) fast-green dye. The working concentration was 0.25 mM for *glra1*MOex4, 0.5 mM for *glra1*MOex7, 0.5 mM for *glrbb*MOex5, and 0.5 mM for control MO, respectively. MOs were injected into WT embryos at the 1–2 cell stage, with 2 nl working solution per embryo. Embryos were sorted 6–8 hrs after injection, and only morphants in which the MO bolus had evenly dissipated were later analyzed for behavioral phenotypes. The specificity of altered pre-RNA splicing in *glra1* and *glrbb* genes caused by MO injection was examined by RT-PCR analysis with RNA harvested from MO-injected embryos at 28 hpf (Figure 4.2B and D).

Immunohistochemistry and quantification of synaptic puncta

Cryosectioning and antibody staining of zebrafish embryonic spinal cords were performed as described in Chapter 2. Anti-gephyrin (clone mAb7a, mouse IgG1, 1:500, Synaptic Systems, Göttingen, Germany), and a pan anti-GlyR α subunits (clone mAb4a,

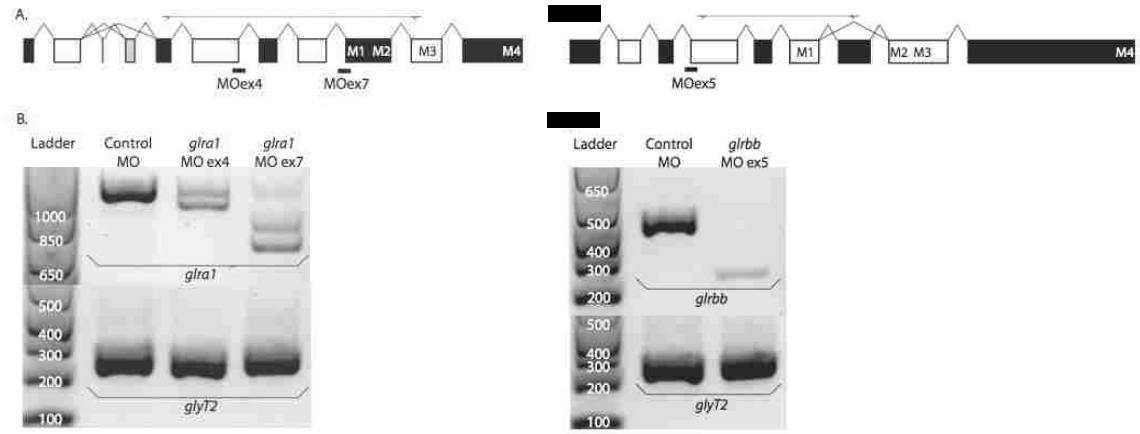
A.
M1 M2
M3
M4
MOex4
MOex7
M1
M2 M3
M4
MOex5
B.
Ladder
Control MO
glra1 MO ex4
glra1 MO ex7
1000
850
650
glra1
500
400
300
200
100
glyT2
Ladder
Control MO
glrbb MO ex5
650
500
400
300
200
glrbb
500
400
300
200
100
glyT2

[redacted]

mouse IgG1, 1:100, Synaptic Systems)[171] were used as primary antibodies. Alexa 488- and Alexa 568-conjugated donkey anti-mouse IgGs were used as secondary antibodies (1:2000, Life Technologies, Carlsbad, CA). Double staining with anti-gephyrin and anti-GlyR α subunit antibodies was performed sequentially. Stained sections were mounted in Vectashield/DAPI and images were captured on a confocal microscope using a 1.4 NA 63 × oil objective. Stained GlyR α subunit and gephyrin puncta were identified using custom Matlab programs as described in Chapter 2. For GlyR α subunit and gephyrin puncta co-localization analysis, puncta in the three-dimensional stack were first found by custom Matlab programs[117, 118]. Then the three-dimensional location of each voxel in all GlyR α subunit puncta and gephyrin puncta were compared in Matlab to identify the colocalized puncta.

Behavior analyses

A high-speed camera (1024 Photron FASTCAM, San Diego, CA) was used to record spontaneous and touch-evoked behaviors of 17 to 50 hpf control, *glra1*, and *glrbb* morphants. Embryos were manually dechorionated. Spastic behaviors were characteristic of all groups just after dechorionation. Therefore, behavioral assays were conducted at least 1 hr after dechorionation. Videos were scored by hand to categorize behaviors and quantify behavior durations.

Statistics

Data were tested for independence, normality and homogeneity of variance, before they were analyzed by ANOVA. Bonferroni correction was applied for *post hoc* student's t-tests.

Results

Glycinergic synaptogenesis differs in control, glra1, and glrbb morphant zebrafish

To compare the impact of knocking down GlyR α1 and βb subunits on glycinergic synaptogenesis, we carried out immunostaining in 24 and 48 hpf spinal cord transverse sections, double-labeling GlyR α subunits, which are required for glycine binding function of GlyR, and the post-synaptic scaffolding protein gephyrin, which clusters GlyRs at post-synapses. At 24 and 48 hpf, many spinal cord cells are still actively dividing progenitors[137], which locate in the middle of the spinal cord, surrounded by differentiated neurons that have exited the cell cycle; these differentiated neurons include Rohon Beard sensory neurons, some interneuron types[182], and primary motor neurons[120] (Figure 4.3; diagrams). Since motor neurons serve as an interface between the central nervous system and the muscles that generate motor behaviors, for immunostainings of GlyR and gephyrin, we focused on regions around the largest nuclei in the motor neuron domain (Figure 4.3; white boxes), which are likely primary motor neurons. GlyR α and gephyrin staining were both characterized by bright puncta which reflect clustering of these proteins at post-synaptic densities. Interestingly, in control morphants, GlyR α puncta and gephyrin puncta do not colocalize until 48 hpf (Figure 4.3A and 4.4B). In 24 hpf control morphants, gephyrin puncta are enriched exclusively on the lateral domain occupied by differentiated neurons,

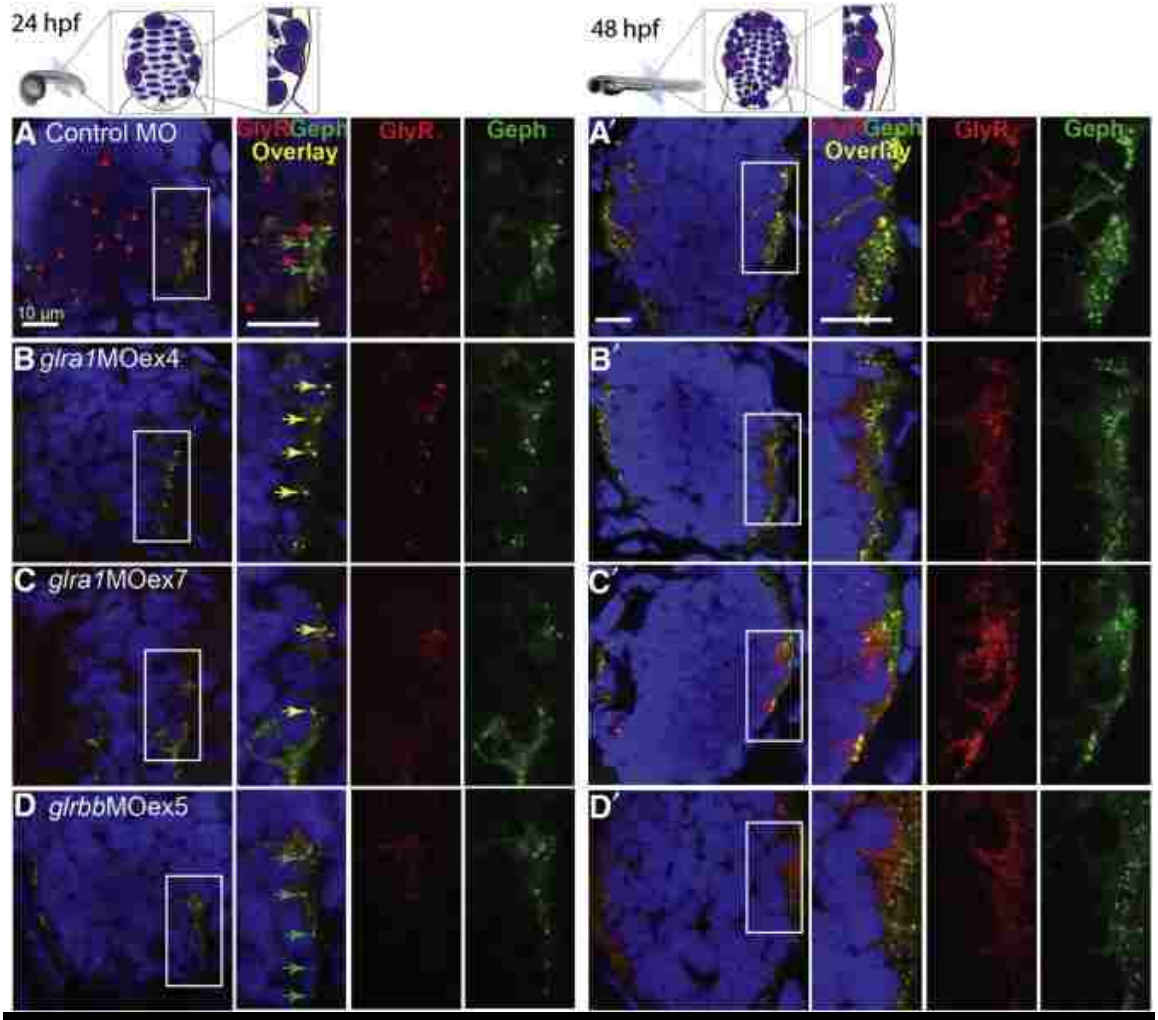
24 hpf
48 hpf
A Control MO
GlyR Geph
Overlay
GlyR
Geph
10 µm
A′
B glra1MOex4
B′
C glra1MOex7
C′
D glrbbMOex5
D′

while GlyR α puncta also decorate the middle progenitors (Figure 4.3A; red arrowheads); and there is little overlap between GlyR α and gephyrin staining even when expressed on the same neurons (Figure 4.3A; red and green arrowheads). By 48 hpf, more neurons have differentiated and formed more synapses, which are enriched in the lateral spinal cord as described in Chapter 2. In 48 hpf control morphants, GlyR α and gephyrin puncta are both enriched in the lateral spinal cord, and colocalize with each other (Figure 4.3A′).

In contrast to control morphants, *glra1* morphants with either *glra1*MOex4 or *glra1*MOex7 exhibit GlyR α-gephyrin colocalization at 24 hpf. In both *glra1* morphants at 24 hpf, GlyR α puncta in the middle spinal cord are dramatically reduced, with remaining GlyR α puncta enriched in the lateral spinal cord, colocalizing with gephyrin puncta (Figure 4.3B and C). This pattern in *glra1* morphants persists at 48 hpf, though GlyR α and gephyrin puncta are enriched more laterally relative to nuclei than in control morphants (Figure 4.3B′ and C′).

In *glrbb* morphants, at 24 hpf, GlyR α puncta are not only missing from the middle of the spinal cord, but are also reduced in the lateral spinal cord. Gephyrin puncta still occur in the lateral spinal cord in 24 hpf *glrbb* morphants with the absence of GlyR α puncta (Figure 4.3D). At 48 hpf, despite of visible diffuse GlyR α staining in the lateral spinal cord of *glrbb* morphants, there are no clear GlyR α puncta. Since the puncta staining pattern likely reflects post-synaptic clustering of GlyRs, this staining pattern in 24 hpf *glrbb* morphants indicates that GlyR α subunits are being expressed but fail to cluster at post-synapses. Gephyrin puncta are smaller than those in control and *glra1* morphants, and locate even more laterally relative to nuclei than in either *glra1* or control morphants (Figure 4.3D′).

In summary, both *glra1* and *glrbb* morphants exhibit reduced punctate GlyR α staining. In *glra1* morphants, this reduction occurred mostly in the middle spinal cord at 24 hpf; though remaining GlyR α still form in the lateral spinal cord, which presumably consist of other GlyR α subunits, colocalizing with gephyrin puncta. In *glrbb* morphants, GlyR α puncta are lost in both the middle and lateral spinal cord, which is likely explained by a failure of GlyRs to cluster at post-synaptic densities.

GlyR α puncta reduction shows different patterns in glra1 and glrbb morphants

Given the disrupted glycinergic synaptogenesis in *glra1* and *glrbb* morphants, we quantitatively analyzed the density of GlyR α puncta and the colocalization of GlyR α and gephyrin puncta in all the morphants. At 24 hpf, the expression regions of GlyR α puncta in spinal cord transverse sections are very different in control, *glra1* and *glrbb* morphants, making it difficult to conduct accurate comparison of GlyR α puncta density in different morphants. At 48 hpf, both *glra1*MOex4 and *glra1*MOex7 morphants exhibit significantly lower density of GlyR α puncta than control morphants ($p < 0.05$ for both *glra1*MOex4 and *glra1*MOex7), while GlyR α density in *glrbb* morphants is comparable with that in control morphants ($F(3,16) = 4.39$, $p = 0.02$; Table 4.1). Surprisingly, gephyrin density is maintained at the control morphant level in all *glra1* and *glrbb* morphants ($F(3,16) = 2.03$, $p = 0.15$; Figure 4.4A; Table 4.1).

The colocalization of GlyR α and gephyrin puncta also shows different patterns in different morphants. In control morphants, the proportion of GlyR α puncta colocalized with gephyrin is smaller at 24 hpf than at 48 hpf (Figure 4.3A and A′, and Figure 4.4A and C; Table 4.1). Curiously, at 24 hpf, while both *glra1*MOex4 and *glra1*MOex7 morphants

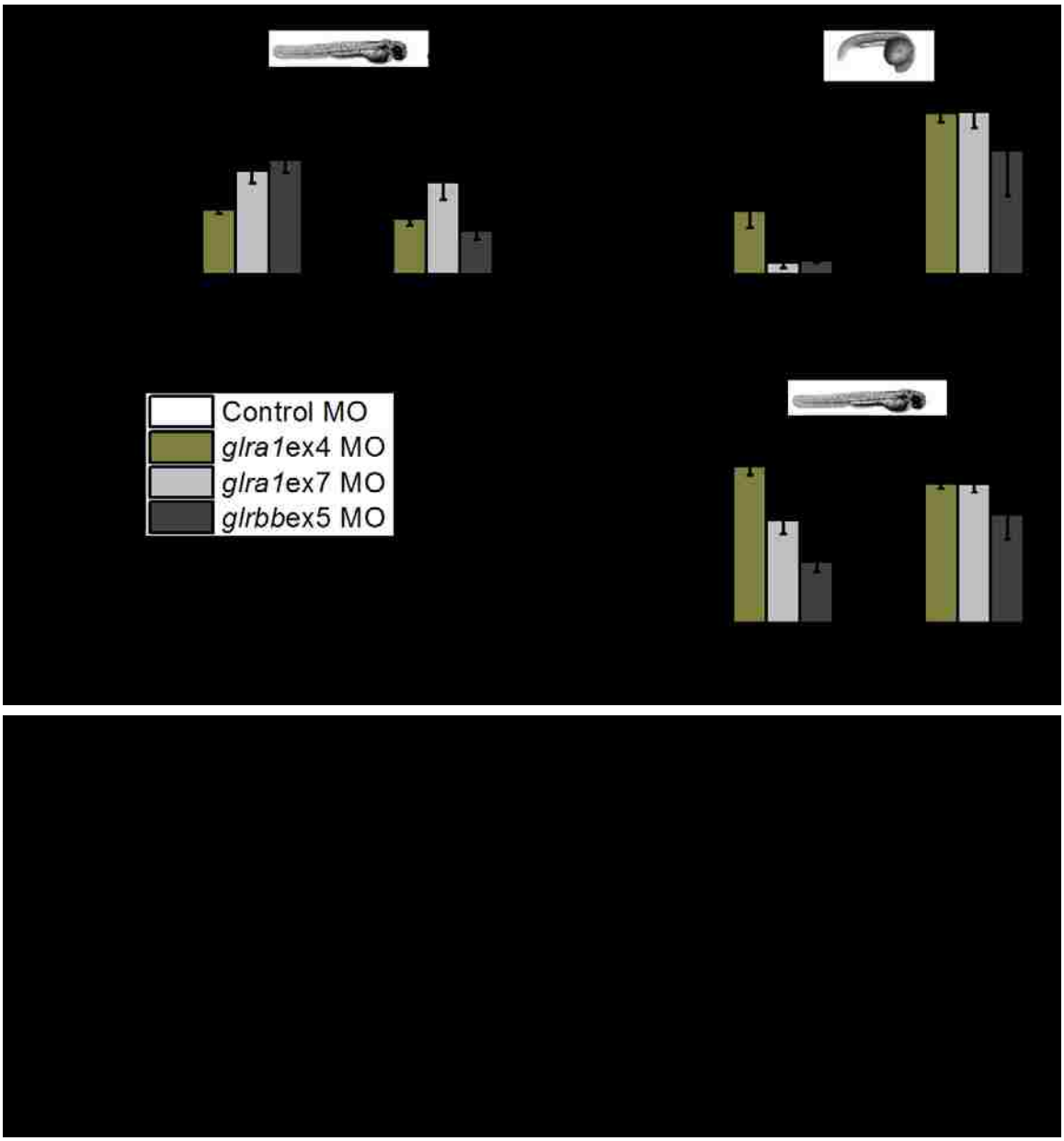

exhibit lateral colocalization of GlyR α and gephyrin puncta (Figure 4.3B and C), only *glra1*MOex4 morphants have significantly more GlyR α colocalized with gephyrin. *glra1*MOex7 morphants actually have a similar proportion of GlyR α colocalized with gephyrin as control morphants. As with *glra1*MOex7, *glrbb* morphants also exhibit significantly fewer GlyR α puncta colocalized with gephyrin (Figure 4.4B; Table 4.1).

Table 4.1 GlyR α and gephyrin puncta density and colocalization in morphants at 24 and 48 hpf

Numbers show GlyR α and gephyrin (GPHN) puncta densities, and proportions of GlyR α and gephyrin puncta colocalized with each other. Numbers correspond to the data in Figure 4.4. Numbers are shown in means +/- SEMs. 24 hpf: Control MO n = 7 fish, *glra1*ex4 MO n = 36fish, *glra1*ex7 MO n = 3 fish, *glrbb*ex5 MO n = 3 fish; 48 hpf: Control MO n = 6 fish, *glra1*ex4 MO n = 3 fish, *glra1*ex7 MO n = 7 fish, *glrbb*ex5 MO n = 5 fish.

			Control MO	***glra1*ex4 MO**	***glra1*ex7 MO**	***glrbb*ex5 MO**
Puncta density (μm^{-2}) 48 hpf		**GlyR α**	0.5332 ± 0.0889	0.1997 ± 0.0126	0.3182 ± 0.0381	0.3565 ± 0.0452
		GPHN	0.2352 ± 0.0367	0.1721 ± 0.0227	0.2844 ± 0.0537	0.1349 ± 0.0279
Proportion with colocalization	**24 hpf**	**GlyR α**	3.57 ± 0.41 %	27.85 ± 7.53 %	4.66 ± 2.32 %	5.65 ± 0.88 %
		GPHN	57.33 ± 3.94 %	71.22 ± 4.56 %	71.55 ± 7.21 %	57.76 ± 20.51 %
	48 hpf	**GlyR α**	47.44 ± 5.02 %	59.49 ± 4.25 %	45.65 ± 6.33 %	27.06 ± 4.66 %
		GPHN	66.05 ± 4.54 %	61.87 ± 2.46 %	61.34 ± 3.84 %	48.05 ± 10.92 %

At 48 hpf, the colocalization pattern changes; compared to 24 hpf, all the morphants have higher proportions of GlyR α puncta colocalized with gephyrin (Table 4.1). While *glra1*MOex4 morphants still have the largest proportion of GlyR α colocalized with gephyrin, the only significant difference observed exists between *glra1*MOex4 and *glrbb* morphants. Unlike *glra1*MOex4, *glra1*MOex7 morphants have similar colocalization proportion as control morphants (Figure 4.4C), which is probably due to a large number of peri-nuclear GlyR α puncta that fail to colocalize with gephyrin (Figure 4.4C′). This pattern likely represents GlyRs trapped intracellularly. This difference between *glra1*MOex4 and *glra1*MOex7 morphants can be explained by a failure of the GlyR α antibody to detect

intracellular GlyRs in *glra1*MOex4 morphants, since this antibody targets amino acids 96-105 that are missing in *glra1*MOex4 morphant α1 subunit. This also indicates that the GlyR α puncta observed in *glra1*MOex4 morphants likely consist of other GlyR α subunits. On the other hand, the significant difference between *glra1*MOex4 and *glrbb* morphants also shows that the colocalization between GlyR and gephyrin is disrupted in *glrbb* morphants.

In summary, our quantitative analysis reveals that knocking down the α1 and βb subunits leads to different patterns of glycinergic synaptogenesis: knocking down the α1 subunit leads to a reduction of GlyR puncta while knocking down the βb subunit disrupts the colocalization of GlyR and gephyrin.

glrbb morphants exhibit more severe motor defects than glra1 morphants

Compared to control morphants, both *glra1* and *glrbb* morphants exhibit spastic and erratic behaviors during 24-36 hpf. Spastic behaviors are characterized by hitches, defined as pauses that interrupt the smooth progression of alternating left-right bending during movements. Behaviors of these morphants were also erratic, lacking stereotypy when elicited multiple times. Compared to control morphants, *glra1* and *glrbb* morphants exhibit significantly longer latency from rest to the first coil ($F(3,334) = 15.8225$, $p = 0.0001$; $p < 0.05$ for all the three pairwise comparisons; control MO 109 ± 1.21 ms, n = 83 fish, *glra1*MOex4 296 ± 1.87 ms, n = 93 fish, *glra1*MOex7 444 ± 5.81 ms, n = 93 fish; *glrbb*MOex5 241 ± 3.97 ms, n = 69 fish; Figure 4.5A). Hitches were also observed in all *glra1* and *glrbb* morphants (Figure 4.5B). In addition to lengthened latency and spasticity, *glrbb* morphants also exhibit the accordion phenotype, which is characterized by

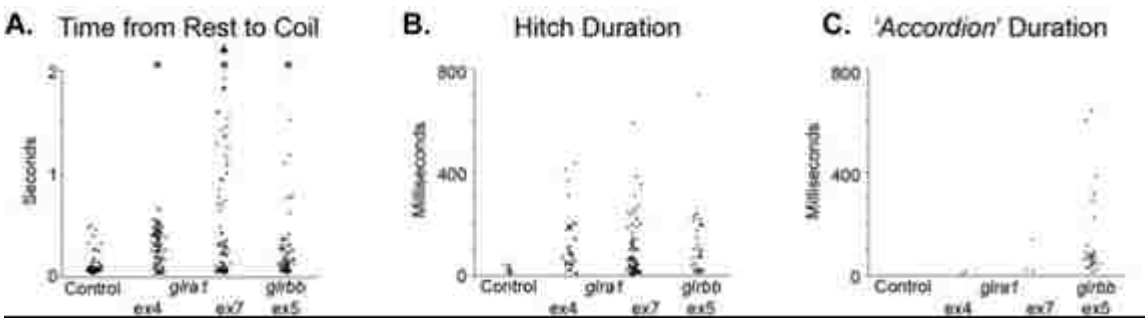

simultaneous bilateral contraction of trunk muscles that shortens the body axis[178] (Figure 4.5C).

In summary, *glra1* and *glrbb* morphants both exhibit defects in embryonic rhythmic motor behaviors. However, similar to human patients with mutations in *GLRA1* and *GLRB* genes, *glrbb* morphants also exhibit more severe motor defects than *glra1* morphants, especially with the accordion phenotype.

Discussion

Our study demonstrated that knocking down *glrbb* gene disrupts colocalization of GlyR and gephyrin, which corresponds to the more severe accordion phenotype compared to *glra1* morphants. Our findings are consistent with the clinical phenotypes of human startle disease patients with mutations in *GLRB* gene, and indicates that such clinical phenotypes

are likely associated with lack of interaction between GlyR and post-synaptic scaffolding protein gephyrin.

Knocking down GlyR α1 and βb subunits impose different impacts on motor behaviors and glycinergic synaptogenesis

In this study, knocking down the βb subunit leads to an accordion phenotype which is caused by a lack of proper inhibition in the spinal circuit. This phenotype is nearly absent in the *glrα1* morphants, suggesting the βb subunit leads to a more severe defects in glycine transmission. Therefore, the binding of GlyRs to gephyrin is critical for synaptic glycine transmission. The GlyR puncta are nearly absent pattern in *glrbb* morphant (Figure 4.3D and D′), which is consistent with a previous study which demonstrated that the clustering of GlyRs at post-synapses is completely dependent on gephyrin, and is very sensitive to disruption of their interaction with gephyrin[206]. In addition, previous studies have shown that the GlyR α4a subunit is also important for glycine transmission in zebrafish spinal cord[171, 207]. Therefore, in *glra1* morphants, GlyR α puncta can still be observed in the immunostaining, indicating that other α subunits, likely α4a subunits, substitute the α1 subunit, thus leads to a less severe phenotype.

Although there is a decrease of GlyR puncta in both *glra1* and *glrbb* morphants, none of the morphants exhibits changes in the number of gephyrin puncta. Even in *glrbb* morphants which exhibit dimmer gephyrin puncta, the number of the puncta remains at the control level. This suggests that the knockdown of GlyR subunits decreases the number of functional glycinergic synapses, but does not change the number of glycinergic synapses formed. This is unexpected since a previous study have found that knocking down γ2-

$GABA_A$ receptors in rat hippocampal culture decreases the density of gephyrin puncta[69]. Such difference in results may be due to the distinct interaction between the receptor and gephyrin[206]. Alternatively, it could also be a time-dependent phenomenon. Since morpholino knockdown are only reliably effective in the first couple of days[200], we did not examine long-term impacts on the number of gephyrin puncta. Future study with long-term knockdown of the GlyR βb subunit would better elucidate how the number of inhibitory synapses is impacted after disruption of GlyR clustering. Despite of the lack of change in gephyrin puncta number in the *glra1* and *glrbb* morphants, gephyrin puncta distribution shifts to the very lateral in the spinal cord in all the *glra1* and *glrbb* morphants, suggesting that knocking down functional receptors alters the spatial pattern of glycinergic synaptogenesis.

Impacts of knocking down GlyR subunits on early spinal cord development

Both *glra1* and *glrbb* morphants lack the GlyRs form puncta in the middle of the spinal cord, a region occupied by precursors in 24 hpf control morphants. While the roles of GlyRs in the spinal precursors at 24 hpf still need to be elucidated in future studies, since the activation of GlyRs depolarizes the post-synaptic neurons in early development of the nervous system, it is possible that those GlyRs provide needed activity for the differentiation of the precursors[138]. Therefore, the lack of medial GlyR puncta in 24 hpf *glra1* and *glrbb* may cause potential changes in the spinal circuit development.

Conclusions

By knocking down GlyR α1 and βb subunits with splice site-targeting morpholinos, we determined the role of these subunits in glycinergic synaptogenesis and rhythmic motor

behaviors. We found that a deduction of GlyR puncta in *glra1* morphants, and disrupted colocalization of GlyR and gephyrin in *glrbb* morphants. In all these morphants, the spatial pattern of gephyrin puncta alters without a change in puncta numbers. The defects in glycine transmission in morphants leads to defects in rhythmic motor behaviors; both *glra1* and *glrbb* morphants exhibit spastic and erratic behaviors, while *glrbb* morphants also exhibit the bilateral contraction "accordion" phenotype. Our results indicate that the binding of βb subunit to gephyrin is critical for glycinergic transmission and the formation of functional glycinergic synapses, and that the failure of GlyR clustering at post-synapses is associated with the additional accordion phenotype. Our study also provides meaningful insights into understanding the neuronal mechanisms of human startle disease, and offers a valuable reference for future work that aim to model startle disease in zebrafish.

Chapter 5: Future Perspectives

In these studies, we investigated the spatial and temporal patterning of synapses that associates to E/I balance in zebrafish spinal cord circuit. In Chapter 2, we found a stable medial-lateral (M-L) pattern of excitatory and inhibitory synapses and neuronal processes at the systems level, which is maintained during circuit development. This suggests a stable pattern of excitatory and inhibitory synapses does exist at the systems level during circuit development. In Chapter 3, we found that this systems pattern is still maintained in the presence of genetic perturbation of E/I balance in the *glycine transporter 1* (*glyt1*) mutant, however, synapse spatial patterns do change in subtle scales at the beginning of E/I balance re-establishment in the *glyt1* mutants. This indicates that re-establishment of E/I balance after perturbations is associated with changes in synapse spatial patterning, but only at fine scales. In Chapter 4, we found that knocking down GlyR α1 and βb subunits disrupts motor behaviors and glycinergic synaptogenesis via different mechanisms, while both knockdowns alter the spatial patterning of inhibitory synapses. Therefore, multi-level spatial patterings of synapses exist in zebrafish spinal circuits, and are regulated in different ways in response to perturbations of E/I balance.

These findings lead to a model for the spatial patterning of excitatory and inhibitory synapses in zebrafish spinal cord: the system-level patterning provides a stable framework for the general distributions of excitatory and inhibitory synapses, which is fundamental for the circuit function and robust in developmental changes and genetic or environmental perturbations; the fine-scale patterning of synapses is flexible, allowing multiple resolutions for the spatial patterning, and alters in a timely manner in response to E/I balance perturbations. In other words, flexible fine-scale patterning changes to serve as a

"buffering zone" to maintain the stable, systems-level patterning by subtle changes of synapse distributions.

This model explains the observations during spinal cord development, in the *glyt1* mutants, and in the *glra1* and *glrbb* morphants, but still needs to be tested by future studies. Due to the natural re-establishment of E/I balance, the zebrafish *glyt1* mutant provides a feasible system for testing this hypothetic model. Since the *glyt1* mutants used in our study carries the weakest allele compare to other available ones[177, 178], the "buffering" functions of fine-scale patterning of synapses can be tested by comparing changes in the fine-scale synapse patterning in *glyt1* mutants with weak and strong alleles. For the systems-level synapse patterning, if it is fundamental for E/I balance, then it would be required for the motor recovery of the *glyt1* mutant. Since the *glyt1* mutant recovery is activity-dependent (my unpublished data), examining the systems-level patterning in *glyt1* mutants with activity blockage will likely provide insights into the association between the systems-level patterning and E/I balance re-establishment. However, the direct test for the necessity of the systems-level patterning in re-establishment or maintenance of E/I balance would need direct manipulation of synapse patterns, which requires better understanding of the causal mechanisms of synapse patterning, an important topic for further studies.

Elucidating the relationship between E/I balance and spatial patterning of synapses at different levels is an essential step to understand the connectivity and the formation of *in vivo* neural circuits, and to predict possible alterations in the circuit wiring in varied circumstances, e.g. at specific development stages or in particular diseases. Given the association between synaptogenesis, E/I balance and many neurological disorders in

humans[5, 7, 176, 208], this understanding would also shed light on potential treatments of these neurological disorders.

References

1. Mongeon, R., M.R. Gleason, M.A. Masino, J.R. Fetcho, G. Mandel, P. Brehm, and J.E. Dallman, *Synaptic homeostasis in a zebrafish glial glycine transporter mutant.* J Neurophysiol, 2008. **100**(4): p. 1716-23.

2. Ganser, L.R. and J.E. Dallman, *Glycinergic synapse development, plasticity, and homeostasis in zebrafish.* Front Mol Neurosci, 2009. **2**: p. 30.

3. Goulding, M., *Circuits controlling vertebrate locomotion: moving in a new direction.* Nat Rev Neurosci, 2009. **10**(7): p. 507-18.

4. Brustein, E., L. Saint-Amant, R.R. Buss, M. Chong, J.R. Mcdearmid, and P. Drapeau, *Steps during the development of the zebrafish locomotor network.* J Physiol Paris, 2003. **97**(1): p. 77-86.

5. Eichler, S.A. and J.C. Meier, *E-I balance and human diseases - from molecules to networking.* Front Mol Neurosci, 2008. **1**: p. 2.

6. Harvey, R.J., M. Topf, K. Harvey, and M.I. Rees, *The genetics of hyperekplexia: more than startle!* Trends Genet, 2008. **24**(9): p. 439-47.

7. Cline, H., *Synaptogenesis: a balancing act between excitation and inhibition.* Curr Biol, 2005. **15**(6): p. R203-5.

8. Gatto, C.L. and K. Broadie, *Genetic controls balancing excitatory and inhibitory synaptogenesis in neurodevelopmental disorder models.* Front Synaptic Neurosci, 2010. **2**: p. 4.

9. Davis, G.W., *Homeostatic control of neural activity: from phenomenology to molecular design.* Annu Rev Neurosci, 2006. **29**: p. 307-23.

10. Turrigiano, G., *Homeostatic signaling: the positive side of negative feedback.* Curr Opin Neurobiol, 2007. **17**(3): p. 318-24.

11. Davis, G.W., *Homeostatic signaling and the stabilization of neural function.* Neuron, 2013. **80**(3): p. 718-28.

12. Turrigiano, G.G., K.R. Leslie, N.S. Desai, L.C. Rutherford, and S.B. Nelson, *Activity-dependent scaling of quantal amplitude in neocortical neurons.* Nature, 1998. **391**(6670): p. 892-6.

13. Hartman, K.N., S.K. Pal, J. Burrone, and V.N. Murthy, *Activity-dependent regulation of inhibitory synaptic transmission in hippocampal neurons.* Nat Neurosci, 2006. **9**(5): p. 642-9.

14. Rocha, M. and M. Sur, *Rapid acquisition of dendritic spines by visual thalamic neurons after blockade of N-methyl-D-aspartate receptors.* Proc Natl Acad Sci U S A, 1995. **92**(17): p. 8026-30.

15. Burrone, J., M. O'byrne, and V.N. Murthy, *Multiple forms of synaptic plasticity triggered by selective suppression of activity in individual neurons.* Nature, 2002. **420**(6914): p. 414-8.

16. Wierenga, C.J., K. Ibata, and G.G. Turrigiano, *Postsynaptic expression of homeostatic plasticity at neocortical synapses.* J Neurosci, 2005. **25**(11): p. 2895-905.

17. Buckby, L.E., T.P. Jensen, P.J. Smith, and R.M. Empson, *Network stability through homeostatic scaling of excitatory and inhibitory synapses following inactivity in CA3 of rat organotypic hippocampal slice cultures.* Mol Cell Neurosci, 2006. **31**(4): p. 805-16.

18. Ibata, K., Q. Sun, and G.G. Turrigiano, *Rapid synaptic scaling induced by changes in postsynaptic firing.* Neuron, 2008. **57**(6): p. 819-26.

19. Levi, S., C. Schweizer, H. Bannai, O. Pascual, C. Charrier, and A. Triller, *Homeostatic regulation of synaptic GlyR numbers driven by lateral diffusion.* Neuron, 2008. **59**(2): p. 261-73.

20. Davis, G.W. and C.S. Goodman, *Synapse-specific control of synaptic efficacy at the terminals of a single neuron.* Nature, 1998. **392**(6671): p. 82-6.

21. Diantonio, A., S.A. Petersen, M. Heckmann, and C.S. Goodman, *Glutamate receptor expression regulates quantal size and quantal content at the Drosophila neuromuscular junction.* J Neurosci, 1999. **19**(8): p. 3023-32.

22. Goold, C.P. and G.W. Davis, *The BMP ligand Gbb gates the expression of synaptic homeostasis independent of synaptic growth control.* Neuron, 2007. **56**(1): p. 109-23.

23. Knott, G.W., C. Quairiaux, C. Genoud, and E. Welker, *Formation of dendritic spines with GABAergic synapses induced by whisker stimulation in adult mice.* Neuron, 2002. **34**(2): p. 265-73.

24. Chen, J.L., K.L. Villa, J.W. Cha, P.T. So, Y. Kubota, and E. Nedivi, *Clustered dynamics of inhibitory synapses and dendritic spines in the adult neocortex.* Neuron, 2012. **74**(2): p. 361-73.

25. Kishore, S. and J.R. Fetcho, *Homeostatic regulation of dendritic dynamics in a motor map in vivo.* Nat Commun, 2013. **4**: p. 2086.

26. Desai, N.S., R.H. Cudmore, S.B. Nelson, and G.G. Turrigiano, *Critical periods for experience-dependent synaptic scaling in visual cortex.* Nat Neurosci, 2002. **5**(8): p. 783-9.

27. Maffei, A., S.B. Nelson, and G.G. Turrigiano, *Selective reconfiguration of layer 4 visual cortical circuitry by visual deprivation.* Nat Neurosci, 2004. **7**(12): p. 1353-9.

28. Goel, A., B. Jiang, L.W. Xu, L. Song, A. Kirkwood, and H.K. Lee, *Cross-modal regulation of synaptic AMPA receptors in primary sensory cortices by visual experience.* Nat Neurosci, 2006. **9**(8): p. 1001-3.

29. Goel, A. and H.K. Lee, *Persistence of experience-induced homeostatic synaptic plasticity through adulthood in superficial layers of mouse visual cortex.* J Neurosci, 2007. **27**(25): p. 6692-700.

30. Maffei, A. and G.G. Turrigiano, *Multiple modes of network homeostasis in visual cortical layer 2/3.* J Neurosci, 2008. **28**(17): p. 4377-84.

31. Deeg, K.E. and C.D. Aizenman, *Sensory modality-specific homeostatic plasticity in the developing optic tectum.* Nat Neurosci, 2011. **14**(5): p. 548-50.

32. Keck, T., Georg b. Keller, R.I. Jacobsen, Ulf t. Eysel, T. Bonhoeffer, and M. Hübener, *Synaptic scaling and homeostatic plasticity in the mouse visual cortex in vivo.* Neuron, 2013. **80**(2): p. 327-334.

33. Knogler, L.D., M. Liao, and P. Drapeau, *Synaptic scaling and the development of a motor network.* J Neurosci, 2010. **30**(26): p. 8871-81.

34. Borodinsky, L.N., C.M. Root, J.A. Cronin, S.B. Sann, H.L. Gu, and N.C. Spitzer, *Activity-dependent homeostatic specification of transmitter expression in embryonic neurons.* Nature, 2004. **429**: p. 523-30.

35. West, A.E. and M.E. Greenberg, *Neuronal activity-regulated gene transcription in synapse development and cognitive function.* Cold Spring Harb Perspect Biol, 2011. **3**(6).

36. Vitureira, N., M. Letellier, and Y. Goda, *Homeostatic synaptic plasticity: from single synapses to neural circuits.* Curr Opin Neurobiol, 2012. **22**(3): p. 516-521.

37. Liu, Z., J. Golowasch, E. Marder, and L.F. Abbott, *A model neuron with activity-dependent conductances regulated by multiple calcium sensors.* J Neurosci, 1998. **18**(7): p. 2309-20.

38. Sutton, M.A., N.R. Wall, G.N. Aakalu, and E.M. Schuman, *Regulation of dendritic protein synthesis by miniature synaptic events.* Science, 2004. **304**(5679): p. 1979-83.

39. Sutton, M.A., A.M. Taylor, H.T. Ito, A. Pham, and E.M. Schuman, *Postsynaptic decoding of neural activity: eEF2 as a biochemical sensor coupling miniature synaptic transmission to local protein synthesis.* Neuron, 2007. **55**(4): p. 648-61.

40. Laplante, M. and D.M. Sabatini, *mTOR signaling in growth control and disease.* Cell, 2012. **149**(2): p. 274-93.

41. Bateup, H.S., C.A. Johnson, C.L. Denefrio, J.L. Saulnier, K. Kornacker, and B.L. Sabatini, *Excitatory/inhibitory synaptic imbalance leads to hippocampal hyperexcitability in mouse models of tuberous sclerosis.* Neuron, 2013. **78**(3): p. 510-22.

42. Penney, J., K. Tsurudome, E.H. Liao, F. Elazzouzi, M. Livingstone, M. Gonzalez, N. Sonenberg, and A.P. Haghighi, *TOR is required for the retrograde regulation of synaptic homeostasis at the Drosophila neuromuscular junction.* Neuron, 2012. **74**(1): p. 166-78.

43. Muller, M. and G.W. Davis, *Transsynaptic control of presynaptic Ca(2)(+) influx achieves homeostatic potentiation of neurotransmitter release.* Curr Biol, 2012. **22**(12): p. 1102-8.

44. Muller, M., E.C. Pym, A. Tong, and G.W. Davis, *Rab3-GAP controls the progression of synaptic homeostasis at a late stage of vesicle release.* Neuron, 2011. **69**(4): p. 749-62.

45. Weyhersmuller, A., S. Hallermann, N. Wagner, and J. Eilers, *Rapid active zone remodeling during synaptic plasticity.* J Neurosci, 2011. **31**(16): p. 6041-52.

46. Muller, M., K.S. Liu, S.J. Sigrist, and G.W. Davis, *RIM controls homeostatic plasticity through modulation of the readily-releasable vesicle pool.* J Neurosci, 2012. **32**(47): p. 16574-85.

47. Goddard, C.A., D.A. Butts, and C.J. Shatz, *Regulation of CNS synapses by neuronal MHC class I.* Proc Natl Acad Sci U S A, 2007. **104**(16): p. 6828-33.

48. Jakawich, S.K., H.B. Nasser, M.J. Strong, A.J. Mccartney, A.S. Perez, N. Rakesh, C.J. Carruthers, and M.A. Sutton, *Local presynaptic activity gates homeostatic changes in presynaptic function driven by dendritic BDNF synthesis.* Neuron, 2010. **68**(6): p. 1143-58.

49. Steinmetz, C.C. and G.G. Turrigiano, *Tumor necrosis factor-alpha signaling maintains the ability of cortical synapses to express synaptic scaling.* J Neurosci, 2010. **30**(44): p. 14685-90.

50. Hu, J.H., J.M. Park, S. Park, B. Xiao, M.H. Dehoff, S. Kim, T. Hayashi, M.K. Schwarz, R.L. Huganir, P.H. Seeburg, D.J. Linden, and P.F. Worley, *Homeostatic scaling requires group I mGluR activation mediated by Homer1a.* Neuron, 2010. **68**(6): p. 1128-42.

51. Pak, D.T. and M. Sheng, *Targeted protein degradation and synapse remodeling by an inducible protein kinase.* Science, 2003. **302**(5649): p. 1368-73.

52. Seeburg, D.P., M. Feliu-Mojer, J. Gaiottino, D.T. Pak, and M. Sheng, *Critical role of CDK5 and Polo-like kinase 2 in homeostatic synaptic plasticity during elevated activity.* Neuron, 2008. **58**(4): p. 571-83.

53. Seeburg, D.P. and M. Sheng, *Activity-induced Polo-like kinase 2 is required for homeostatic plasticity of hippocampal neurons during epileptiform activity.* J Neurosci, 2008. **28**(26): p. 6583-91.

54. Lee, K.J., Y. Lee, A. Rozeboom, J.Y. Lee, N. Udagawa, H.S. Hoe, and D.T. Pak, *Requirement for Plk2 in orchestrated ras and rap signaling, homeostatic structural plasticity, and memory.* Neuron, 2011. **69**(5): p. 957-73.

55. Chowdhury, S., J.D. Shepherd, H. Okuno, G. Lyford, R.S. Petralia, N. Plath, D. Kuhl, R.L. Huganir, and P.F. Worley, *Arc/Arg3.1 interacts with the endocytic machinery to regulate AMPA receptor trafficking.* Neuron, 2006. **52**(3): p. 445-59.

56. Shepherd, J.D., G. Rumbaugh, J. Wu, S. Chowdhury, N. Plath, D. Kuhl, R.L. Huganir, and P.F. Worley, *Arc/Arg3.1 mediates homeostatic synaptic scaling of AMPA receptors.* Neuron, 2006. **52**(3): p. 475-84.

57. Chang, M.C., J.M. Park, K.A. Pelkey, H.L. Grabenstatter, D. Xu, D.J. Linden, T.P. Sutula, C.J. Mcbain, and P.F. Worley, *Narp regulates homeostatic scaling of excitatory synapses on parvalbumin-expressing interneurons.* Nat Neurosci, 2010. **13**(9): p. 1090-7.

58. Blackman, M.P., B. Djukic, S.B. Nelson, and G.G. Turrigiano, *A critical and cell-autonomous role for MeCP2 in synaptic scaling up.* J Neurosci, 2012. **32**(39): p. 13529-36.

59. Qiu, Z., E.L. Sylwestrak, D.N. Lieberman, Y. Zhang, X.Y. Liu, and A. Ghosh, *The Rett syndrome protein MeCP2 regulates synaptic scaling.* J Neurosci, 2012. **32**(3): p. 989-94.

60. Zhong, X., H. Li, and Q. Chang, *MeCP2 phosphorylation is required for modulating synaptic scaling through mGluR5.* J Neurosci, 2012. **32**(37): p. 12841-7.

61. Bloodgood, B.L., N. Sharma, H.A. Browne, A.Z. Trepman, and M.E. Greenberg, *The activity-dependent transcription factor NPAS4 regulates domain-specific inhibition.* Nature, 2013. **503**(7474): p. 121-5.

62. Ehlers, M.D., *Activity level controls postsynaptic composition and signaling via the ubiquitin-proteasome system.* Nat Neurosci, 2003. **6**(3): p. 231-42.

63. Jakawich, S.K., R.M. Neely, S.N. Djakovic, G.N. Patrick, and M.A. Sutton, *An essential postsynaptic role for the ubiquitin proteasome system in slow homeostatic synaptic plasticity in cultured hippocampal neurons.* Neuroscience, 2010. **171**(4): p. 1016-31.

64. Bingol, B. and E.M. Schuman, *Activity-dependent dynamics and sequestration of proteasomes in dendritic spines.* Nature, 2006. **441**(7097): p. 1144-8.

65. Prange, O., T.P. Wong, K. Gerrow, Y.T. Wang, and A. El-Husseini, *A balance between excitatory and inhibitory synapses is controlled by PSD-95 and neuroligin.* Proc Natl Acad Sci U S A, 2004. **101**(38): p. 13915-20.

66. Keith, D. and A. El-Husseini, *Excitation control: balancing PSD-95 function at the synapse.* Front Mol Neurosci, 2008. **1**: p. 4.

67. Sun, Q. and G.G. Turrigiano, *PSD-95 and PSD-93 play critical but distinct roles in synaptic scaling up and down.* J Neurosci, 2011. **31**(18): p. 6800-8.

68. Varley, Z.K., R. Pizzarelli, R. Antonelli, S.H. Stancheva, M. Kneussel, E. Cherubini, and P. Zacchi, *Gephyrin regulates GABAergic and glutamatergic synaptic transmission in hippocampal cell cultures.* J Biol Chem, 2011. **286**(23): p. 20942-51.

69. Yu, W. and A.L. De Blas, *Gephyrin expression and clustering affects the size of glutamatergic synaptic contacts.* J Neurochem, 2008. **104**(3): p. 830-45.

70. Anggono, V., R.L. Clem, and R.L. Huganir, *PICK1 loss of function occludes homeostatic synaptic scaling.* J Neurosci, 2011. **31**(6): p. 2188-96.

71. Chih, B., H. Engelman, and P. Scheiffele, *Control of excitatory and inhibitory synapse formation by neuroligins.* Science, 2005. **307**(5713): p. 1324-8.

72. Chubykin, A.A., D. Atasoy, M.R. Etherton, N. Brose, E.T. Kavalali, J.R. Gibson, and T.C. Sudhof, *Activity-dependent validation of excitatory versus inhibitory synapses by neuroligin-1 versus neuroligin-2.* Neuron, 2007. **54**(6): p. 919-31.

73. Wang, G., J. Gilbert, and H.Y. Man, *AMPA receptor trafficking in homeostatic synaptic plasticity: functional molecules and signaling cascades.* Neural Plast, 2012. **2012**: p. 825364.

74. Glebov, O.O., C.M. Tigaret, J.R. Mellor, and J.M. Henley, *Clathrin-independent trafficking of AMPA receptors.* J Neurosci, 2015. **35**(12): p. 4830-6.

75. Perez-Otano, I. and M.D. Ehlers, *Homeostatic plasticity and NMDA receptor trafficking.* Trends Neurosci, 2005. **28**(5): p. 229-38.

76. Moscato, E.H., X. Peng, A. Jain, T.D. Parsons, J. Dalmau, and R.J. Balice-Gordon, *Acute mechanisms underlying antibody effects in anti-N-methyl-D-aspartate receptor encephalitis.* Ann Neurol, 2014. **76**(1): p. 108-19.

77. Rutherford, L.C., S.B. Nelson, and G.G. Turrigiano, *BDNF has opposite effects on the quantal amplitude of pyramidal neuron and interneuron excitatory synapses.* Neuron, 1998. **21**(3): p. 521-30.

78. Correa, S.A., C.J. Hunter, O. Palygin, S.C. Wauters, K.J. Martin, C. Mckenzie, K. Mckelvey, R.G. Morris, Y. Pankratov, J.S. Arthur, and B.G. Frenguelli, *MSK1 regulates homeostatic and experience-dependent synaptic plasticity.* J Neurosci, 2012. **32**(38): p. 13039-51.

79. Beattie, E.C., D. Stellwagen, W. Morishita, J.C. Bresnahan, B.K. Ha, M. Von Zastrow, M.S. Beattie, and R.C. Malenka, *Control of synaptic strength by glial TNFalpha.* Science, 2002. **295**(5563): p. 2282-5.

80. Stellwagen, D., E.C. Beattie, J.Y. Seo, and R.C. Malenka, *Differential regulation of AMPA receptor and GABA receptor trafficking by tumor necrosis factor-alpha.* J Neurosci, 2005. **25**(12): p. 3219-28.

81. Stellwagen, D. and R.C. Malenka, *Synaptic scaling mediated by glial TNF-alpha.* Nature, 2006. **440**(7087): p. 1054-9.

82. Mcgeachie, A.B., L.A. Cingolani, and Y. Goda, *Stabilising influence: integrins in regulation of synaptic plasticity.* Neurosci Res, 2011. **70**(1): p. 24-9.

83. Wang, H.L., Z. Zhang, M. Hintze, and L. Chen, *Decrease in calcium concentration triggers neuronal retinoic acid synthesis during homeostatic synaptic plasticity.* J Neurosci, 2011. **31**(49): p. 17764-71.

84. Sarti, F., J. Schroeder, J. Aoto, and L. Chen, *Conditional RARalpha knockout mice reveal acute requirement for retinoic acid and RARalpha in homeostatic plasticity.* Front Mol Neurosci, 2012. **5**: p. 16.

85. Chao, H.T., H.Y. Zoghbi, and C. Rosenmund, *MeCP2 controls excitatory synaptic strength by regulating glutamatergic synapse number.* Neuron, 2007. **56**(1): p. 58-65.

86. Lin, Y., B.L. Bloodgood, J.L. Hauser, A.D. Lapan, A.C. Koon, T.K. Kim, L.S. Hu, A.N. Malik, and M.E. Greenberg, *Activity-dependent regulation of inhibitory synapse development by Npas4.* Nature, 2008. **455**(7217): p. 1198-204.

87. Banovic, D., O. Khorramshahi, D. Owald, C. Wichmann, T. Riedt, W. Fouquet, R. Tian, S.J. Sigrist, and H. Aberle, *Drosophila neuroligin 1 promotes growth and postsynaptic differentiation at glutamatergic neuromuscular junctions.* Neuron, 2010. **66**(5): p. 724-38.

88. Levinson, J.N. and A. El-Husseini, *Building excitatory and inhibitory synapses: balancing neuroligin partnerships.* Neuron, 2005. **48**(2): p. 171-4.

89. Varoqueaux, F., G. Aramuni, R.L. Rawson, R. Mohrmann, M. Missler, K. Gottmann, W. Zhang, T.C. Sudhof, and N. Brose, *Neuroligins determine synapse maturation and function.* Neuron, 2006. **51**(6): p. 741-54.

90. Niell, C.M., M.P. Meyer, and S.J. Smith, *In vivo imaging of synapse formation on a growing dendritic arbor.* Nat Neurosci, 2004. **7**(3): p. 254-60.

91. Meyer, M.P. and S.J. Smith, *Evidence from in vivo imaging that synaptogenesis guides the growth and branching of axonal arbors by two distinct mechanisms.* J Neurosci, 2006. **26**(13): p. 3604-14.

92. Nikolaou, N. and M.P. Meyer, *Imaging circuit formation in zebrafish.* Dev Neurobiol, 2012. **72**(3): p. 346-357.

93. Corbetta, S., S. Gualdoni, G. Ciceri, M. Monari, E. Zuccaro, V.L. Tybulewicz, and I. De Curtis, *Essential role of Rac1 and Rac3 GTPases in neuronal development.* FASEB J, 2009. **23**(5): p. 1347-57.

94. Vicario-Abejon, C., D. Owens, R. Mckay, and M. Segal, *Role of neurotrophins in central synapse formation and stabilization.* Nat Rev Neurosci, 2002. **3**(12): p. 965-74.

95. Kellom, M., M. Basselin, V.L. Keleshian, M. Chen, S.I. Rapoport, and J.S. Rao, *Dose-dependent changes in neuroinflammatory and arachidonic acid cascade markers with synaptic marker loss in rat lipopolysaccharide infusion model of neuroinflammation.* BMC Neurosci, 2012. **13**: p. 50.

96. Rao, J.S., M. Kellom, H.W. Kim, S.I. Rapoport, and E.A. Reese, *Neuroinflammation and synaptic loss.* Neurochem Res, 2012. **37**(5): p. 903-10.

97. Shen, K. and P. Scheiffele, *Genetics and cell biology of building specific synaptic connectivity.* Annu Rev Neurosci, 2010. **33**: p. 473-507.

98. Liu, G., *Local structural balance and functional interaction of excitatory and inhibitory synapses in hippocampal dendrites.* Nat Neurosci, 2004. **7**(4): p. 373-9.

99. Gulyás, A.I., M. Megías, Z. Emri, and T.F. Freund, *Total number and ratio of excitatory and inhibitory synapses converging onto single interneurons of different types in the CA1 area of the rat hippocampus.* J Neurosci, 1999. **19**(22): p. 10082-97.

100. Megias, M., Z. Emri, T.F. Freund, and A.I. Gulyas, *Total number and distribution of inhibitory and excitatory synapses on hippocampal CA1 pyramidal cells.* Neuroscience, 2001. **102**(3): p. 527-540.

101. Tripodi, M. and S. Arber, *Regulation of motor circuit assembly by spatial and temporal mechanisms.* Curr Opin Neurobiol, 2012. **22**(4): p. 615-23.

102. Baier, H., *Synaptic laminae in the visual system: molecular mechanisms forming layers of perception.* Annu Rev Cell Dev Biol, 2013. **29**: p. 385-416.

103. Mclean, D.L., M.A. Masino, I.Y. Koh, W.B. Lindquist, and J.R. Fetcho, *Continuous shifts in the active set of spinal interneurons during changes in locomotor speed.* Nat Neurosci, 2008. **11**(12): p. 1419-29.

104. Mclean, D.L. and J.R. Fetcho, *Spinal Interneurons Differentiate Sequentially from Those Driving the Fastest Swimming Movements in Larval Zebrafish to Those Driving the Slowest Ones.* J Neurosci, 2009. **29**(43): p. 13566-13577.

105. Kinkhabwala, A., M. Riley, M. Koyama, J. Monen, C. Satou, Y. Kimura, S. Higashijima, and J. Fetcho, *A structural and functional ground plan for neurons in the hindbrain of zebrafish.* Proc Natl Acad Sci U S A, 2011. **108**(3): p. 1164-9.

106. Brustein, E., N. Marandi, Y. Kovalchuk, P. Drapeau, and A. Konnerth, *"In vivo" monitoring of neuronal network activity in zebrafish by two-photon Ca(2+) imaging.* Pflugers Arch, 2003. **446**(6): p. 766-73.

107. Higashijima, S., G. Mandel, and J.R. Fetcho, *Distribution of prospective glutamatergic, glycinergic, and GABAergic neurons in embryonic and larval zebrafish.* J Comp Neurol, 2004. **480**(1): p. 1-18.

108. Craig, A.M., G. Banker, W. Chang, M.E. Mcgrath, and A.S. Serpinskaya, *Clustering of gephyrin at GABAergic but not glutamatergic synapses in cultured rat hippocampal neurons.* J Neurosci, 1996. **16**(10): p. 3166-77.

109. Wiegand, T. and K.A. Moloney, *Rings, circles, and null-models for point pattern analysis in ecology.* Oikos, 2004. **104**(2): p. 209-229.

110. Wiegand, T. and K.A. Moloney, *Handbook of spatial point-pattern analysis in ecology*. Chapman & Hall/CRDC applied environmental statistics. 2014, Boca Raton, FL: Chapman and Hall/CRC press. 1 online resource.

111. Mclean, D.L., J. Fan, S. Higashijima, M.E. Hale, and J.R. Fetcho, *A topographic map of recruitment in spinal cord.* Nature, 2007. **446**(7131): p. 71-5.

112. Miyasaka, N., K. Morimoto, T. Tsubokawa, S. Higashijima, H. Okamoto, and Y. Yoshihara, *From the olfactory bulb to higher brain centers: genetic visualization of secondary olfactory pathways in zebrafish.* J Neurosci, 2009. **29**(15): p. 4756-67.

113. Kimmel, C.B., W.W. Ballard, S.R. Kimmel, B. Ullmann, and T.F. Schilling, *Stages of embryonic development of the zebrafish.* Dev Dyn, 1995. **203**(3): p. 253-310.

114. Fong, D.K., A. Rao, F.T. Crump, and A.M. Craig, *Rapid synaptic remodeling by protein kinase C: reciprocal translocation of NMDA receptors and calcium/calmodulin-dependent Kinase II.* J Neurosci, 2002. **22**(6): p. 2153-64.

115. Ganser, L.R., Q. Yan, V.M. James, R. Kozol, M. Topf, R.J. Harvey, and J.E. Dallman, *Distinct phenotypes in zebrafish models of human startle disease.* Neurobiol Dis, 2013. **60**: p. 139-51.

116. Ogino, K., S.L. Ramsden, N. Keib, G. Schwarz, R.J. Harvey, and H. Hirata, *Duplicated gephyrin genes showing distinct tissue distribution and alternative splicing patterns mediate molybdenum cofactor biosynthesis, glycine receptor clustering, and escape behavior in zebrafish.* J Biol Chem, 2011. **286**(1): p. 806-17.

117. Morgan, J.L., T. Schubert, and R.O. Wong, *Developmental patterning of glutamatergic synapses onto retinal ganglion cells.* Neural Dev, 2008. **3**: p. 8.

118. Soto, F., A. Bleckert, R. Lewis, Y. Kang, D. Kerschensteiner, A.M. Craig, and R.O. Wong, *Coordinated increase in inhibitory and excitatory synapses onto retinal ganglion cells during development.* Neural Dev, 2011. **6**: p. 31.

119. Hale, M.E., D.A. Ritter, and J.R. Fetcho, *A confocal study of spinal interneurons in living larval zebrafish.* J Comp Neurol, 2001. **437**(1): p. 1-16.

120. Myers, P.Z., J.S. Eisen, and M. Westerfield, *Development and axonal outgrowth of identified motoneurons in the zebrafish.* J Neurosci, 1986. **6**(8): p. 2278-89.

121. Morgan, J.L., F. Soto, R.O. Wong, and D. Kerschensteiner, *Development of cell type-specific connectivity patterns of converging excitatory axons in the retina.* Neuron, 2011. **71**(6): p. 1014-21.

122. Bleckert, A., E.D. Parker, Y. Kang, R. Pancaroglu, F. Soto, R. Lewis, A.M. Craig, and R.O. Wong, *Spatial relationships between GABAergic and glutamatergic synapses on the dendrites of distinct types of mouse retinal ganglion cells across development.* PLoS One, 2013. **8**(7): p. e69612.

123. Kim, J., T. Zhao, R.S. Petralia, Y. Yu, H. Peng, E. Myers, and J.C. Magee, *mGRASP enables mapping mammalian synaptic connectivity with light microscopy.* Nat Methods, 2012. **9**(1): p. 96-102.

124. Druckmann, S., L. Feng, B. Lee, C. Yook, T. Zhao, J.C. Magee, and J. Kim, *Structured synaptic connectivity between hippocampal regions.* Neuron, 2014.

125. Brown, A.G. and R.E. Fyffe, *Direct observations on the contacts made between Ia afferent fibres and alpha-motoneurones in the cat's lumbosacral spinal cord.* J Physiol, 1981. **313**: p. 121-40.

126. Fyffe, R.E.W., *Spatial distribution of recurrent inhibitory synapses on spinal motoneurons in the cat.* J Neurophysiol, 1991. **65**(5): p. 1134-49.

127. Burke, R.E. and L.L. Glenn, *Horseradish peroxidase study of the spatial and electrotonic distribution of group Ia synapses on type-identified ankle extensor motoneurons in the cat.* J Comp Neurol, 1996. **372**(3): p. 465-85.

128. Grande, G., S. Armstrong, M. Neuber-Hess, and P.K. Rose, *Distribution of contacts from vestibulospinal axons on the dendrites of splenius motoneurons.* J Comp Neurol, 2005. **491**(4): p. 339-51.

129. Grande, G., T.V. Bui, and P.K. Rose, *Distribution of vestibulospinal contacts on the dendrites of ipsilateral splenius motoneurons: an anatomical substrate for push-pull interactions during vestibulocollic reflexes.* Brain Res, 2010. **1333**: p. 9-27.

130. Rotterman, T.M., P. Nardelli, T.C. Cope, and F.J. Alvarez, *Normal distribution of VGLUT1 synapses on spinal motoneuron dendrites and their reorganization after nerve injury.* J Neurosci, 2014. **34**(10): p. 3475-92.

131. Eaton, R.C., R.D. Farley, C.B. Kimmel, and E. Schabtach, *Functional development in the Mauthner cell system of embryos and larvae of the zebra fish.* J Neurobiol, 1977. **8**(2): p. 151-72.

132. Schmitt, E.A. and J.E. Dowling, *Early retinal development in the zebrafish, Danio rerio: light and electron microscopic analyses.* J Comp Neurol, 1999. **404**(4): p. 515-36.

133. Higgs, D.M., A.K. Rollo, M.J. Souza, and A.N. Popper, *Development of form and function in peripheral auditory structures of the zebrafish (Danio rerio).* J Acoust Soc Am, 2003. **113**(2): p. 1145-54.

134. Zeddies, D.G. and R.R. Fay, *Development of the acoustically evoked behavioral response in zebrafish to pure tones.* J Exp Biol, 2005. **208**(Pt 7): p. 1363-72.

135. Lu, Z. and A.A. Desmidt, *Early development of hearing in zebrafish.* J Assoc Res Otolaryngol, 2013. **14**(4): p. 509-21.

136. Kim, H., J. Shin, S. Kim, J. Poling, H.C. Park, and B. Appel, *Notch-regulated oligodendrocyte specification from radial glia in the spinal cord of zebrafish embryos.* Dev Dyn, 2008. **237**(8): p. 2081-9.

137. Park, H.-C., A. Mehta, J.S. Richardson, and B. Appel, *olig2 Is Required for Zebrafish Primary Motor Neuron and Oligodendrocyte Development.* Dev Biol, 2002. **248**(2): p. 356-368.

138. Spitzer, N.C., *Electrical activity in early neuronal development.* Nature, 2006. **444**(7120): p. 707-12.

139. Yang, X., L. Li, S. Arber, Y. Tanabe, C. Birchmeier, C. William, T.M. Jessell, and S.J. Burden, *Patterning of muscle acetylcholine receptor gene expression in the absence of motor innervation.* Neuron, 2001. **30**: p. 399-410.

140. Lefebvre, J.L., L. Jing, S. Becaficco, C. Franzini-Armstrong, and M. Granato, *Differential requirement for MuSK and dystroglycan in generating patterns of neuromuscular innervation.* Proc Natl Acad Sci U S A, 2007. **104**(7): p. 2483-8.

141. Okabe, S., *Birth, growth and elimination of a single synapse.* Anat Sci Int, 2002. **77**(4): p. 203-210.

142. Wyatt, R.M. and R.J. Balice-Gordon, *Activity-dependent elimination of neuromuscular synapses.* J Neurocytol, 2003. **32**(5-8): p. 777-794.

143. Kano, M. and K. Hashimoto, *Synapse elimination in the central nervous system.* Curr Opin Neurobiol, 2009. **19**(2): p. 154-161.

144. Burke, R.E. and A.L. Karanas, *Demonstration of a medial to lateral gradient in the density of cholinergic neuropil in the rat striatum.* Neurosci Lett, 1990. **108**(1-2): p. 58-64.

145. Altar, C.A., M. Dugich-Djordjevic, M. Armanini, and C. Bakhit, *Medial-to-lateral gradient of neostriatal NGF receptors: relationship to cholinergic neurons and NGF-like lmmunoreactivity.* J Neurosci, 1991. **11**(3): p. 828-836.

146. Song, L., Y. Liu, Y. Yu, X. Duan, S. Qi, and Y. Liu, *Shh signaling guides spatial pathfinding of raphespinal tract axons by multidirectional repulsion.* Cell Res, 2012. **22**(4): p. 697-716.

147. Brierley, D.J., E. Blanc, O.V. Reddy, K. Vijayraghavan, and D.W. Williams, *Dendritic targeting in the leg neuropil of Drosophila: the role of midline signalling molecules in generating a myotopic map.* PLoS Biol, 2009. **7**(9): p. e1000199.

148. Mauss, A., M. Tripodi, J.F. Evers, and M. Landgraf, *Midline signalling systems direct the formation of a neural map by dendritic targeting in the Drosophila motor system.* PLoS Biol, 2009. **7**(9): p. e1000200.

149. Furrer, M.P., S. Kim, B. Wolf, and A. Chiba, *Robo and Frazzled/DCC mediate dendritic guidance at the CNS midline.* Nat Neurosci, 2003. **6**(3): p. 223-30.

150. Rajagopalan, S., V. Vivancos, E. Nicolas, and B.J. Dickson, *Selecting a longitudinal pathway: Robo receptors specify the lateral position of axons in the Drosophila CNS.* Cell, 2000. **103**(7): p. 1033-45.

151. Kastenhuber, E., U. Kern, J.L. Bonkowsky, C.B. Chien, W. Driever, and J. Schweitzer, *Netrin-DCC, Robo-Slit, and heparan sulfate proteoglycans coordinate lateral positioning of longitudinal dopaminergic diencephalospinal axons.* J Neurosci, 2009. **29**(28): p. 8914-26.

152. Reeber, S.L., N. Sakai, Y. Nakada, J. Dumas, K. Dobrenis, J.E. Johnson, and Z. Kaprielian, *Manipulating Robo expression in vivo perturbs commissural axon pathfinding in the chick spinal cord.* J Neurosci, 2008. **28**(35): p. 8698-708.

153. Thisse, B., S. Pflumio, M. Fürthauer, B. Loppin, V. Heyer, A. Degrave, R. Woehl, A. Lux, T. Steffan, X.Q. Charbonnier, and C. Thisse, *Expression of the zebrafish genome during embryogenesis (NIH R01 RR15402).* ZFIN Direct Data Submission (http://zfin.org), 2001.

154. Thisse, C. and B. Thisse, *High throughput expression analysis of zf-models consortium clones.* ZFIN Direct Data Submission (http://zfin.org), 2005.

155. Thisse, B., G.J. Wright, and C. Thisse, *Embryonic and larval expression patterns from a large scale screening for novel low affinity extracellular protein interactions.* ZFIN Direct Data Submission (http://zfin.org), 2008.

156. Challa, A.K., C.E. Beattie, and M.A. Seeger, *Identification and characterization of roundabout orthologs in zebrafish.* Mech Dev, 2001. **102**(1-2): p. 249-53.

157. Challa, A.K., M.L. Mcwhorter, C. Wang, M.A. Seeger, and C.E. Beattie, *Robo3 isoforms have distinct roles during zebrafish development.* Mech Dev, 2005. **122**(10): p. 1073-86.

158. Samant, G.V., M.O. Schupp, M. Francois, S. Moleri, R.K. Kothinti, C.Z. Chun, I. Sinha, S. Sellars, N. Leigh, K. Pramanik, M.A. Horswill, I. Remadevi, K. Li, G.A. Wilkinson, N.M. Tabatabai, M. Beltrame, P. Koopman, and R. Ramchandran, *Sox factors transcriptionally regulate ROBO4 gene expression in developing vasculature in zebrafish.* J Biol Chem, 2011. **286**(35): p. 30740-7.

159. Bonner, J., M. Letko, O.B. Nikolaus, L. Krug, A. Cooper, B. Chadwick, P. Conklin, A. Lim, C.B. Chien, and R.I. Dorsky, *Midline crossing is not required for subsequent pathfinding decisions in commissural neurons.* Neural Dev, 2012. **7**: p. 18.

160. Tran, T.S., E. Carlin, R. Lin, E. Martinez, J.E. Johnson, and Z. Kaprielian, *Neuropilin2 regulates the guidance of post-crossing spinal commissural axons in a subtype-specific manner.* Neural Dev, 2013. **8**: p. 15.

161. Spiegel, I., A.R. Mardinly, H.W. Gabel, J.E. Bazinet, C.H. Couch, C.P. Tzeng, D.A. Harmin, and M.E. Greenberg, *Npas4 regulates excitatory-inhibitory balance within neural circuits through cell-type-specific gene programs.* Cell, 2014. **157**(5): p. 1216-29.

162. Clark, P.J. and F.C. Evans, *Distance to nearest neighbor as a measure of spatial relationships in populations.* Ecology, 1954. **35**(4): p. 445-453.

163. Spruston, N., *Pyramidal neurons: dendritic structure and synaptic integration.* Nat Rev Neurosci, 2008. **9**(3): p. 206-21.

164. Branco, T. and M. Hausser, *Synaptic integration gradients in single cortical pyramidal cell dendrites.* Neuron, 2011. **69**(5): p. 885-92.

165. Kim, H.G., M. Beierlein, and B.W. Connors, *Inhibitory control of excitable dendrites in neocortex.* J Neurophysiol, 1995. **74**(4): p. 1810-4.

166. Miles, R., K. Toth, A.I. Gulyas, N. Hajos, and T.F. Freund, *Differences between somatic and dendritic inhibition in the hippocampus.* Neuron, 1996. **16**(4): p. 815-823.

167. Pouille, F. and M. Scanziani, *Enforcement of temporal fidelity in pyramidal cells by somatic feed-forward inhibition.* Science, 2001. **293**(10): p. 1159-63.

168. Berger, T. and H. Luscher, *Timing and precision of spike initiation in layer V pyramidal cells of the rat somatosensory cortex.* Cereb Cortex, 2003. **13**: p. 274-81.

169. Andrasfalvy, B.K. and I. Mody, *Differences between the scaling of miniature IPSCs and EPSCs recorded in the dendrites of CA1 mouse pyramidal neurons.* J Physiol, 2006. **576**(Pt 1): p. 191-6.

170. Perez-Garci, E., M. Gassmann, B. Bettler, and M.E. Larkum, *The GABAB1b isoform mediates long-lasting inhibition of dendritic Ca2+ spikes in layer 5 somatosensory pyramidal neurons.* Neuron, 2006. **50**(4): p. 603-16.

171. Hirata, H., E. Carta, I. Yamanaka, R.J. Harvey, and J.Y. Kuwada, *Defective glycinergic synaptic transmission in zebrafish motility mutants.* Front Mol Neurosci, 2010. **2**: p. 26.

172. Grillner, S. and T.M. Jessell, *Measured motion: searching for simplicity in spinal locomotor networks.* Curr Opin Neurobiol, 2009. **19**(6): p. 572-86.

173. Schneider Gasser, E.M., C.J. Straub, P. Panzanelli, O. Weinmann, M. Sassoe-Pognetto, and J.M. Fritschy, *Immunofluorescence in brain sections: simultaneous detection of presynaptic and postsynaptic proteins in identified neurons.* Nat Protoc, 2006. **1**(4): p. 1887-97.

174. Gross, G.G., J.A. Junge, R.J. Mora, H.B. Kwon, C.A. Olson, T.T. Takahashi, E.R. Liman, G.C. Ellis-Davies, A.W. Mcgee, B.L. Sabatini, R.W. Roberts, and D.B. Arnold, *Recombinant probes for visualizing endogenous synaptic proteins in living neurons.* Neuron, 2013. **78**(6): p. 971-85.

175. Fortin, D.A., S.E. Tillo, G. Yang, J.C. Rah, J.B. Melander, S. Bai, O. Soler-Cedeno, M. Qin, B.V. Zemelman, C. Guo, T. Mao, and H. Zhong, *Live imaging of endogenous PSD-95 using ENABLED: a conditional strategy to fluorescently label endogenous proteins.* J Neurosci, 2014. **34**(50): p. 16698-712.

176. Nelson, S.B. and V. Valakh, *Excitatory/Inhibitory Balance and Circuit Homeostasis in Autism Spectrum Disorders.* Neuron, 2015. **87**(4): p. 684-698.

177. Cui, W.W., S.E. Low, H. Hirata, L. Saint-Amant, R. Geisler, R.I. Hume, and J.Y. Kuwada, *The zebrafish shocked gene encodes a glycine transporter and is essential for the function of early neural circuits in the CNS.* J Neurosci, 2005. **25**(28): p. 6610-6620.

178. Granato, M., F.J. Van Eeden, U. Schach, T. Trowe, M. Brand, M. Furutani-Seiki, P. Haffter, M. Hammerschmidt, C.P. Heisenberg, Y.J. Jiang, D.A. Kane, R.N. Kelsh, M.C. Mullins, J. Odenthal, and C. Nusslein-Volhard, *Genes controlling*

and mediating locomotion behavior of the zebrafish embryo and larva. Development, 1996. **123**: p. 399-413.

179. Bakkar, W., C.L. Ma, M. Pabba, P. Khacho, Y.L. Zhang, E. Muller, M. Martina, and R. Bergeron, *Chronically saturating levels of endogenous glycine disrupt glutamatergic neurotransmission and enhance synaptogenesis in the CA1 region of mouse hippocampus.* Synapse, 2011. **65**(11): p. 1181-95.

180. Clemente, D., A. Porteros, E. Weruaga, J.R. Alonso, F.J. Arenzana, J. Aijon, and R. Arevalo, *Cholinergic elements in the zebrafish central nervous system: Histochemical and immunohistochemical analysis.* J Comp Neurol, 2004. **474**(1): p. 75-107.

181. Kozol, R.A., H.N. Cukier, B. Zou, V. Mayo, S. De Rubeis, G. Cai, A.J. Griswold, P.L. Whitehead, J.L. Haines, J.R. Gilbert, M.L. Cuccaro, E.R. Martin, J.D. Baker, J.D. Buxbaum, M.A. Pericak-Vance, and J.E. Dallman, *Two knockdown models of the autism genes SYNGAP1 and SHANK3 in zebrafish produce similar behavioral phenotypes associated with embryonic disruptions of brain morphogenesis.* Hum Mol Genet, 2015.

182. Higashijima, S., M. Schaefer, and J.R. Fetcho, *Neurotransmitter properties of spinal interneurons in embryonic and larval zebrafish.* J Comp Neurol, 2004. **480**(1): p. 19-37.

183. Dale, N., A. Roberts, O.P. Ottersen, and J. Storm-Mathisen, *The morphology and distribution of 'Kolmer-Agduhr cells', a class of cerebrospinal-fluid-contacting neurons revealed in the frog embryo spinal cord by GABA immunocytochemistry.* Proc R Soc Lond B Biol Sci, 1987. **232**(1267): p. 193-203.

184. Kanungo, J., Y.L. Zheng, B. Mishra, and H.C. Pant, *Zebrafish Rohon-Beard neuron development: cdk5 in the midst.* Neurochem Res, 2009. **34**(6): p. 1129-37.

185. Xue, M., B.V. Atallah, and M. Scanziani, *Equalizing excitation-inhibition ratios across visual cortical neurons.* Nature, 2014. **511**(7511): p. 596-600.

186. Fogarty, M.J., R. Kanjhan, M.C. Bellingham, and P.G. Noakes, *Glycinergic neurotransmission: a potent regulator of embryonic motor neuron dendritic morphology and synaptic plasticity.* J Neurosci, 2016. **36**(1): p. 80-87.

187. Siskova, Z., D. Justus, H. Kaneko, D. Friedrichs, N. Henneberg, T. Beutel, J. Pitsch, S. Schoch, A. Becker, H. Von Der Kammer, and S. Remy, *Dendritic structural degeneration is functionally linked to cellular hyperexcitability in a mouse model of Alzheimer's disease.* Neuron, 2014. **84**(5): p. 1023-33.

188. Magee, J.C., *Dendritic integration of excitatory synaptic input.* Nat Rev Neurosci, 2000. **1**(3): p. 181-90.

189. Williams, S.R. and G.J. Stuart, *Role of dendritic synapse location in the control of action potential output.* Trends Neurosci, 2003. **26**(3): p. 147-54.

190. Narayanan, R. and D. Johnston, *Functional maps within a single neuron.* J Neurophysiol, 2012. **108**(9): p. 2343-2351.

191. Stuart, G.J. and N. Spruston, *Dendritic integration: 60 years of progress.* Nat Neurosci, 2015. **18**(12): p. 1713-21.

192. Chung, S.K., J.F. Vanbellinghen, J.G. Mullins, A. Robinson, J. Hantke, C.L. Hammond, D.F. Gilbert, M. Freilinger, M. Ryan, M.C. Kruer, A. Masri, C. Gurses, C. Ferrie, K. Harvey, R. Shiang, J. Christodoulou, F. Andermann, E. Andermann, R.H. Thomas, R.J. Harvey, J.W. Lynch, and M.I. Rees, *Pathophysiological mechanisms of dominant and recessive GLRA1 mutations in hyperekplexia.* J Neurosci, 2010. **30**(28): p. 9612-20.

193. Bakker, M.J., J.G. Van Dijk, A.M. Van Den Maagdenberg, and M.A. Tijssen, *Startle syndromes.* Lancet Neurol, 2006. **5**(6): p. 513-24.

194. Cote, S. and P. Drapeau, *Regulation of spinal interneuron differentiation by the paracrine action of glycine.* Dev Neurobiol, 2012. **72**(2): p. 208-14.

195. Shiang, R., S.G. Ryan, Y.Z. Zhu, A.F. Hahn, P. O'connell, and J.J. Wasmuth, *Mutations in the alpha 1 subunit of the inhibitory glycine receptor cause the dominant neurologic disorder, hyperekplexia.* Nat Genet, 1993. **5**(4): p. 351-8.

196. Rees, M.I., T.M. Lewis, J.B. Kwok, G.R. Mortier, P. Govaert, R.G. Snell, P.R. Schofield, and M.J. Owen, *Hyperekplexia associated with compound heterozygote mutations in the beta-subunit of the human inhibitory glycine receptor (GLRB).* Hum Mol Genet, 2002. **11**(7): p. 853-60.

197. Al-Owain, M., D. Colak, A. Al-Bakheet, N. Al-Hashmi, T. Shuaib, A. Al-Hemidan, H. Aldhalaan, Z. Rahbeeni, M. Al-Sayed, B. Al-Younes, P.T. Ozand, and N. Kaya, *Novel mutation in GLRB in a large family with hereditary hyperekplexia.* Clin Genet, 2012. **81**(5): p. 479-84.

198. Chung, S.K., A. Bode, T.D. Cushion, R.H. Thomas, C. Hunt, S.E. Wood, W.O. Pickrell, C.J. Drew, S. Yamashita, R. Shiang, S. Leiz, A.C. Longardt, V. Raile, B. Weschke, R.D. Puri, I.C. Verma, R.J. Harvey, D.D. Ratnasinghe, M. Parker, C. Rittey, A. Masri, L. Lingappa, O.W. Howell, J.F. Vanbellinghen, J.G. Mullins, J.W. Lynch, and M.I. Rees, *GLRB is the third major gene of effect in hyperekplexia.* Hum Mol Genet, 2013. **22**(5): p. 927-40.

199. Lee, C.G., M.J. Kwon, H.J. Yu, S.H. Nam, J. Lee, C.S. Ki, and M. Lee, *Clinical features and genetic analysis of children with hyperekplexia in Korea.* J Child Neurol, 2013. **28**(1): p. 90-4.

200. Eisen, J.S. and J.C. Smith, *Controlling morpholino experiments: don't stop making antisense.* Development, 2008. **135**(10): p. 1735-43.

201. Burgess, H.A. and M. Granato, *Sensorimotor gating in larval zebrafish.* J Neurosci, 2007. **27**(18): p. 4984-94.

202. Hurley, I.A., R.L. Mueller, K.A. Dunn, E.J. Schmidt, M. Friedman, R.K. Ho, V.E. Prince, Z. Yang, M.G. Thomas, and M.I. Coates, *A new time-scale for ray-finned fish evolution.* Proc Biol Sci, 2007. **274**(1609): p. 489-98.

203. Hirata, H., L. Saint-Amant, G.B. Downes, W.W. Cui, W. Zhou, M. Granato, and J.Y. Kuwada, *Zebrafish bandoneon mutants display behavioral defects due to a mutation in the glycine receptor beta-subunit.* Proc Natl Acad Sci U S A, 2005. **102**(23): p. 8345-50.

204. Draper, B.W., P.A. Morcos, and C.B. Kimmel, *Inhibition of zebrafish fgf8 pre-mRNA splicing with morpholino oligos: a quantifiable method for gene knockdown.* Genesis, 2001. **30**(3): p. 154-6.

205. Lynch, J.W., *Molecular structure and function of the glycine receptor chloride channel.* Physiol Rev, 2004. **84**(4): p. 1051-95.

206. Levi, S., S.M. Logan, K.R. Tovar, and A.M. Craig, *Gephyrin is critical for glycine receptor clustering but not for the formation of functional GABAergic synapses in hippocampal neurons.* J Neurosci, 2004. **24**(1): p. 207-17.

207. Mcdearmid, J.R., M. Liao, and P. Drapeau, *Glycine receptors regulate interneuron differentiation during spinal network development.* Proc Natl Acad Sci U S A, 2006. **103**(25): p. 9679-84.

208. Rubenstein, J.L. and M.M. Merzenich, *Model of autism: increased ratio of excitation/inhibition in key neural systems.* Genes Brain Behav, 2003. **2**(5): p. 255-67.